RDECOM TR 10-D-112

**U.S. ARMY RESEARCH,
DEVELOPMENT AND
ENGINEERING COMMAND**

TITLE: Design and Experimental Results for the S414 Airfoil

AUTHOR: **Dan M. Somers and Mark D. Maughmer**

COMPANY NAME: **Airfoils, Incorporated**

COMPANY ADDRESS: **122 Rose Drive
Port Matilda PA 16870-7535**

DATE: **August 2010**

FINAL REPORT: **Contract Number W911W6-07-C-0047, SBIR Phase II,
Topic Number A06-006, Proposal Number A2-2972**

Prepared for:

U.S. ARMY RESEARCH, DEVELOPMENT AND ENGINEERING COMMAND, AVIATION APPLIED TECHNOLOGY DIRECTORATE, FORT EUSTIS, VA 23604-5577

AIRFOILS, INCORPORATED
122 ROSE DRIVE
PORT MATILDA, PA 16870-7535 USA
WEBSITE WWW AIRFOILS.COM
TELEPHONE (814) 357-0500
FACSIMILE (814) 357-0357

DESIGN AND EXPERIMENTAL RESULTS FOR THE S414 AIRFOIL

DAN M. SOMERS
AIRFOILS, INCORPORATED

MARK D. MAUGHMER
THE PENNSYLVANIA STATE UNIVERSITY

AUGUST 2010

ABSTRACT

A 14.22-percent-thick, slotted, natural-laminar-flow (SNLF) airfoil, the S414, intended for rotorcraft applications has been designed and analyzed theoretically and verified experimentally in The Pennsylvania State University Low-Speed, Low-Turbulence Wind Tunnel. The two primary objectives of high maximum lift and low profile drag have been achieved. The constraint on the airfoil thickness has been satisfied. The airfoil exhibits an abrupt stall. Comparisons of the theoretical and experimental results show good agreement overall. Comparisons with the S406 and S411 airfoils, which have similar design specifications, confirm the achievement of the objectives.

INTRODUCTION

Blade profile drag is a major contributor to the total vehicle drag for most rotorcraft. In general, to maximize rotor lift-to-drag ratio for low-speed flight, the following figure of merit FOM should be maximized:

$$\text{FOM} = \frac{c_{l,\max}}{c_{d,\text{cruise}}}$$

where $c_{l,\max}$ is the section maximum lift coefficient for the retreating blade and $c_{d,\text{cruise}}$ is the cruise section profile-drag coefficient for the advancing blade. (See ref. 1.) (Note that the figure of merit is expressed in terms of section (i.e., airfoil) characteristics, not aircraft characteristics.) The figure of merit can be interpreted as follows. Increasing maximum lift coefficient delays the onset of stall-flutter on the retreating blade, subject to the constraints of roll trim. Decreasing section profile-drag coefficient reduces the profile drag of the advancing blade. This figure of merit applies to almost all classes of aircraft. For high-speed flight, the figure of merit reduces to $1/\sqrt{c_{d,\text{cruise}}}$. (See ref. 2.)

Three approaches have become accepted for the reduction of profile drag. One approach is to employ a high-lift system (e.g., leading-edge slat plus double- or triple-slotted, Fowler flap) to achieve a higher maximum lift coefficient. (See, for example, ref. 3.) This approach has several disadvantages. Almost no laminar flow can be achieved because of the disturbances introduced by the slat, which results in a high section profile-drag coefficient. High-lift systems also usually generate large, negative pitching-moment coefficients. Such systems are complex, both mechanically and structurally, resulting in higher weight and cost. This approach has been adopted for the wings of all current transport aircraft. Active high-lift systems (e.g., blown flaps and circulation control) have demonstrated very high lift coefficients, but the cost, complexity, and potentially disastrous failure modes have prevented their adoption in production aircraft.

A second approach is to employ a natural-laminar-flow (NLF) airfoil to achieve a lower profile-drag coefficient. (See, for example, ref. 4.) By appropriate airfoil shaping, extensive (≥ 30-percent chord) laminar flow can be achieved on both the upper and lower surfaces. The extent of laminar flow is limited to about 70-percent chord by the pressure-

recovery gradient along the aft portion of the airfoil. The recovery gradient becomes steeper as the extent of the favorable pressure gradient along the forward portion of the airfoil increases, eventually reaching a limit beyond which trailing-edge separation occurs, resulting in a lower maximum lift coefficient and, correspondingly, a lower figure of merit. Leading-edge sweep and radial pressure gradients also restrict the extent of laminar flow because they introduce crossflow instabilities that lead to transition. This approach can provide a blade profile-drag reduction of about 50 percent compared to a conventional, turbulent-flow blade and has been adopted for the wings of most current general-aviation aircraft, including business jets, as well as unmanned aerial vehicles and all sailplanes. It does, however, require more stringent construction techniques.

A third approach is to employ a laminar-flow-control (LFC) airfoil to achieve a lower profile-drag coefficient. (See, for example, ref. 5.) By incorporating suction through porous or slotted, blade skins, 100-percent-chord laminar flow can be achieved on both the upper and lower surfaces. LFC systems are very complex, mechanically, structurally, and operationally, resulting in higher weight and cost. This approach can provide a blade profile-drag reduction of about 75 percent compared to a conventional, turbulent-flow blade but has yet to be adopted for any production aircraft, fixed- or rotary-wing.

For the present effort, a new approach, called a slotted, natural-laminar-flow (SNLF) airfoil (ref. 6), is employed. The SNLF airfoil concept is similar in nature to the slotted, supercritical airfoil concept (ref. 7), in that it employs a slot to allow a pressure recovery that would not be possible for a single-element airfoil.

Almost all airfoils in use on rotorcraft today were developed, however, under the assumption that extensive laminar flow is not likely on a rotor. (See ref. 8, for example.) For the present application, however, given the low Reynolds numbers, the achievement of laminar flow warrants exploration, acknowledging that questions remain about the effects of sweep and radial pressure gradients.

The airfoil designed under the present effort is intended for the rotor of a small helicopter having a torsionally stiff blade capable of handling much larger pitching moments than historically accepted. To complement the design effort, an investigation was conducted in The Pennsylvania State University Low-Speed, Low-Turbulence Wind Tunnel (ref. 9) to obtain the basic, low-speed, two-dimensional aerodynamic characteristics of the airfoil. The results have been compared with predictions from the method of reference 10. The results have also been compared with those for the S406 and S411 airfoils (refs. 11 and 12, respectively), which have similar design specifications.

SYMBOLS

Values are given in both SI and U.S. Customary Units. Measurements and calculations were made in U.S. Customary Units.

C_p pressure coefficient, $\frac{p_l - p_\infty}{q_\infty}$

c airfoil chord, mm (in.)

c_c section chord-force coefficient, $\oint C_p d\left(\frac{z}{c}\right)$

c_d section profile-drag coefficient, $\int_{\text{Wake}} c_d' d\left(\frac{h}{c}\right)$, except post stall, $c_n \sin\alpha + c_c \cos\alpha$

c_d' point drag coefficient (ref. 13)

c_l section lift coefficient, $c_n / \cos\alpha - c_d \tan\alpha$

c_m section pitching-moment coefficient about quarter-chord point, $-\oint C_p\left(\frac{x}{c} - 0.25\right) d\left(\frac{x}{c}\right) + \oint C_p\left(\frac{z}{c}\right) d\left(\frac{z}{c}\right)$

c_n section normal-force coefficient, $-\oint C_p d\left(\frac{x}{c}\right)$

h horizontal width in wake profile, mm (in.)

M free-stream Mach number

p static pressure, Pa (lbf/ft^2)

q dynamic pressure, Pa (lbf/ft^2)

R Reynolds number based on free-stream conditions and airfoil chord

t airfoil thickness, mm (in.)

x airfoil abscissa, mm (in.)

y model span station, $y = 0$ at midspan, mm (in.)

z airfoil ordinate, mm (in.)

α	angle of attack relative to x-axis, deg

Subscripts:

ae	aft element
l	local point on airfoil
ll	lower limit of low-drag range
max	maximum
min	minimum
ul	upper limit of low-drag range
0	zero lift
∞	free-stream conditions

Abbreviation:

SNLF	slotted, natural laminar flow

AIRFOIL DESIGN

OBJECTIVES AND CONSTRAINTS

The airfoil design specifications are contained in table I. Two primary objectives are evident. The first objective is to achieve a maximum lift coefficient of 1.25 at a Mach number of 0.30 and a Reynolds number of 0.97×10^6 and a maximum lift coefficient of 1.20 at a Mach number of 0.40 and a Reynolds number of 1.29×10^6. A requirement related to this objective is that the maximum lift coefficient not decrease significantly with transition fixed near the leading edge on both surfaces. In addition, the airfoil should exhibit docile stall characteristics. The second objective is to obtain low profile-drag coefficients from a lift coefficient of 0.10 at a Mach number of 0.70 and a Reynolds number of 2.26×10^6 to a lift coefficient of 0.65 at a Mach number of 0.45 and a Reynolds number of 1.45×10^6.

One major constraint was placed on the design of the airfoil. The airfoil thickness should equal about 14-percent chord.

The specifications for this airfoil are similar to those for the S406 airfoil (ref. 11) and identical to those for the S411 airfoil (ref. 12), but with no constraint on the zero-lift pitching-moment coefficient.

PHILOSOPHY

Given the above objectives and constraints, certain characteristics of the design are apparent. The following sketch illustrates a drag polar that meets the goals for this design.

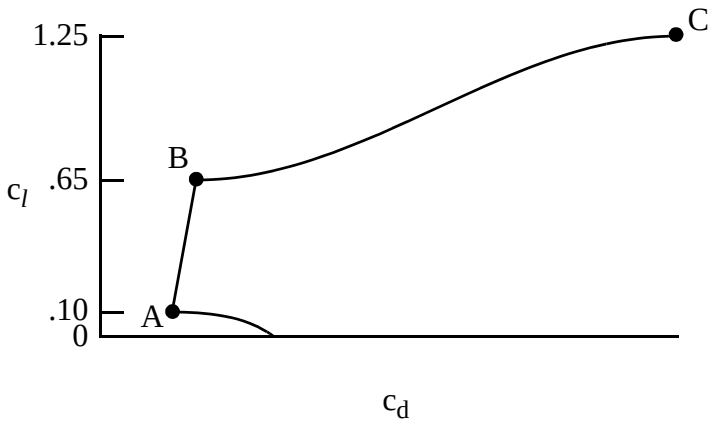

Sketch 1

The desired airfoil shape can be traced to the pressure distributions that occur at the various points in sketch 1. Point A is the lower limit of the low-drag range of lift coefficients; point B, the upper limit. The drag coefficient increases rapidly outside the low-drag, lift-coefficient range because boundary-layer transition moves quickly toward the leading edge with increasing (or decreasing) lift coefficient. This feature results in a leading edge that produces a suction peak at higher lift coefficients, which ensures that transition on the upper surface will occur very near the leading edge. Thus, the maximum lift coefficient, point C, occurs with turbulent flow along the entire upper surface and, therefore, should be relatively insensitive to roughness at the leading edge.

A two-element airfoil concept is used to meet the design specifications. The pressure distribution near the middle of the low-drag, lift-coefficient range is illustrated in sketch 2.

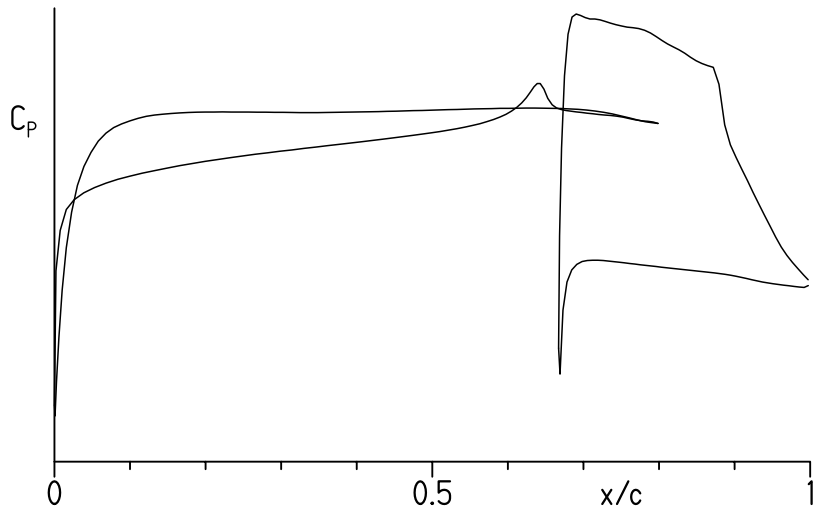

Sketch 2

Because the aft element eliminates the requirement that the pressure at the trailing edge of the fore element recover to free stream (see ref. 14), the favorable pressure gradient can extend farther aft. For the slotted, natural-laminar-flow (SNLF) airfoil concept, the favorable gradient extends along both surfaces of the fore element to near its trailing edge. Thus, the fore element is entirely laminar. (The relatively low Reynolds number allows the laminar flow to survive the short, adverse pressure gradient on the lower surface at about 65-percent chord.) The aft element then provides the necessary recovery to free-stream pressure. Because the wake of the fore element does not impinge on the aft element and because of its low Reynolds number, the aft element can also achieve significant extents of laminar flow.

The SNLF airfoil concept allows the natural laminar flow to be extended beyond the limit previously discussed. Thus, the concept exhibits low section profile-drag coefficients without having to resort to the complexity and cost of laminar flow control. The concept also achieves a high maximum lift coefficient without variable geometry (i.e., the aft element need not be deflected). The SNLF airfoil shape is not radically different from conventional airfoil shapes—no more than conventional, natural-laminar-flow airfoil shapes are from conventional, turbulent-flow airfoil shapes. Unlike conventional airfoils with slotted flaps, however, the SNLF airfoil has no nested configuration; the slot between the fore and aft elements is always open.

EXECUTION

The Eppler Airfoil Design and Analysis Code (refs. 15 and 16), a subcritical, single-element code, was used to design the initial fore- and aft-element shapes. The MSES code (ref. 10), a transonic, multielement code, was used to refine the fore-element shape in the two-element configuration.

The airfoil is designated the S414. The airfoil shape is shown in figure 1. The airfoil coordinates are available from Airfoils, Incorporated. The airfoil thickness is 14.22-percent chord, which satisfies the design constraint.

Because the test Reynolds numbers and particularly the test Mach numbers are much lower than the operational values of the intended application, the airfoil had to be modified for the wind-tunnel test. The modification was restricted to the aft half of the lower surface of the fore element; the aft element was not modified. The design and test airfoil shapes are compared in figure 1. The test shape is thinner around the entry to the slot.

THEORETICAL PROCEDURE

The theoretical results are predicted using the method of reference 10. A critical amplification factor of 9 was specified for the computations. Note that the method of reference 10 does not model the effect of Görtler instabilities (ref. 17) on the laminar boundary layer. A cursory evaluation of this effect indicates that these instabilities will not lead to transition in the concave region of the lower surface of the fore element.

Because the free-stream Mach number for all wind-tunnel test conditions did not exceed 0.2, the flow can be considered essentially incompressible for the purpose of comparing the theoretical and experimental results. This allows the fast, subcritical flow solver of the method of reference 10 to be used.

EXPERIMENTAL PROCEDURE

WIND TUNNEL

The Pennsylvania State University Low-Speed, Low-Turbulence Wind Tunnel (ref. 9) is a closed-throat, single-return, atmospheric tunnel (fig. 2). The test section is 101.3 cm (39.9 in.) high by 147.6 cm (58.1 in.) wide (fig. 3). Electrically actuated turntables provide positioning and attachment for the two-dimensional model. The turntables are flush with the top and bottom tunnel walls and rotate with the model. The axis of rotation coincided with 0.42 chord. The model was mounted vertically between the turntables and the gaps between the model and the turntables were sealed. The turbulence intensity in the test section is approximately 0.05 percent at 46 m/s (150 ft/s).

MODEL

The aluminum, wind-tunnel model was fabricated by Advanced Technologies, Incorporated, Newport News, Virginia, using a numerically controlled milling machine. The model had a chord of 457.2 mm (18.00 in.) and a span of 107.95 cm (42.50 in.) and, thus, extended through both turntables. Upper- and lower-surface orifices were located to one side of midspan at the staggered positions listed in table II. All the orifices were 0.51 mm (0.020 in.) in diameter with their axes perpendicular to the surface. The surfaces of the model were sanded to ensure an aerodynamically smooth finish. The measured model contour was within 0.13 mm (0.005 in.) of the prescribed shape.

WAKE-SURVEY PROBE

A total- and static-pressure, wake-survey probe (fig. 4) was mounted from the top tunnel wall (fig. 3). The probe was positioned 57.2 cm (22.5 in.) from the ceiling and automatically aligned with the wake-centerline streamline. A traverse mechanism incrementally positioned the probe to survey the wake. The increment was 1.27 mm (0.050 in.) for traverses less than 254.0 mm (10.00 in.) and 2.54 mm (0.100 in.) for longer traverses, which were occasionally required near the maximum lift coefficient. The tip of the probe was located 0.7 chord downstream of the trailing edge of the model.

INSTRUMENTATION

Basic tunnel pressures and the wake pressures were measured with precision transducers. Measurements of the pressures on the model were made by an automatic pressure-scanning system utilizing precision transducers. Data were obtained and recorded by an electronic data-acquisition system.

METHODS

The pressures measured on the model were reduced to standard pressure coefficients and numerically integrated to obtain section normal-force and chord-force coefficients and section pitching-moment coefficients about the quarter-chord point. Section profile-drag coefficients were computed from the wake total and static pressures by the method of reference 13. Wake surveys were not performed, however, at most post-stall angles of attack, in which case, the profile-drag coefficients were computed from the normal- and chord-force coefficients.

Standard, low-speed, wind-tunnel boundary corrections (ref. 18) have been applied to the data. The wake-survey-probe total-pressure-tube displacement correction (ref. 13) has been taken into account.

TESTS

The model was tested at Reynolds numbers based on airfoil chord of 0.50×10^6, 0.70×10^6, 1.00×10^6, and 1.50×10^6 with transition free (smooth) and with transition fixed by roughness at 2-percent chord on the upper surface and by serrated tape (ref. 19) at 10-percent chord on the lower surface of the fore element, where the chord is the total chord of the model. The model was also tested with transition fixed on the fore element and with transition fixed by serrated tape at 5-percent chord on the upper surface and 10-percent chord on the lower surface of the aft element, where the chord is the chord of the aft element. The grit roughness was sized near the maximum lift coefficient using the method of reference 20. The grit was sparsely distributed along 3-mm (0.1-in.) wide strips applied to the model with lacquer. The thickness of the serrated tape was determined empirically on each surface for each Reynolds number by increasing the thickness until transition moved forward to the vicinity of the tape, as verified by stethoscope measurements (ref. 5). (See table III.) The thickness on the lower surface of the fore element was determined at an angle of attack of 10° to ensure turbulent flow through the slot, even at high lift coefficients. The thickness on the aft element was determined in the middle of the low-drag, lift-coefficient range.

The Mach number did not exceed 0.2 for any test condition. Thus, the test Mach numbers are much lower than the operational values of the intended application.

Starting from 0°, the angle of attack was increased to post-stall values. The angle of attack was then decreased from 0° to below that for zero lift.

For several test runs, the model surfaces were coated with oil to determine the location as well as the nature of the boundary-layer transition from laminar to turbulent flow and the location of turbulent separation (ref. 21). Oil-flow visualization was also used to verify the two-dimensionality of the flow. In addition, acoustic measurements (ref. 5) were used to confirm the transition locations.

DISCUSSION OF RESULTS

THEORETICAL RESULTS

Pressure Distributions

The pressure distributions for the design airfoil shape predicted using the method of reference 10 at various angles of attack at three of the design conditions are shown in figure 5.

Section Characteristics

The section characteristics of the design airfoil shape at all four design conditions with transition free and with transition fixed on the fore and aft elements are shown in figure 6.

Based on the predictions, all the design objectives and constraints have been met, except that for the lower limit of the low-drag, lift-coefficient range, which is higher than specified.

EXPERIMENTAL RESULTS

Pressure Distributions

The pressure distributions for the test airfoil shape measured at various angles of attack for a Reynolds number of 1.00×10^6 and a Mach number of 0.10 with transition free are shown in figure 7. At an angle of attack of –4.09° (fig. 7(a)), a pressure peak is present on the lower surface of the fore element whereas a favorable pressure gradient extends along the upper surface almost to the trailing edge of the fore element. An adverse pressure gradient occurs along the forward half of the upper surface of the aft element and along essentially the entire lower surface. A short laminar separation bubble, typical of the low Reynolds number of the aft element ($\approx 0.3 \times 10^6$), is discernible on the upper surface around 88-percent chord (i.e., 65 percent of the chord of the aft element) despite the turbulent flow on the lower surface of the fore element. As the angle of attack is increased, the pressure peak on the lower surface of the fore element decreases in magnitude. At an angle of attack of –3.07° (fig. 7(b)), which corresponds approximately to the lower limit of the low-drag, lift-coefficient range, the laminar flow survives the peak and the pressure distribution on the lower surface of the fore element around the slot entry is smoother. At an angle of attack of –2.06° (fig. 7(c)), the peak has almost disappeared and the pressure gradients on both surfaces of the fore element are slightly favorable. As the angle of attack is increased further, the pressure gradient along the majority of the upper surface of the fore element becomes flat (fig. 7(d)) and then increasingly adverse (figs. 7(e) and 7(f)). The pressure distributions within the low-drag range suggest that the flow on both surfaces of the fore element is completely laminar. This was confirmed by oil-flow visualization and acoustic measurements. At an angle of attack of 2.02° (fig. 7(g)), which corresponds to the upper limit of the low-drag range, the gradient on the upper surface of the fore element is still insufficiently adverse to cause transition to move forward significantly. As the angle of attack is increased even further, the pressure peak on the upper surface of the fore element becomes sharper and moves forward (figs. 7(h)–7(r)) until, at an angle of attack of 14.23° (fig. 7(s)), it reaches the leading edge. As the angle of attack is increased still further, the leading-edge peak increases in magnitude (figs. 7(t) and 7(u)). The maximum lift coefficient occurs at an angle of attack of 16.24° (fig. 7(u)). As the angle of attack is increased further, the peak collapses and three fourths of the upper surface of the fore element is separated (figs. 7(v)–7(x)); the upper surface of the aft element remains attached, however. The pressure distribution on the aft element changes little with angle of attack, except through stall (figs. 7(u) and 7(v)), because the incoming flow angle for the aft element is fixed by the fore element.

Section Characteristics

The section characteristics of the test airfoil shape with transition free, with transition fixed on the fore element only, and with transition fixed on the fore and aft elements are

shown in figure 8 and tabulated in the appendix. For a Reynolds number of 1.00×10^6 and a Mach number of 0.10 with transition free (fig. 8(c)), the maximum lift coefficient is 1.85. The stall characteristics are abrupt. For a Reynolds number of 1.50×10^6 and a Mach number of 0.17 with transition free (fig. 8(d)), the lower limit of the low-drag, lift-coefficient range is 0.05, the upper limit is 0.58, and the zero-lift pitching-moment coefficient is –0.124.

The unusual shape of the drag polars, particularly noticeable around the lower limit of the low-drag range for lower Reynolds numbers, is probably the result of an interaction between the wake of the fore element and the laminar separation bubble on the upper surface of the aft element. As the angle of attack approaches the lower or upper limit, transition occurs near the trailing edge of the fore element. The resulting turbulence probably alleviates the laminar separation bubble on the upper surface of the aft element, reducing the drag. Oil-flow visualization shows that the length of the bubble decreases toward the lower limit of the low-drag range.

The effects of Reynolds number on the section characteristics are summarized in figure 9. In general, the lift-curve slope, the maximum lift coefficient, the lower limit of the low-drag range, and the magnitude of the pitching-moment coefficients, including the zero-lift value, increase with increasing Reynolds number. The upper limit of the low-drag range and the profile-drag coefficients decrease with increasing Reynolds number. The zero-lift angle of attack is relatively unaffected by Reynolds number.

The effect of fixing transition on the section characteristics is shown in figure 8. In general, the zero-lift angle of attack and the stall characteristics are relatively unaffected by fixing transition, whereas the lift-curve slope and the magnitude of the pitching-moment coefficients, including the zero-lift value, decrease with transition fixed. The latter results are primarily a consequence of the boundary-layer displacement effect, which decambers the airfoil because the displacement thickness is greater with transition fixed than with transition free. The effect of fixing transition on the maximum lift coefficient is small, varying from a decrease of less than 4 percent to an increase of less than 2 percent. The effect is caused primarily by fixing transition on the fore element. The drag coefficients are, of course, generally affected adversely by the trips.

It should be noted that, for almost all test conditions, the Reynolds number based on local velocity and boundary-layer displacement thickness at the trip locations is too low to support turbulent flow. (See ref. 22.) Accordingly, to force transition, the trip must be so large that it increases the displacement thickness, which abnormally decreases the lift coefficient and the magnitude of the pitching-moment coefficient and increases the drag coefficient. Conversely, at low lift coefficients, the grit roughness on the upper surface of the fore element, which is sized for high lift coefficients, is too small to force transition, resulting in incorrectly low drag coefficients.

The variations of maximum lift coefficient and minimum profile-drag coefficient with Reynolds number are shown in figures 10 and 11, respectively. The maximum lift coefficient increases with increasing Reynolds number, whereas the minimum profile-drag coefficient decreases, which are typical trends for most airfoils.

COMPARISON OF THEORETICAL AND EXPERIMENTAL RESULTS

Pressure Distributions

The comparison of the theoretical and experimental pressure distributions for the test airfoil shape at various angles of attack for a Reynolds number of 1.00×10^6 and a Mach number of 0.10 with transition free is shown in figure 12. At a lift coefficient of 0.28 (fig. 12(a)), which is near the middle of the low-drag range, the agreement between the predicted and measured pressure coefficients and pressure gradients is good. The predicted location of the laminar separation bubble on the upper surface of the aft element is slightly aft of the measured location. At a lift coefficient of 1.04 (fig. 12(b)), the agreement is less precise, particularly with respect to the pressure gradients on the upper surface of the fore element. The predicted locations of the laminar separation bubbles on the upper surfaces of the fore and aft elements are aft of the measured locations. At a lift coefficient of 1.85 (fig. 12(c)), which is the measured maximum lift coefficient, the agreement is worse but still remarkably good, considering the complexity of the configuration.

Section Characteristics

The comparison of the theoretical and experimental section characteristics of the test airfoil shape with transition free is shown in figure 13. In general, the method of reference 10 overpredicts the lift-curve slope, the maximum lift coefficient, the profile-drag coefficients, the upper limit of the low-drag range, and the magnitudes of the zero-lift angle of attack and the pitching-moment coefficients, including the zero-lift value. The overprediction of the maximum lift coefficient decreases from 13 percent for a Reynolds number of 0.50×10^6 to 5 percent for a Reynolds number of 1.50×10^6. The severity of the stall characteristics is underpredicted. Overall, however, the agreement is good, especially considering the complexity of the configuration.

The comparisons of the theoretical and experimental section characteristics with transition fixed on the fore element only and with transition fixed on the fore and aft elements are shown in figures 14 and 15, respectively. In general, the predicted characteristics show similar tendencies as with transition free, although the overall agreement is poorer, probably because of the abnormalities introduced by the trips, as discussed previously.

COMPARISON WITH S406 AND S411 AIRFOILS

The experimental section characteristics of the S414 airfoil for a Reynolds number of 1.0×10^6 and a Mach number of 0.1 with transition free are compared with those of the S406 and S411 airfoils, which have similar design specifications, in figure 16. The S414 airfoil exhibits profile-drag coefficients comparable to those of the S406 airfoil, which are lower than those of the S411 airfoil, but also substantially more negative pitching-moment coefficients and abrupt stall characteristics. The maximum lift coefficients and the profile-drag coefficients at a lift coefficient of 0.4 are compared in figures 17 and 18, respectively. The

maximum lift coefficient of the S414 airfoil with transition free is about 30-percent higher for a Reynolds number of 0.5×10^6, increasing to over 50-percent higher for a Reynolds number of 1.5×10^6.

CONCLUDING REMARKS

A 14.22-percent-thick, slotted, natural-laminar-flow (SNLF) airfoil, the S414, intended for rotorcraft applications has been designed and analyzed theoretically and verified experimentally in The Pennsylvania State University Low-Speed, Low-Turbulence Wind Tunnel. The two primary objectives of a high maximum lift coefficient and low profile-drag coefficients have been achieved. The constraint on the airfoil thickness has been satisfied. The airfoil exhibits abrupt stall characteristics. Comparisons of the theoretical and experimental results show good agreement overall. Comparisons with the S406 and S411 airfoils, which have similar design specifications, confirm the achievement of the objectives.

ACKNOWLEDGMENTS

This effort was sponsored by the U.S. Army. Preston B. Martin served as the technical monitor.

REFERENCES

1. Maughmer, Mark D.; and Somers, Dan M.: Figures of Merit for Airfoil/Aircraft Design Integration. AIAA Paper 88-4416, Sept. 1988.

2. Harris, Franklin D.: Rotary Wing Aerodynamics – Historical Perspective and Important Issues. American Helicopter Soc. National Specialists' Meeting on Aerodynamics and Aeroacoustics, Arlington, TX, Feb. 25–27, 1987.

3. Smith, A. M. O.: High-Lift Aerodynamics. AIAA Paper 74-939, Aug. 1974.

4. Jacobs, Eastman N.: Preliminary Report on Laminar-Flow Airfoils and New Methods Adopted for Airfoil and Boundary-Layer Investigations. NACA WR L-345, 1939 (formerly, NACA ACR).

5. Pfenninger, Werner: Investigations on Reductions of Friction on Wings, in Particular by Means of Boundary Layer Suction. NACA TM 1181, 1947. (Translated from Mitteilungen aus dem Institut für Aerodynamik an der Eidgenössischen Technischen Hochschule Zürich, Nr. 13, 1946.)

6. Somers, Dan M.: Laminar-Flow Airfoil. U.S. Patent 6,905,092 B2, June 2005.

7. Whitcomb, Richard T.; and Clark, Larry R.: An Airfoil Shape for Efficient Flight at Supercritical Mach Numbers. NASA TM X-1109, 1965.

8. Noonan, Kevin W.: Aerodynamic Characteristics of Two Rotorcraft Airfoils Designed for Application to the Inboard Region of a Main Rotor Blade. NASA TP-3009, 1990.

9. Brophy, Christopher M.: Turbulence Management and Flow Qualification of The Pennsylvania State University Low Turbulence, Low Speed, Closed Circuit Wind Tunnel. M. S. Thesis, Pennsylvania State Univ., 1993.

10. Drela, M.: Design and Optimization Method for Multi-Element Airfoils. AIAA Paper 93-0969, Feb. 1993.

11. Somers, Dan M.; and Maughmer, Mark D.: Design and Experimental Results for the S406 Airfoil. U.S. Army RDECOM TR 10-D-107, 2010. (Available from DTIC.)

12. Somers, Dan M.; and Maughmer, Mark D.: Design and Experimental Results for the S411 Airfoil. U.S. Army RDECOM TR 10-D-111, 2010. (Available from DTIC.)

13. Pankhurst, R. C.; and Holder, D. W.: Wind-Tunnel Technique. Sir Isaac Pitman & Sons, Ltd. (London), 1965.

14. Maughmer, Mark D.: Trailing Edge Conditions as a Factor in Airfoil Design. Ph.D. Dissertation, Univ. of Illinois, 1983.

15. Eppler, Richard: Airfoil Design and Data. Springer-Verlag (Berlin), 1990.

16. Eppler, Richard: Airfoil Program System “PROFIL07.” User’s Guide. Richard Eppler, c.2007.

17. Görtler, H.: On the Three-Dimensional Instability of Laminar Boundary Layers on Concave Walls. NACA TM 1375, 1954.

18. Allen, H. Julian; and Vincenti, Walter G.: Wall Interference in a Two-Dimensional-Flow Wind Tunnel, With Consideration of the Effect of Compressibility. NACA Rep. 782, 1944. (Supersedes NACA WR A-63.)

19. Hama, Francis R.: An Efficient Tripping Device. J. Aeronaut. Sci., vol. 24, no. 3, Mar. 1957, pp. 236–237.

20. Braslow, Albert L.; and Knox, Eugene C.: Simplified Method for Determination of Critical Height of Distributed Roughness Particles for Boundary-Layer Transition at Mach Numbers From 0 to 5. NACA TN 4363, 1958.

21. Loving, Donald L.; and Katzoff, S.: The Fluorescent-Oil Film Method and Other Techniques for Boundary-Layer Flow Visualization. NASA MEMO 3-17-59L, 1959.

22. Schubauer, G. B.; and Klebanoff, P. S.: Contributions on the Mechanics of Boundary-Layer Transition. NACA Rep. 1289, 1956.

TABLE I.- AIRFOIL DESIGN SPECIFICATIONS

Parameter	Objective/ Constraint	Mach Number M	Reynolds Number R	Priority
Minimum lift coefficient $c_{l,min}$	0.00	0.70	2.26×10^6	Low
Maximum lift coefficient $c_{l,max}$	1.25 1.20	0.30 0.40	0.97×10^6 1.29×10^6	High
Lower limit of low-drag, lift-coefficient range $c_{l,ll}$	0.10	0.70	2.26×10^6	Medium
Upper limit of low-drag, lift-coefficient range $c_{l,ul}$	0.65	0.45	1.45×10^6	Medium
Zero-lift pitching-moment coefficient $c_{m,0}$	—			
Thickness t/c	0.14			Medium
Other: Maximum lift coefficient $c_{l,max}$ independent of leading-edge roughness Docile stall characteristics Objectives and constraints identical to those for S411 airfoil without $c_{m,0}$ constraint				

TABLE II.- MODEL ORIFICE LOCATIONS

[c = 457.2 mm (18.00 in.)]

(a) Fore element

Upper Surface		Lower Surface	
x/c	y, mm (in.)	x/c	y, mm (in.)
0.00000	–144.38 (–5.684)	0.00181	–162.13 (–6.383)
.00347	–143.59 (–5.653)	.00838	–161.08 (–6.342)
.01305	–142.39 (–5.606)	.01954	–159.92 (–6.296)
.02985	–140.84 (–5.545)	.03424	–158.84 (–6.253)
.05304	–138.83 (–5.466)	.05304	–156.96 (–6.179)
.08189	–136.15 (–5.360)	.07597	–154.83 (–6.096)
.11621	–133.43 (–5.253)	.10166	–152.61 (–6.008)
.15578	–130.33 (–5.131)	.13193	–150.15 (–5.911)
.19969	–126.61 (–4.985)	.16390	–147.25 (–5.797)
.24657	–122.77 (–4.833)	.19995	–144.29 (–5.681)
.29549	–119.10 (–4.689)	.23707	–141.18 (–5.558)
.34643	–114.78 (–4.519)	.27585	–137.95 (–5.431)
.39953	–110.24 (–4.340)	.31623	–134.59 (–5.299)
.45228	–105.83 (–4.167)	.35727	–130.88 (–5.153)
.50313	–101.51 (–3.997)	.39923	–127.51 (–5.020)
.55229	–97.43 (–3.836)	.44062	–124.01 (–4.882)
.59958	–93.68 (–3.688)	.48222	–120.44 (–4.742)
.64303	–90.08 (–3.546)	.52258	–117.09 (–4.610)
.68101	–86.64 (–3.411)	.56177	–113.69 (–4.476)
.71553	–83.92 (–3.304)	.59906	–110.62 (–4.355)
.74485	–81.57 (–3.212)	.61014	–109.70 (–4.319)
.76808	–79.42 (–3.127)	.62182	–108.66 (–4.278)
.78518	–77.99 (–3.071)	.63398	–107.74 (–4.242)
.79502	–76.99 (–3.031)	.64402	–106.53 (–4.194)
.79896	–75.92 (–2.989)	.65521	–105.69 (–4.161)
		.66644	–104.73 (–4.123)
		.67630	–103.99 (–4.094)
		.68618	–103.20 (–4.063)
		.69599	–102.32 (–4.028)
		.72232	–100.17 (–3.944)
		.74522	–98.25 (–3.868)
		.76401	–96.39 (–3.795)
		.77908	–94.96 (–3.739)
		.78934	–94.00 (–3.701)
		.79559	–92.90 (–3.657)

TABLE II.- Concluded

(b) Aft element

Upper Surface		Lower Surface	
x/c	y, mm (in.)	x/c	y, mm (in.)
0.66747	−125.27 (−4.932)	0.67390	−123.42 (−4.859)
.67055	−124.17 (−4.889)	.69391	−121.69 (−4.791)
.67980	−123.29 (−4.854)	.72442	−118.96 (−4.684)
.69643	−121.71 (−4.792)	.76454	−115.76 (−4.557)
.71879	−119.82 (−4.718)	.80994	−112.05 (−4.411)
.74656	−117.35 (−4.620)	.85722	−107.86 (−4.246)
.77855	−114.72 (−4.516)	.90259	−104.27 (−4.105)
.81243	−111.83 (−4.403)	.94270	−100.89 (−3.972)
.84673	−108.97 (−4.290)	.97337	−98.35 (−3.872)
.86526	−107.38 (−4.228)	.99309	−96.38 (−3.794)
.88215	−106.06 (−4.176)		
.89313	−105.04 (−4.136)		
.90370	−104.16 (−4.101)		
.91469	−103.22 (−4.064)		
.92890	−102.16 (−4.022)		
.94272	−100.90 (−3.972)		
.96770	−98.82 (−3.890)		
.98537	−97.33 (−3.832)		
.99591	−96.37 (−3.794)		
1.00000	−95.50 (−3.760)		

TABLE III.- TRIP LOCATIONS AND SIZES

(a) Fore element

R	Upper surface			Lower surface	
	x/c	Grit number	Nominal size, mm (in.)	x/c	Serrated-tape thickness, mm (in.)
0.50×10^6	0.02	80	0.211 (0.0083)	0.10	0.572 (0.0225)
0.70×10^6		90	0.178 (0.0070)		0.457 (0.0180)
1.00×10^6		120	0.124 (0.0049)		
1.50×10^6		180	0.089 (0.0035)		0.343 (0.0135)

(b) Aft element

R	Upper surface		Lower surface	
	$(x/c)_{ae}$	Serrated-tape thickness, mm (in.)	$(x/c)_{ae}$	Serrated-tape thickness, mm (in.)
0.50×10^6	0.05	0.343 (0.0135)	0.10	0.686 (0.0270)
0.70×10^6		0.191 (0.0075)		
1.00×10^6		0.114 (0.0045)		0.610 (0.0240)
1.50×10^6		0.064 (0.0025)		0.457 (0.0180)

Figure 1.- S414 design and test airfoil shapes.

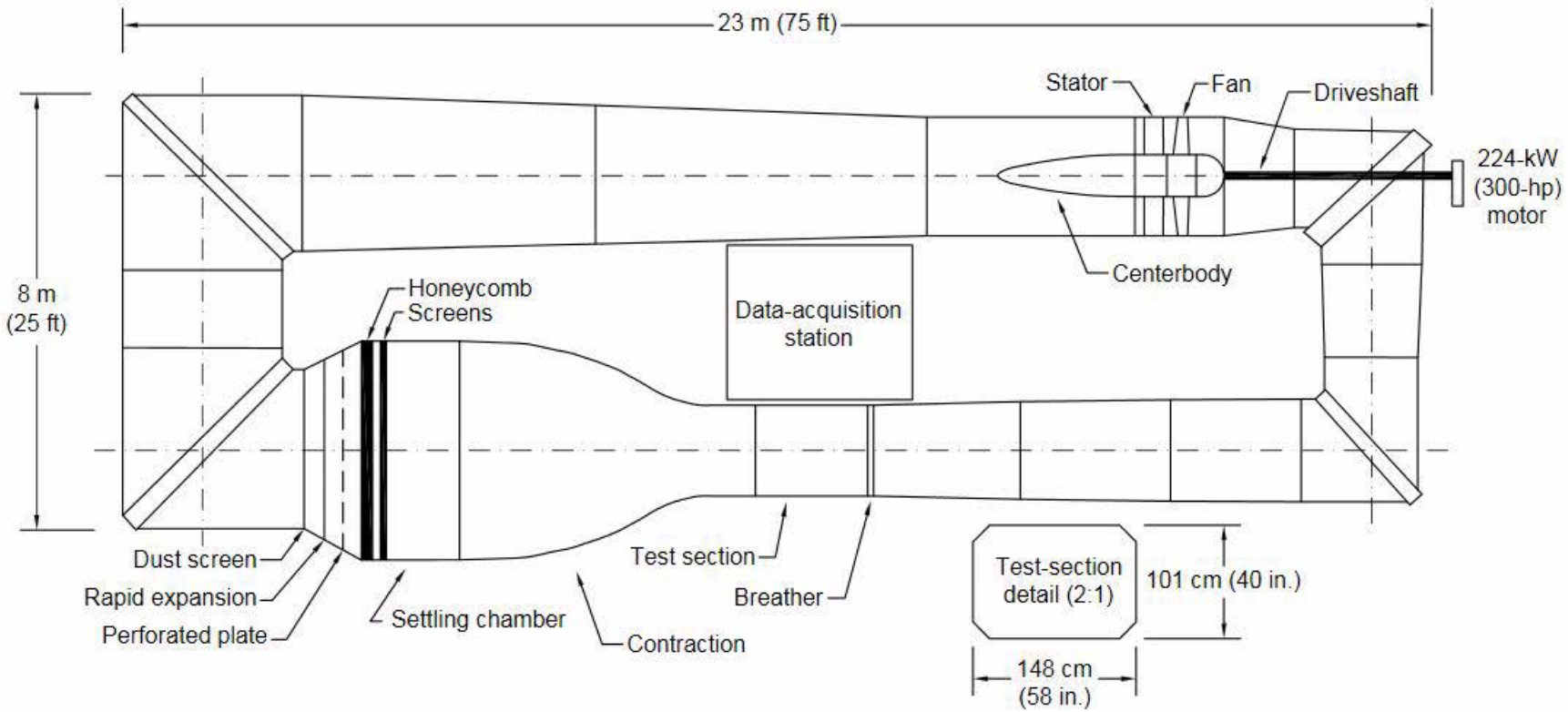

Figure 2.- The Pennsylvania State University Low-Speed, Low-Turbulence Wind Tunnel.

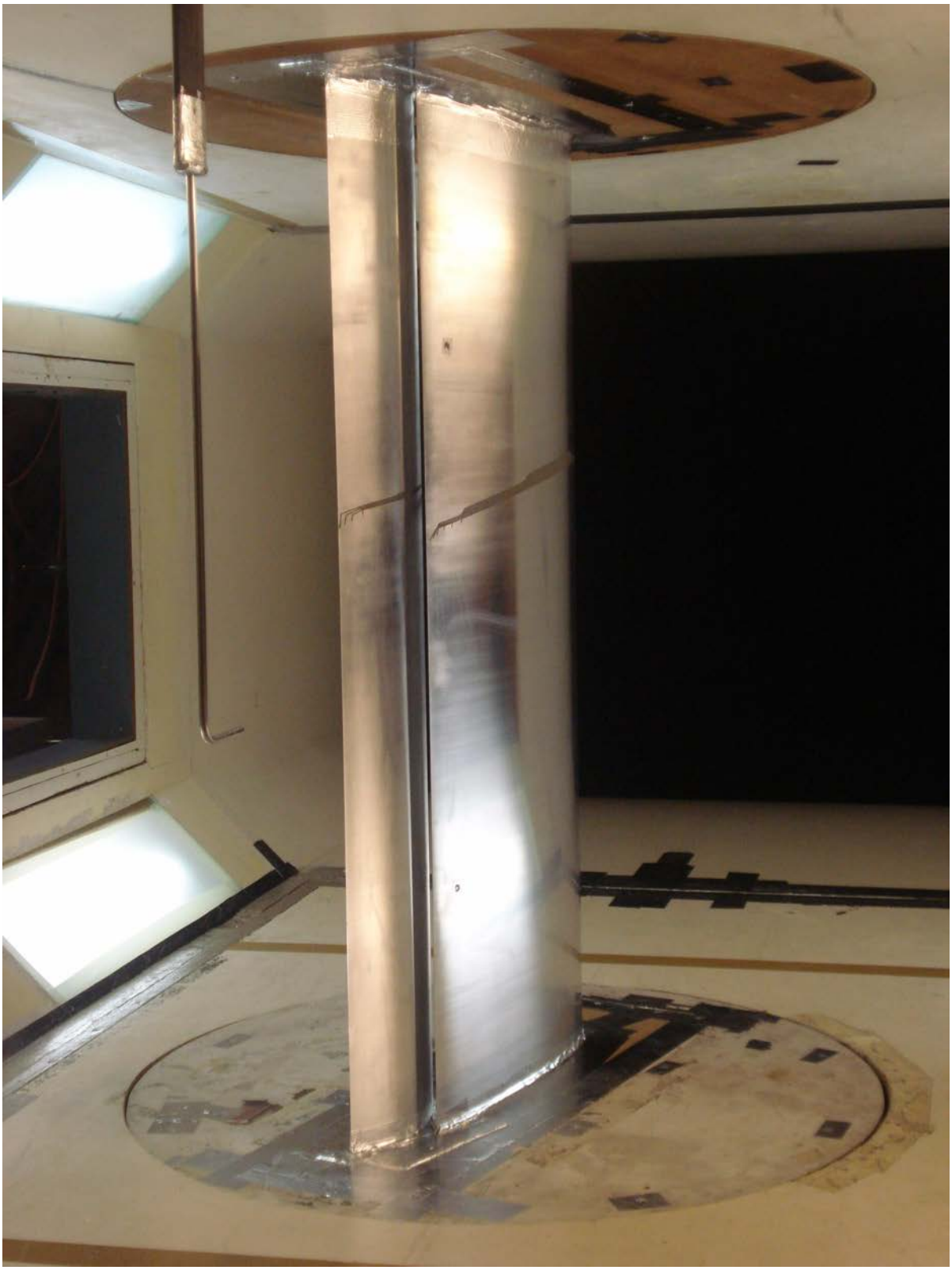

Figure 3.- S414 airfoil model and wake-survey probe mounted in test section.

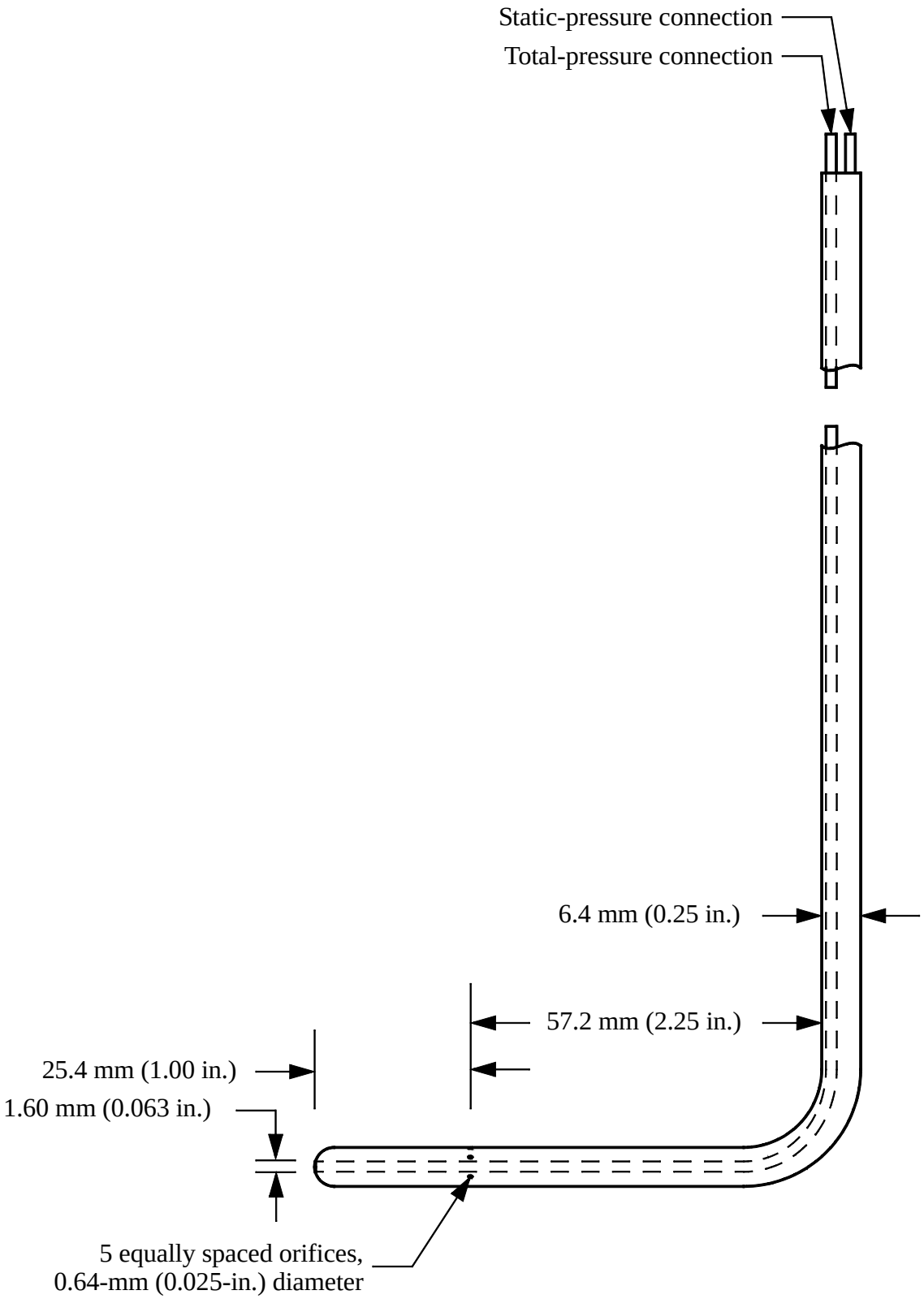

Figure 4.- Wake-survey probe.

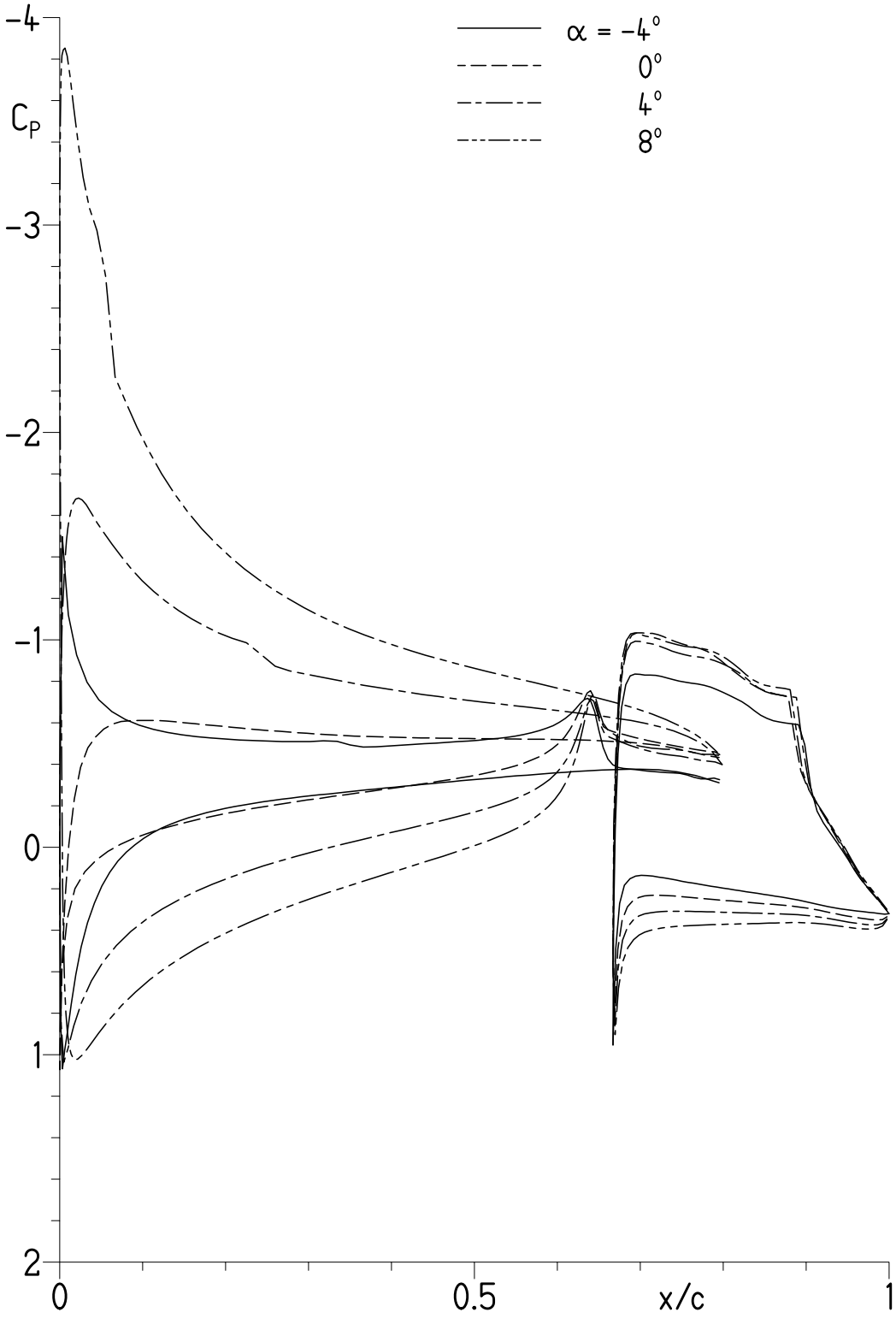

(a) M = 0.30 and R = 0.97×10^6.

Figure 5.- Theoretical pressure distributions for design airfoil shape.

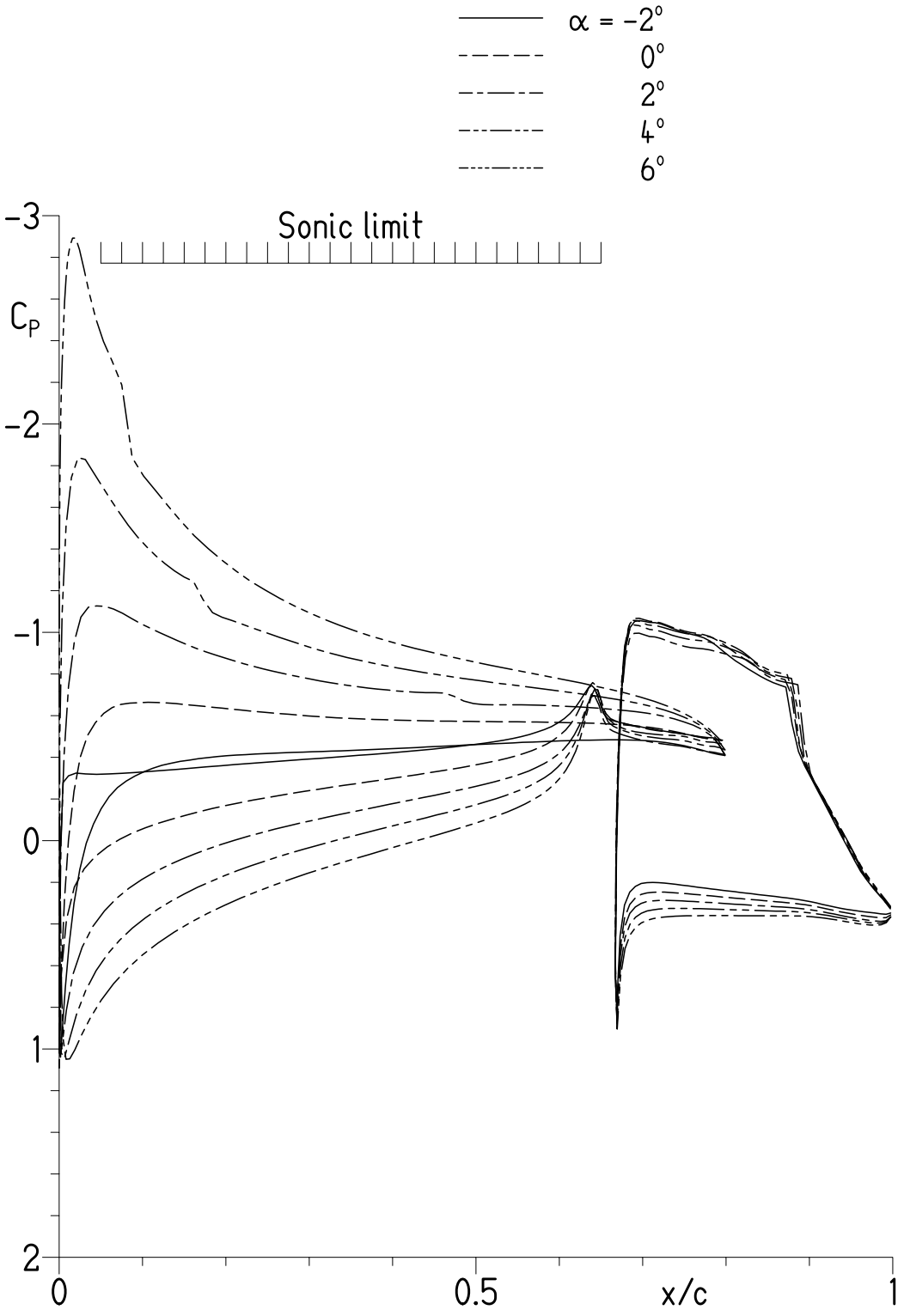

(b) M = 0.45 and R = 1.45×10^6.

Figure 5.- Continued.

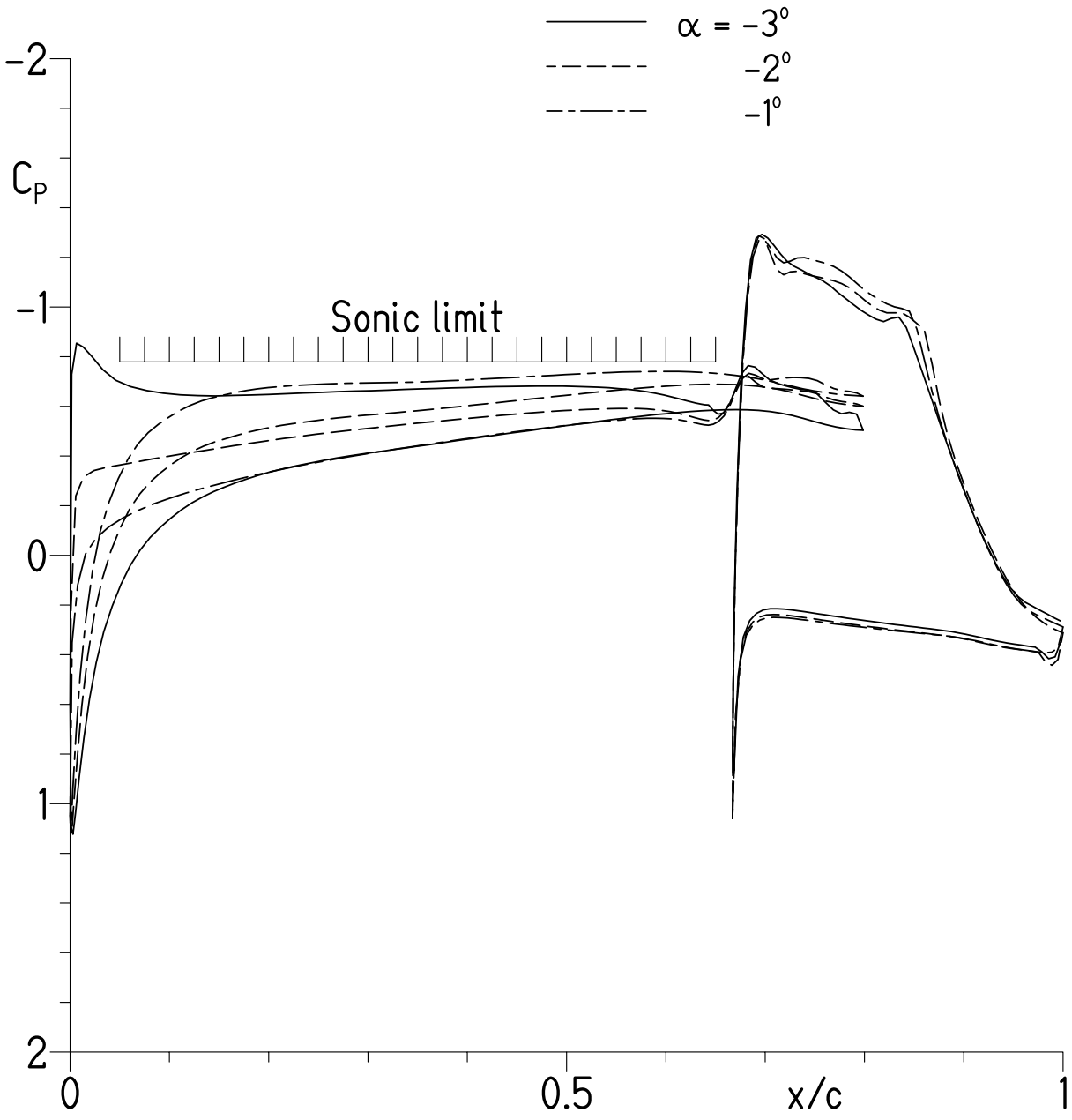

(c) M = 0.70 and R = 2.26×10^6.

Figure 5.- Concluded.

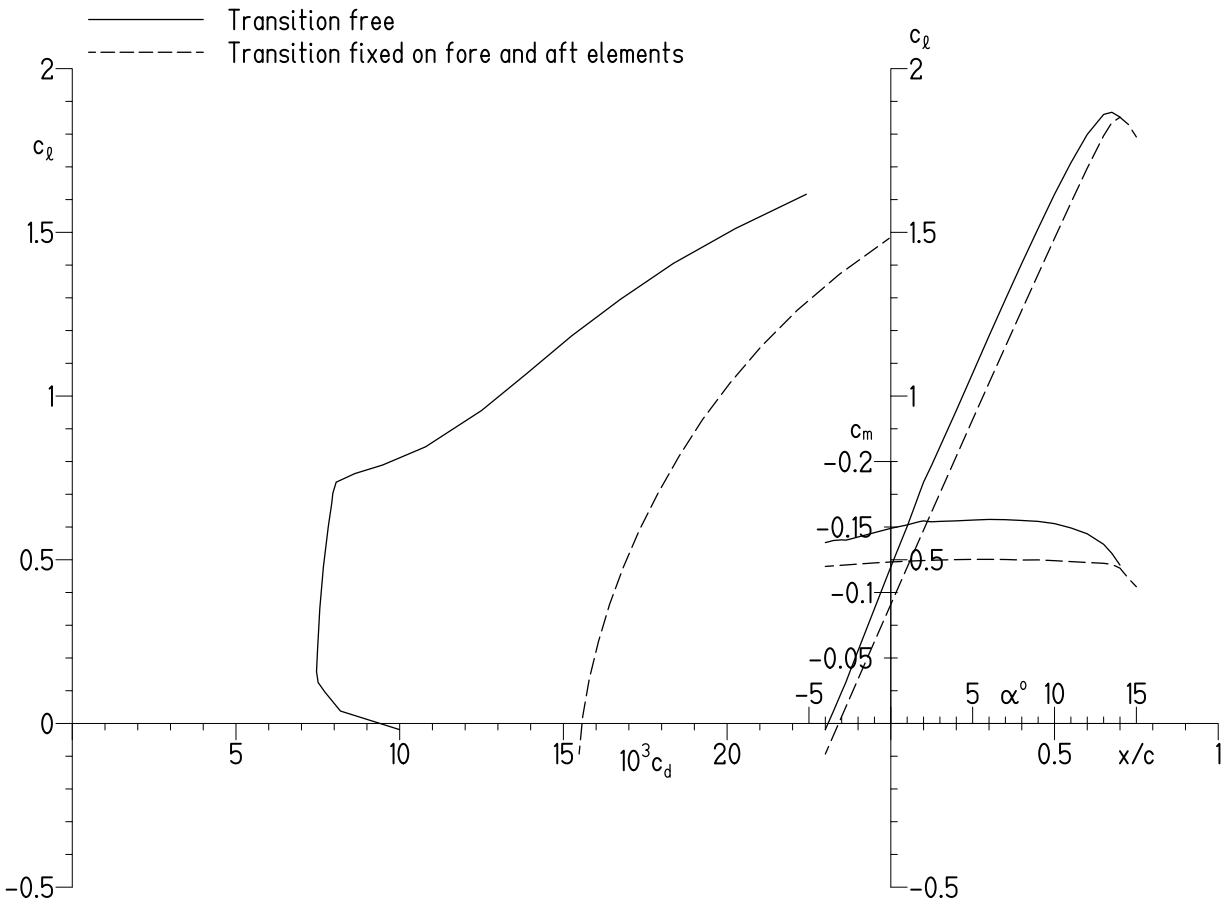

(a) $M = 0.30$ and $R = 0.97 \times 10^6$.

Figure 6.- Theoretical section characteristics of design airfoil shape.

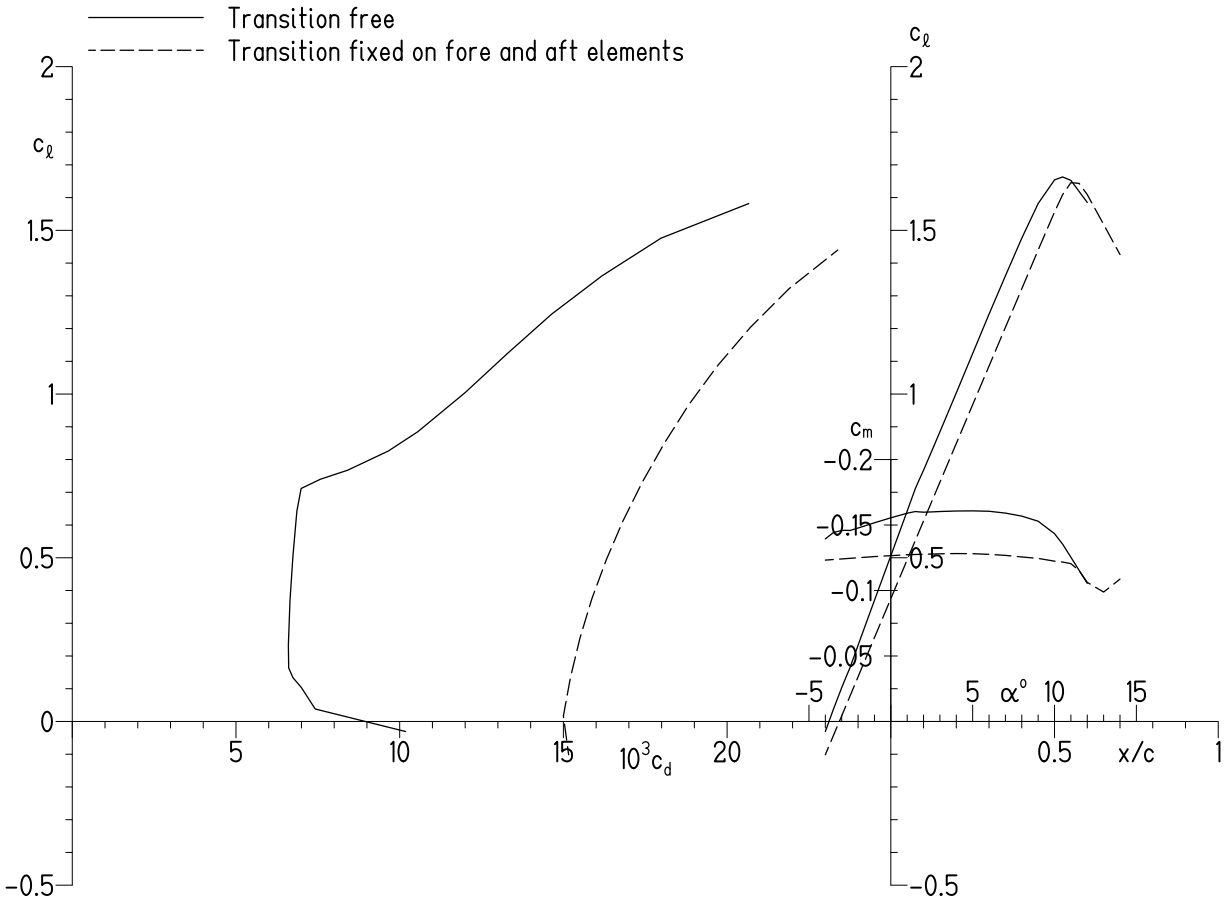

(b) M = 0.40 and R = 1.29×10^6.

Figure 6.- Continued.

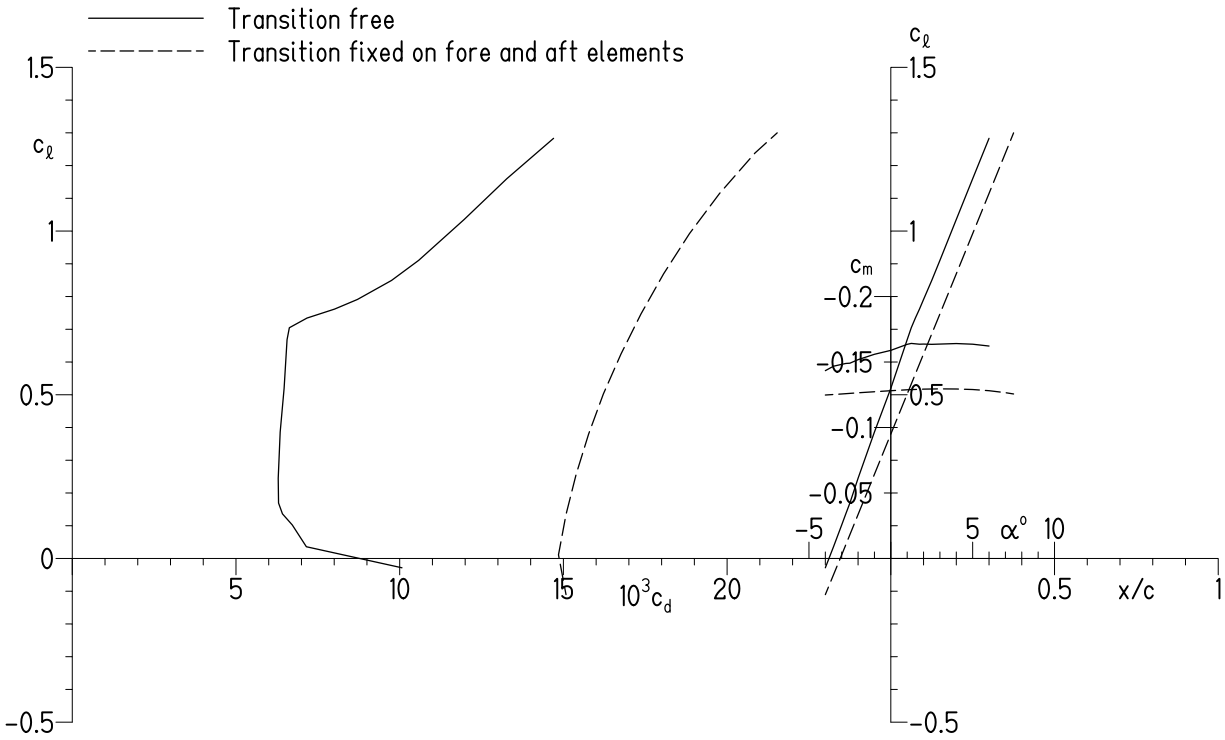

(c) $M = 0.45$ and $R = 1.45 \times 10^6$.

Figure 6.- Continued.

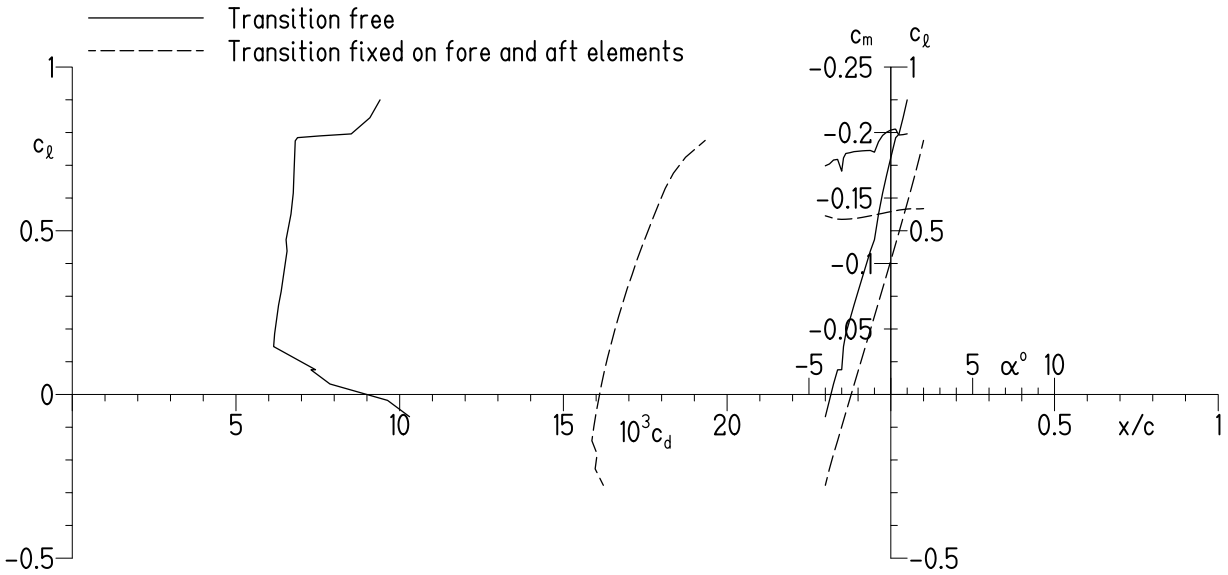

(d) $M = 0.70$ and $R = 2.26 \times 10^6$.

Figure 6.- Concluded.

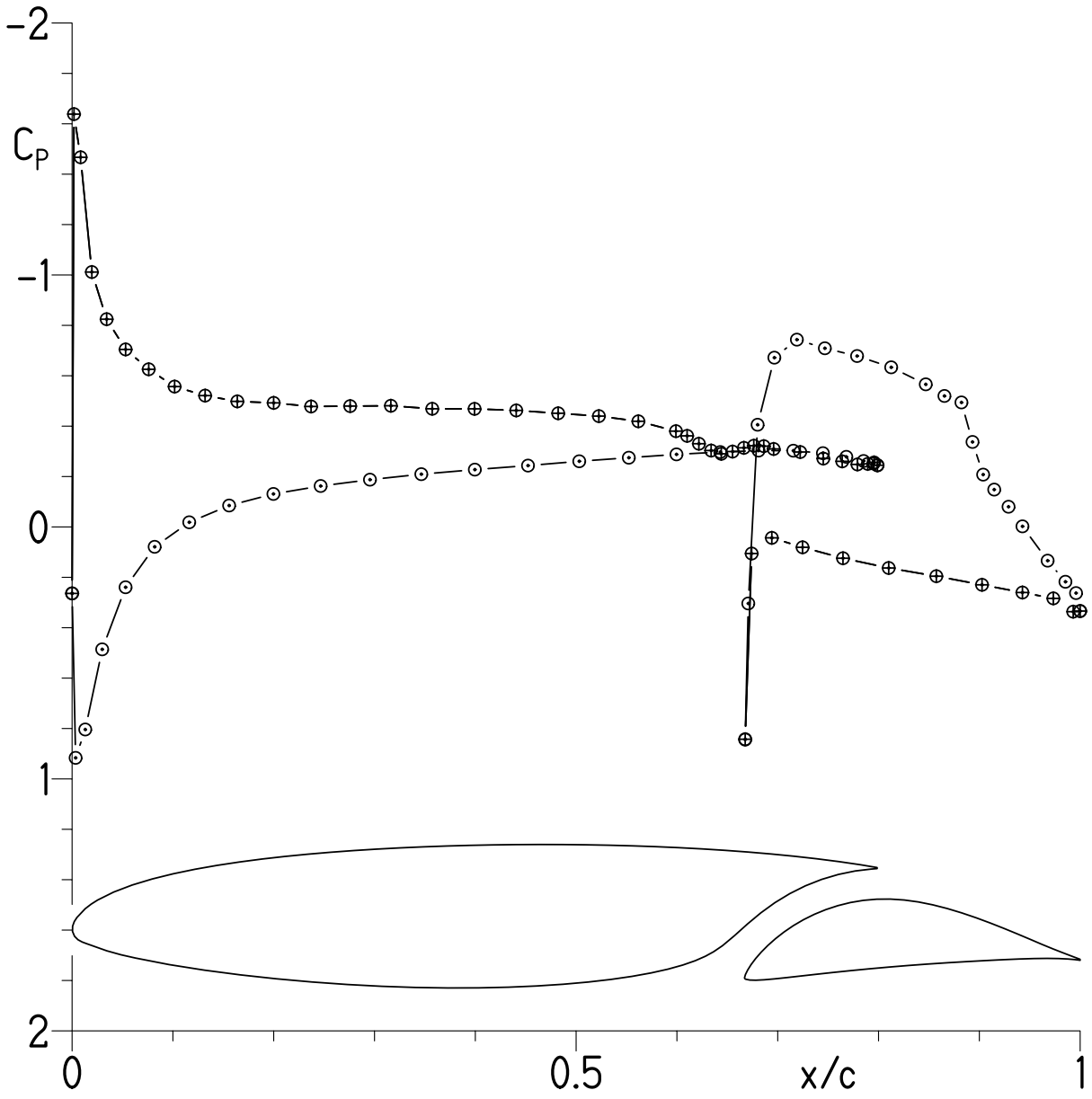

(a) $\alpha = -4.09°$; $c_l = -0.072$; $c_d = 0.01069$; $c_m = -0.1159$.

Figure 7.- Experimental pressure distributions for $R = 1.00 \times 10^6$ and $M = 0.10$ with transition free. Open symbols represent data for upper surface; crossed symbols, data for lower surface.

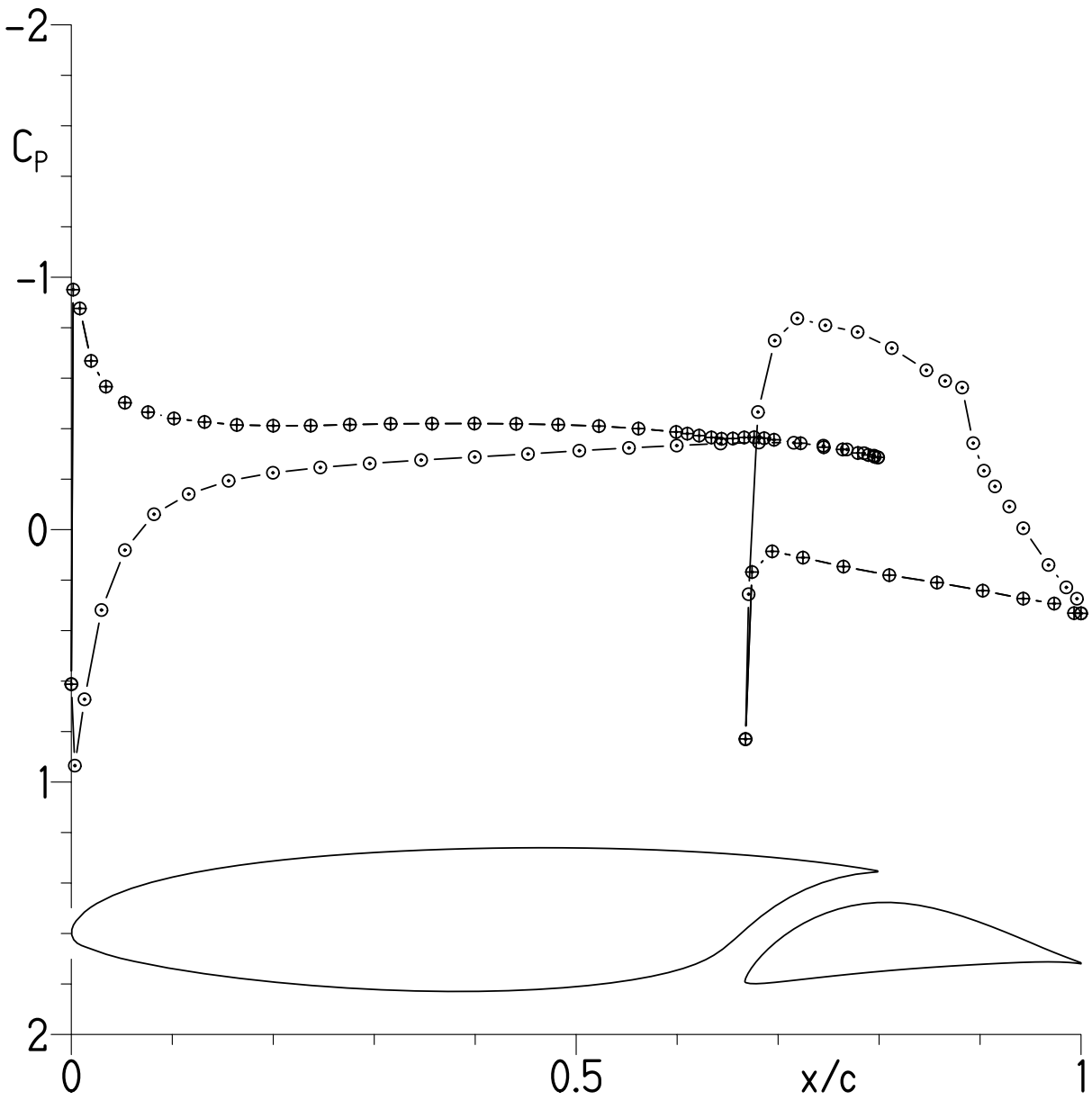

(b) $\alpha = -3.07°$; $c_l = 0.056$; $c_d = 0.00618$; $c_m = -0.1221$.

Figure 7.- Continued.

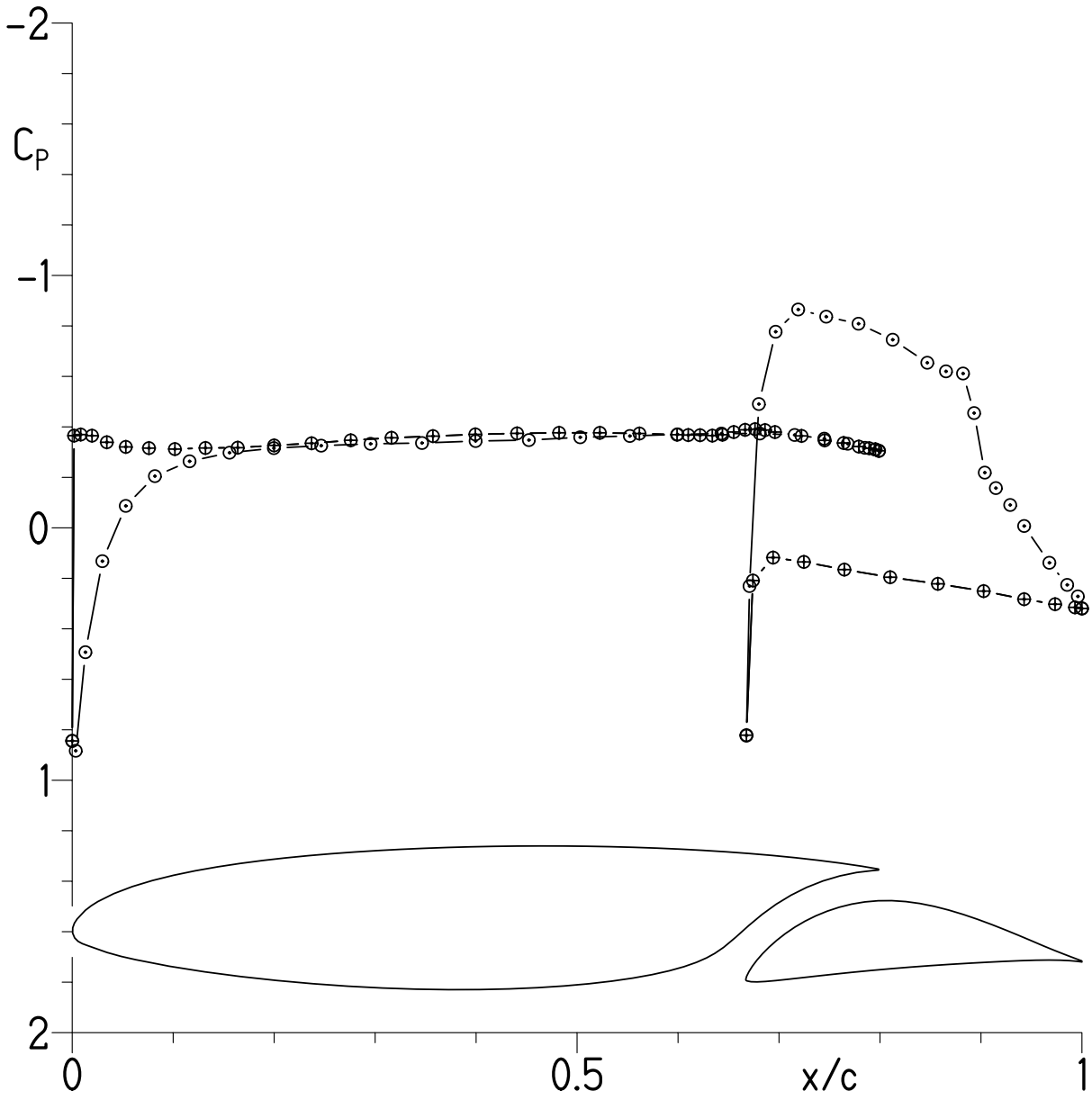

(c) $\alpha = -2.06°$; $c_l = 0.175$; $c_d = 0.00669$; $c_m = -0.1240$.

Figure 7.- Continued.

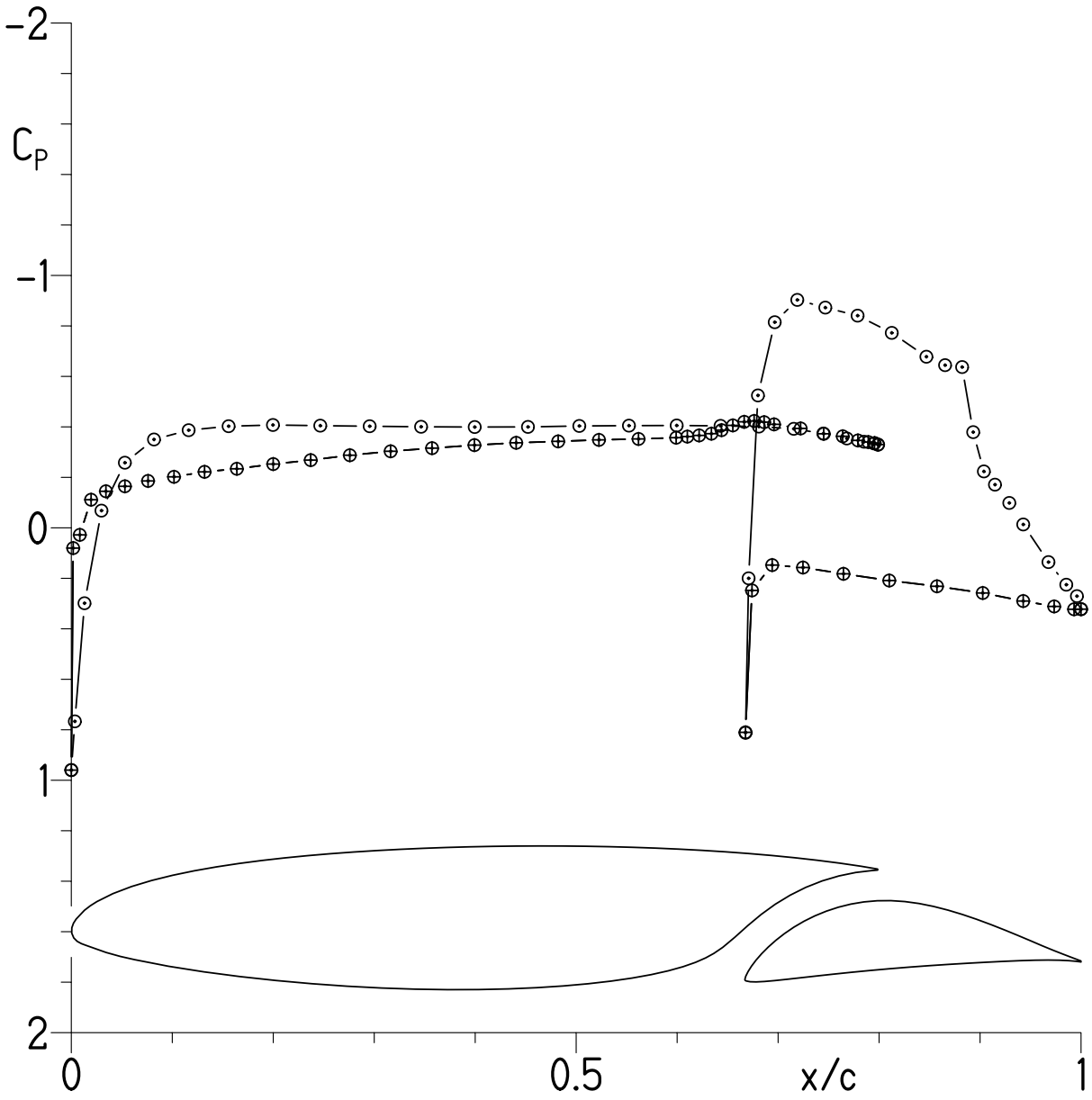

(d) $\alpha = -1.04°$; $c_l = 0.284$; $c_d = 0.00655$; $c_m = -0.1250$.

Figure 7.- Continued.

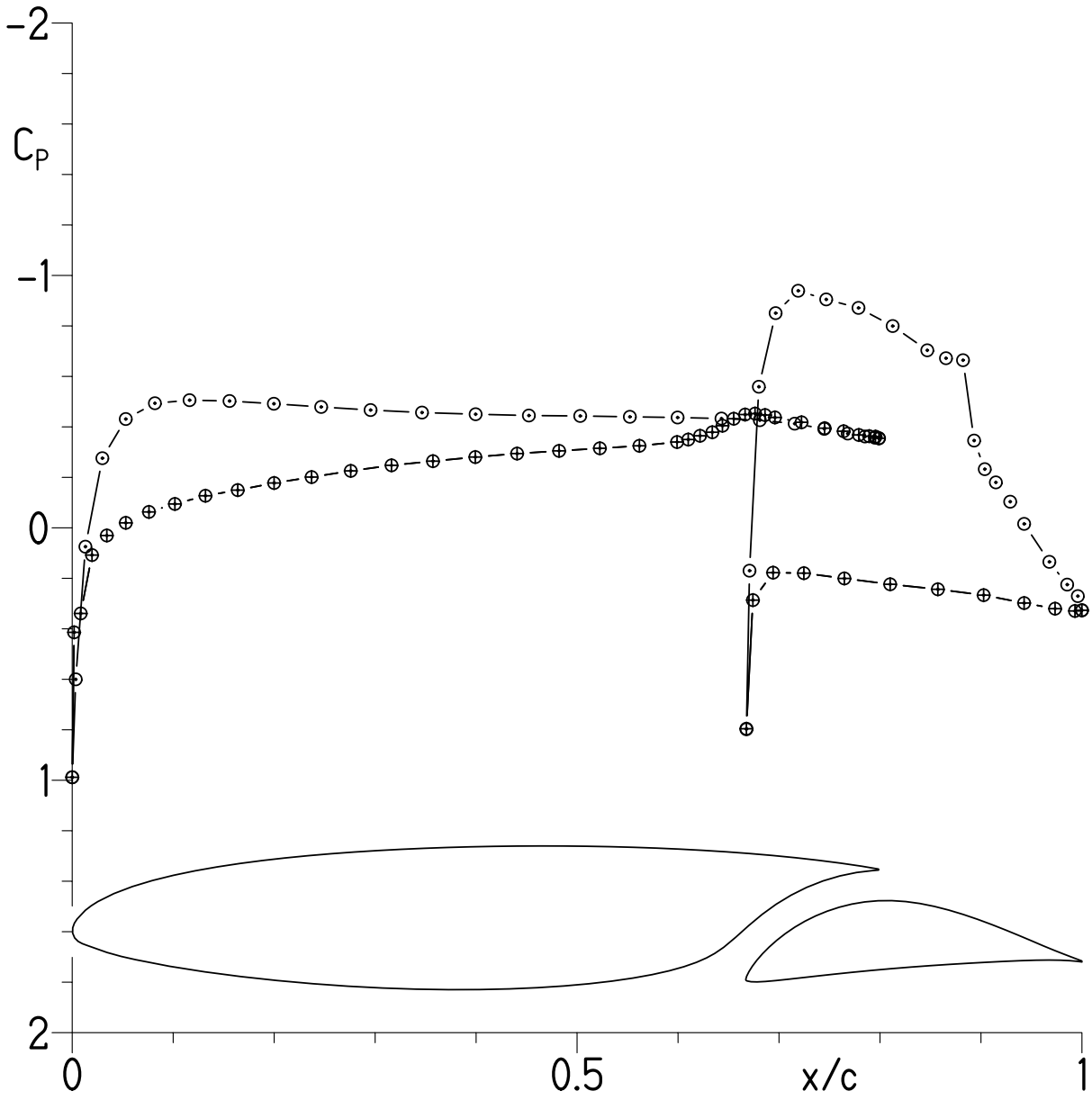

(e) $\alpha = -0.02°$; $c_l = 0.390$; $c_d = 0.00675$; $c_m = -0.1268$.

Figure 7.- Continued.

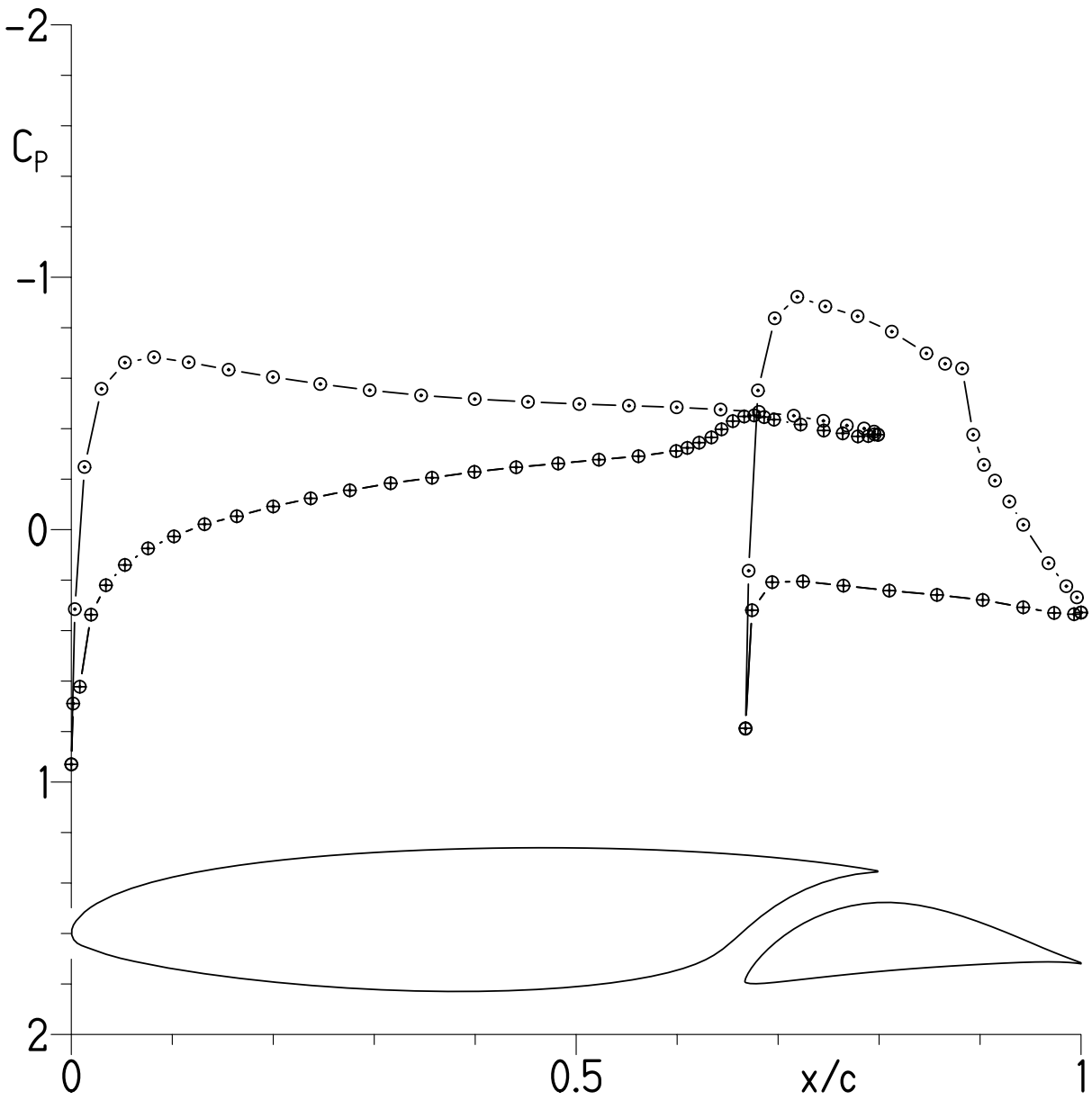

(f) $\alpha = 1.00°$; $c_l = 0.519$; $c_d = 0.00703$; $c_m = -0.1282$.

Figure 7.- Continued.

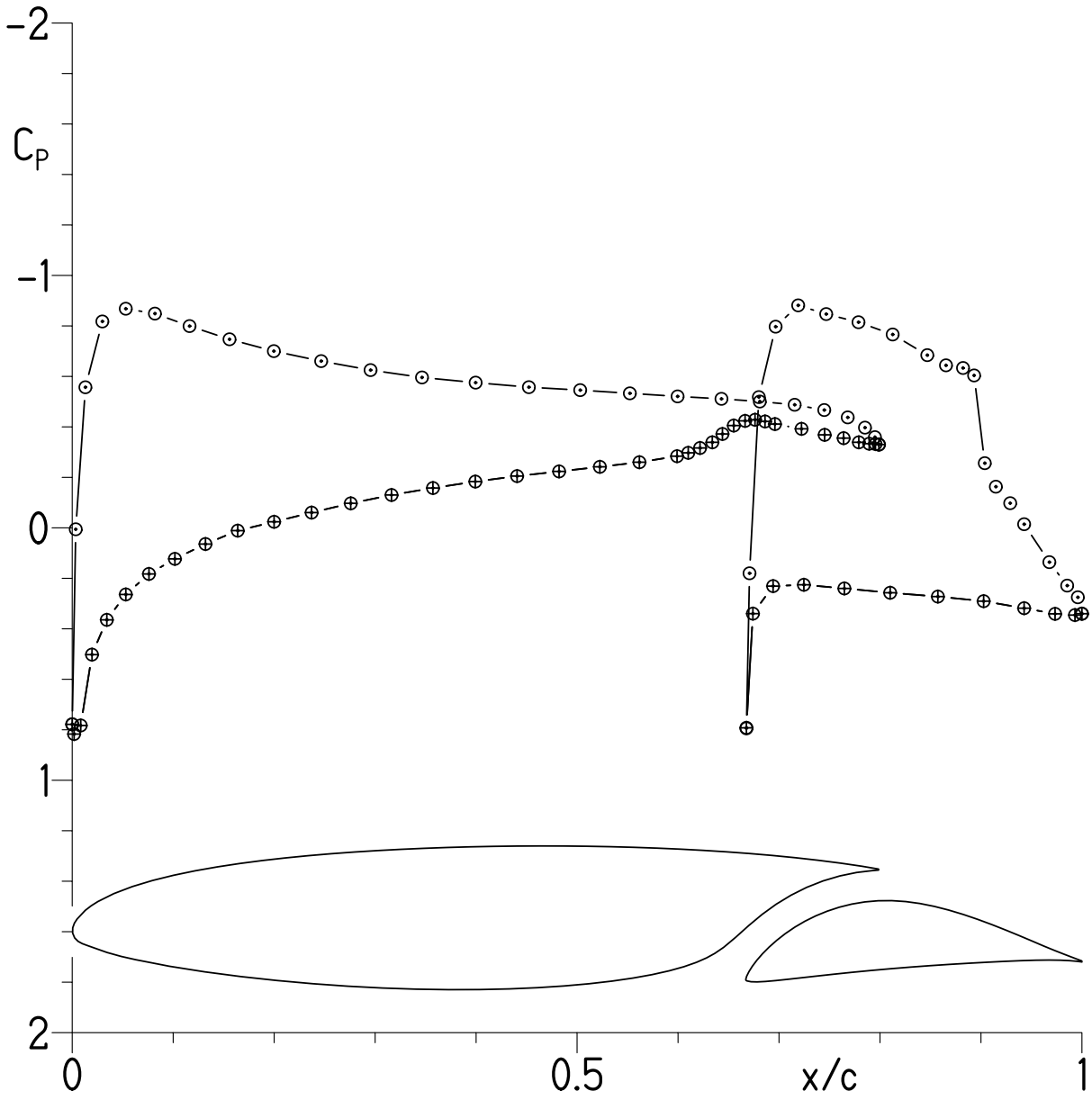

(g) $\alpha = 2.02°$; $c_l = 0.628$; $c_d = 0.00741$; $c_m = -0.1308$.

Figure 7.- Continued.

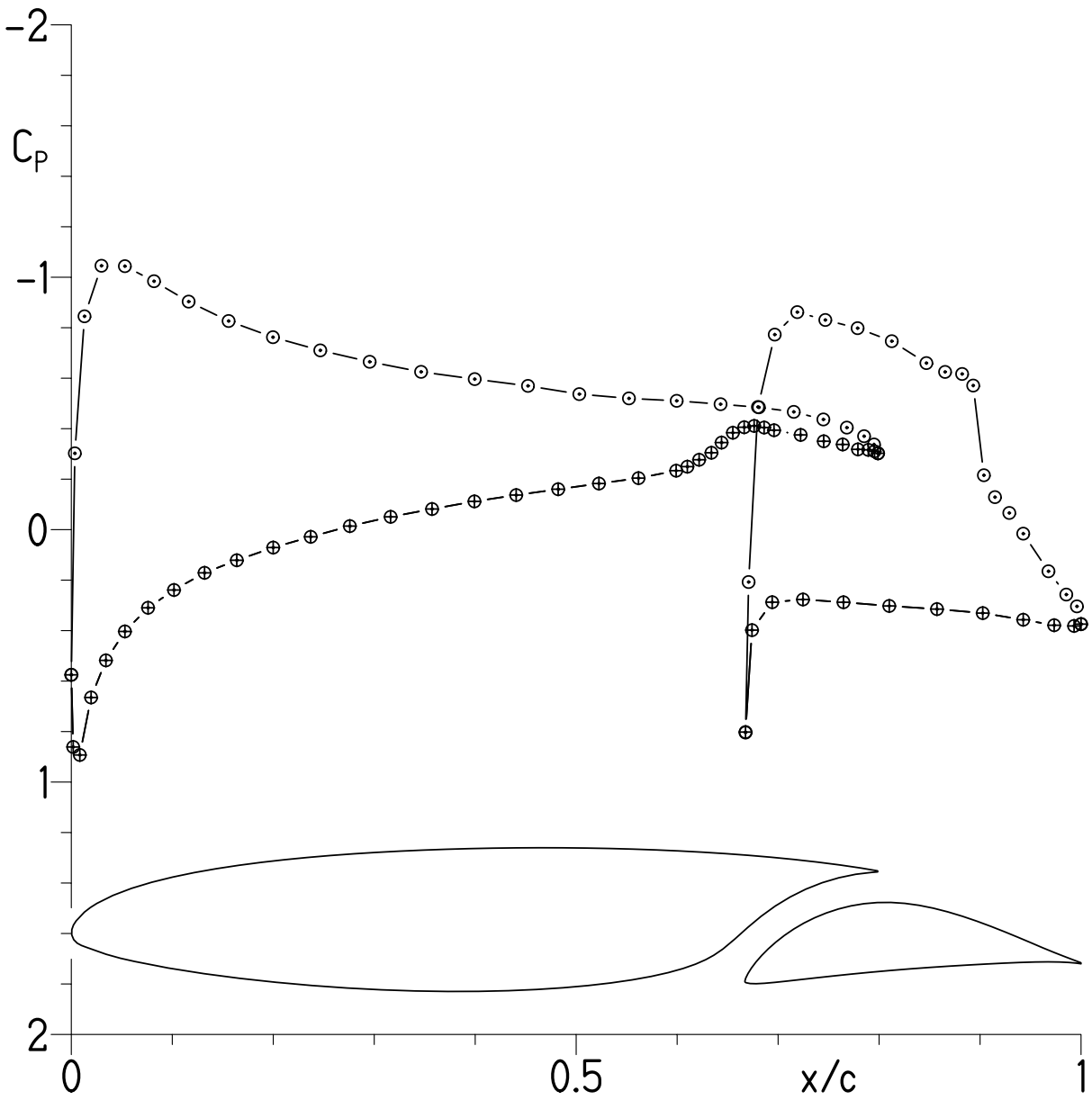

(h) $\alpha = 3.04°$; $c_l = 0.723$; $c_d = 0.01007$; $c_m = –0.1301$.

Figure 7.- Continued.

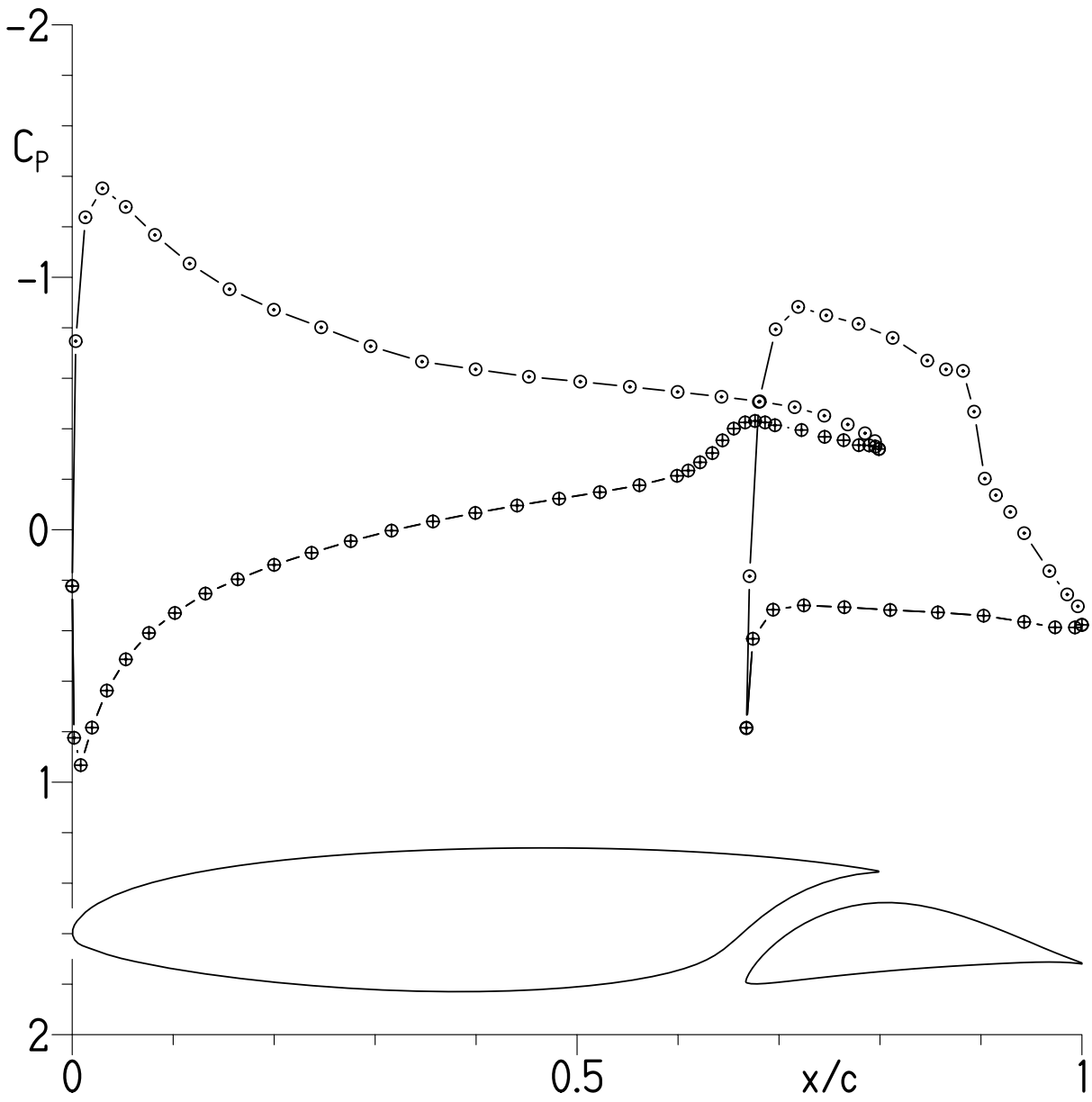

(i) $\alpha = 4.05°$; $c_l = 0.829$; $c_d = 0.01176$; $c_m = -0.1300$.

Figure 7.- Continued.

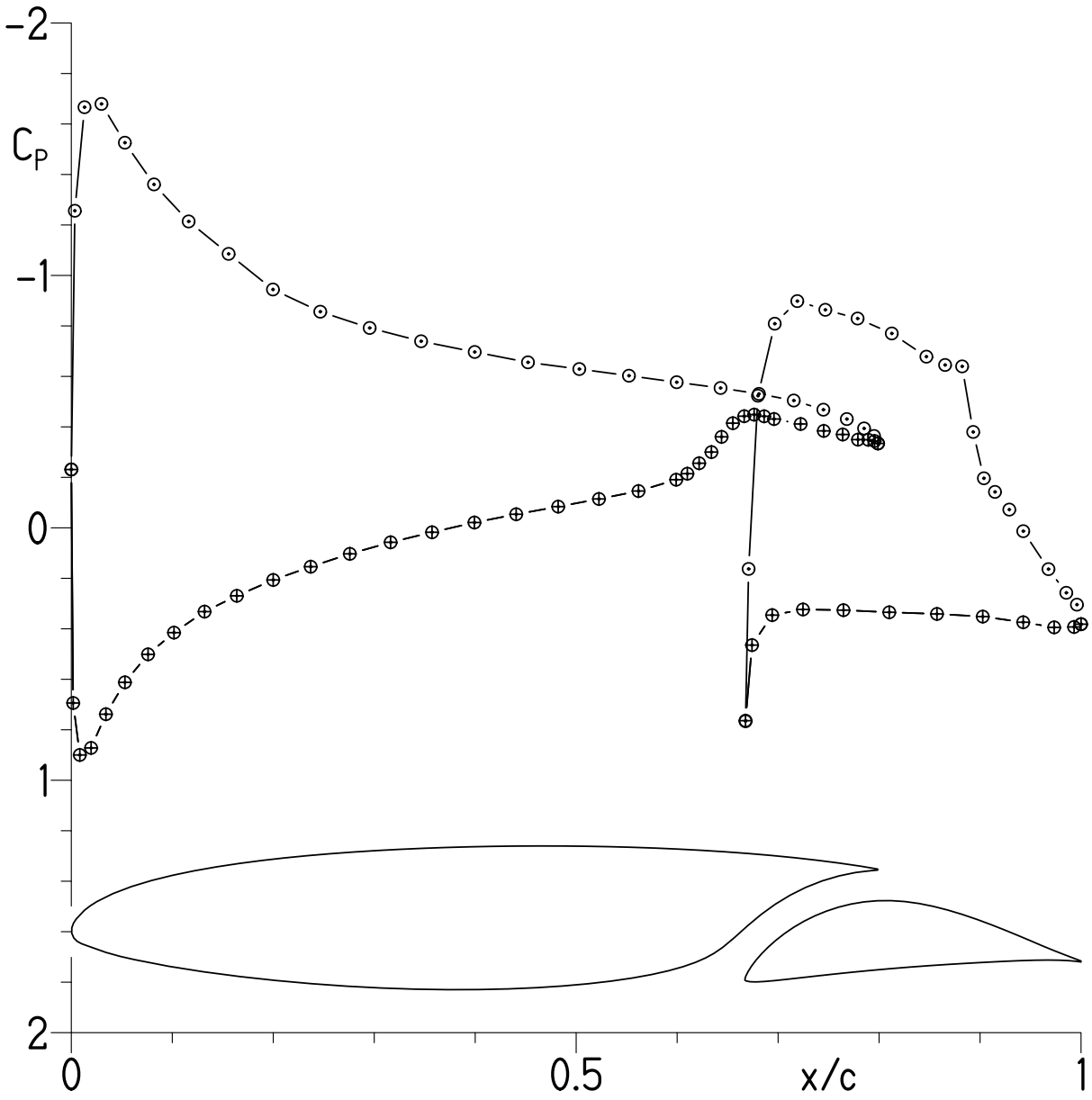

(j) $\alpha = 5.07°$; $c_l = 0.934$; $c_d = 0.01307$; $c_m = -0.1304$.

Figure 7.- Continued.

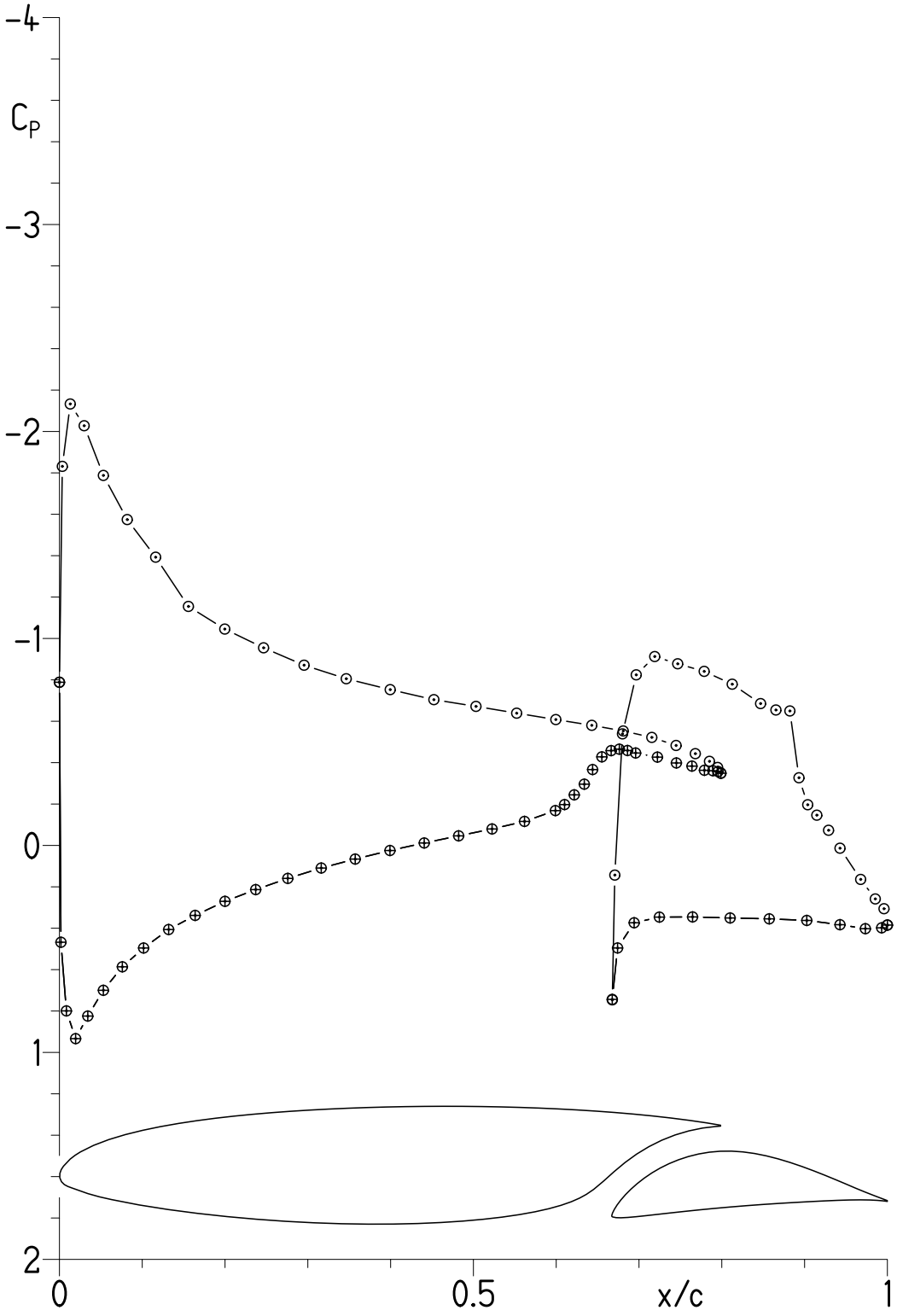

(k) $\alpha = 6.09°$; $c_l = 1.041$; $c_d = 0.01449$; $c_m = -0.1309$.

Figure 7.- Continued.

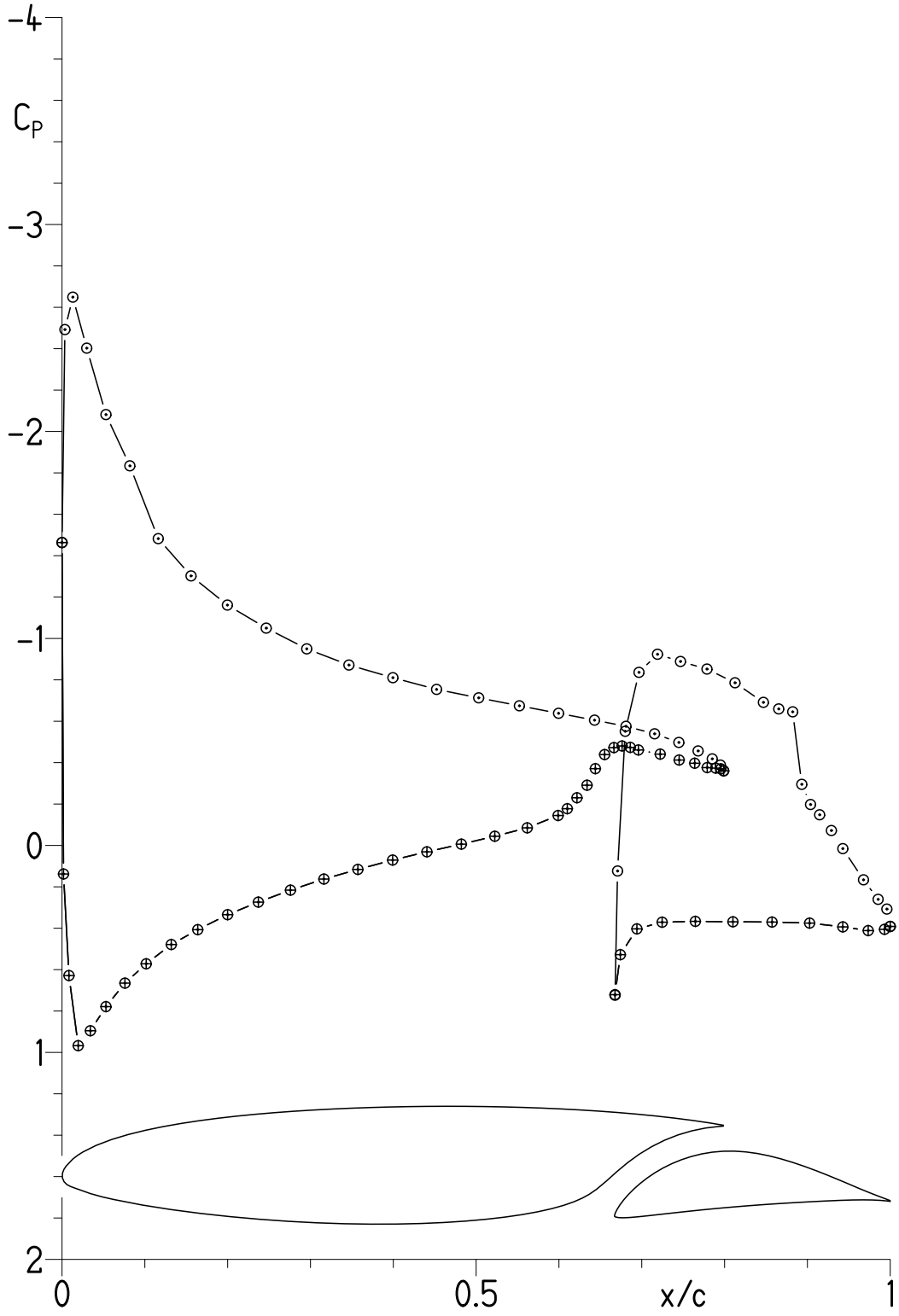

(l) $\alpha = 7.11°$; $c_l = 1.151$; $c_d = 0.01566$; $c_m = -0.1314$.

Figure 7.- Continued.

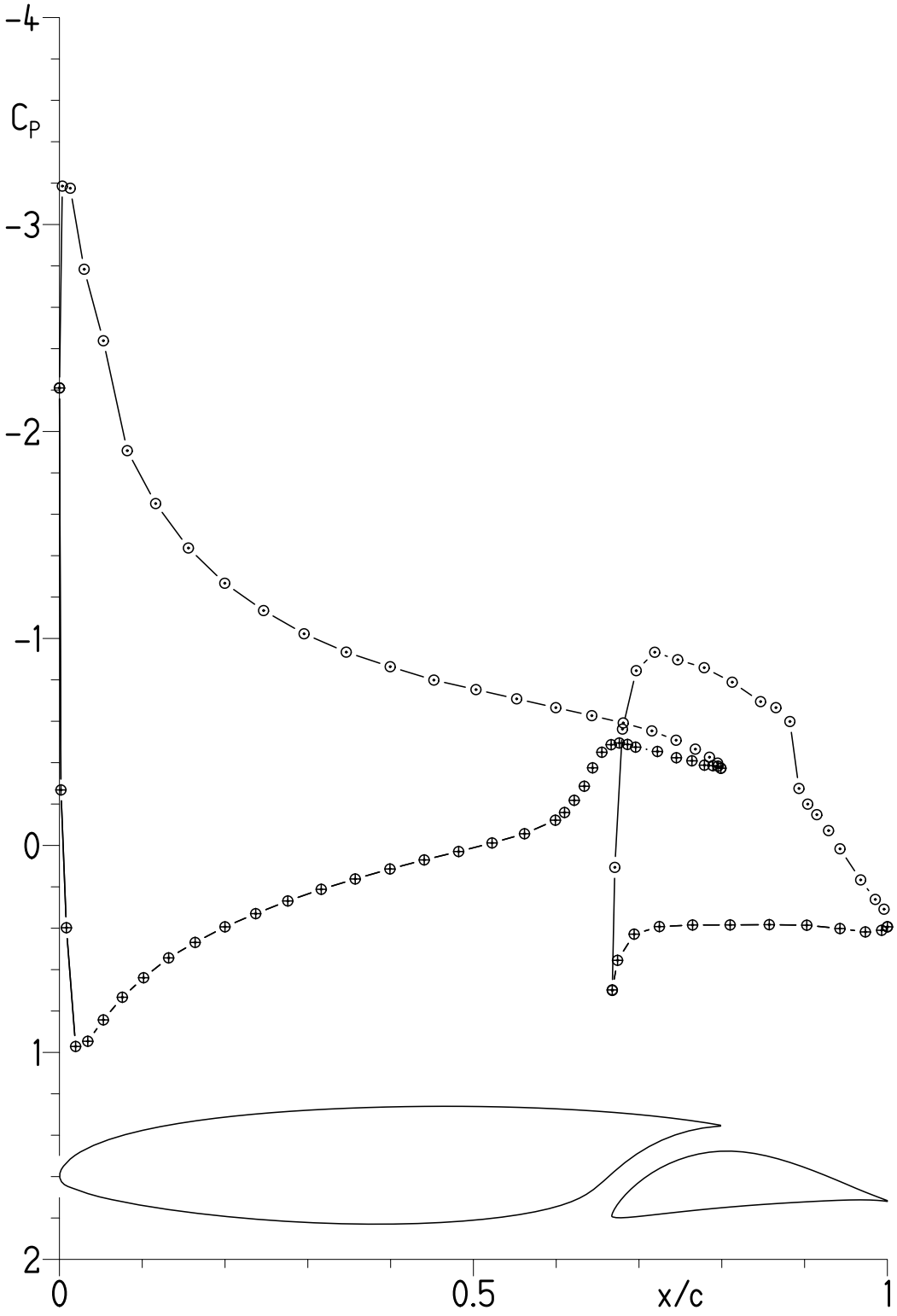

(m) $\alpha = 8.13°$; $c_l = 1.251$; $c_d = 0.01718$; $c_m = -0.1310$.

Figure 7.- Continued.

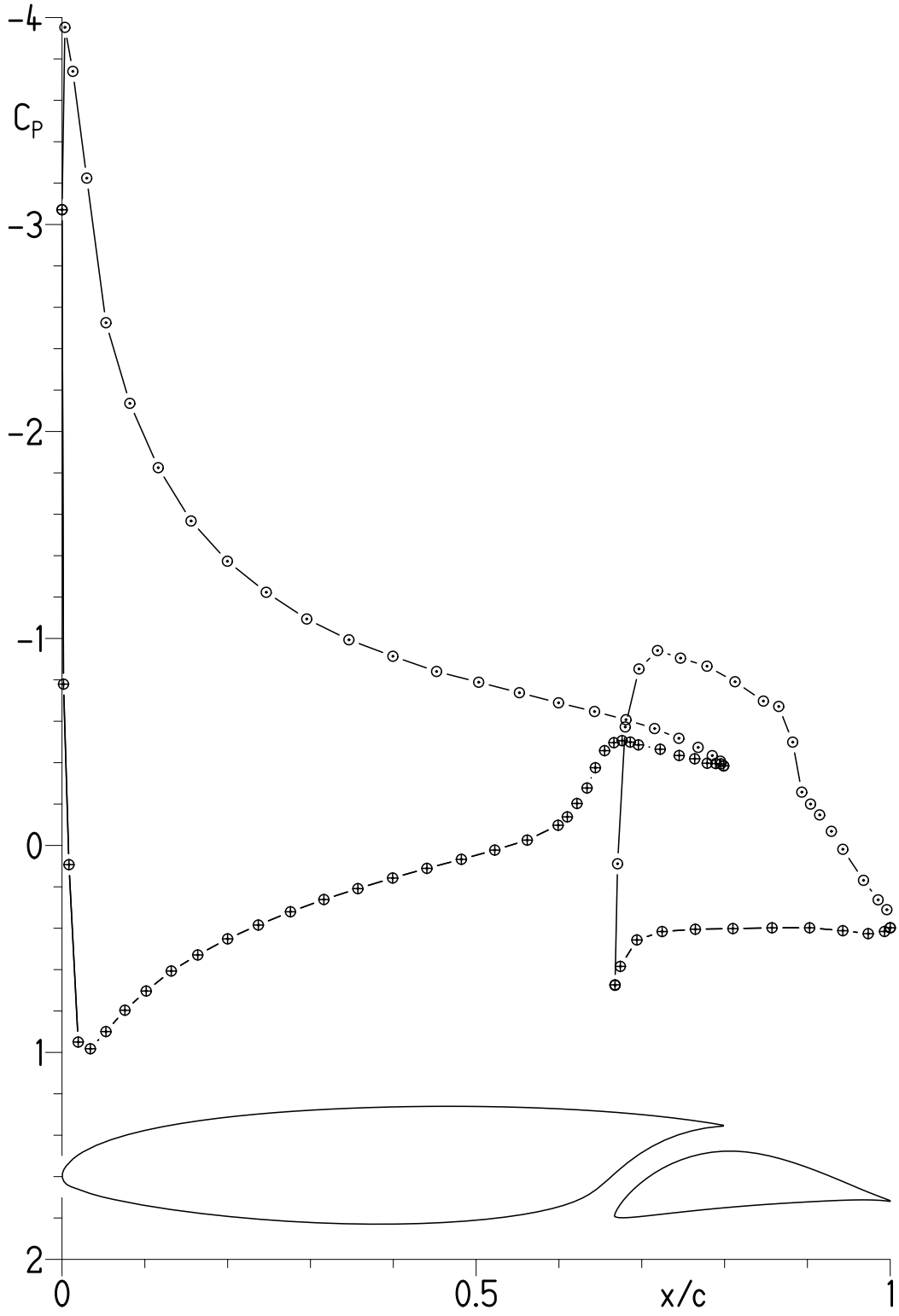

(n) $\alpha = 9.14°$; $c_l = 1.349$; $c_d = 0.01878$; $c_m = -0.1309$.

Figure 7.- Continued.

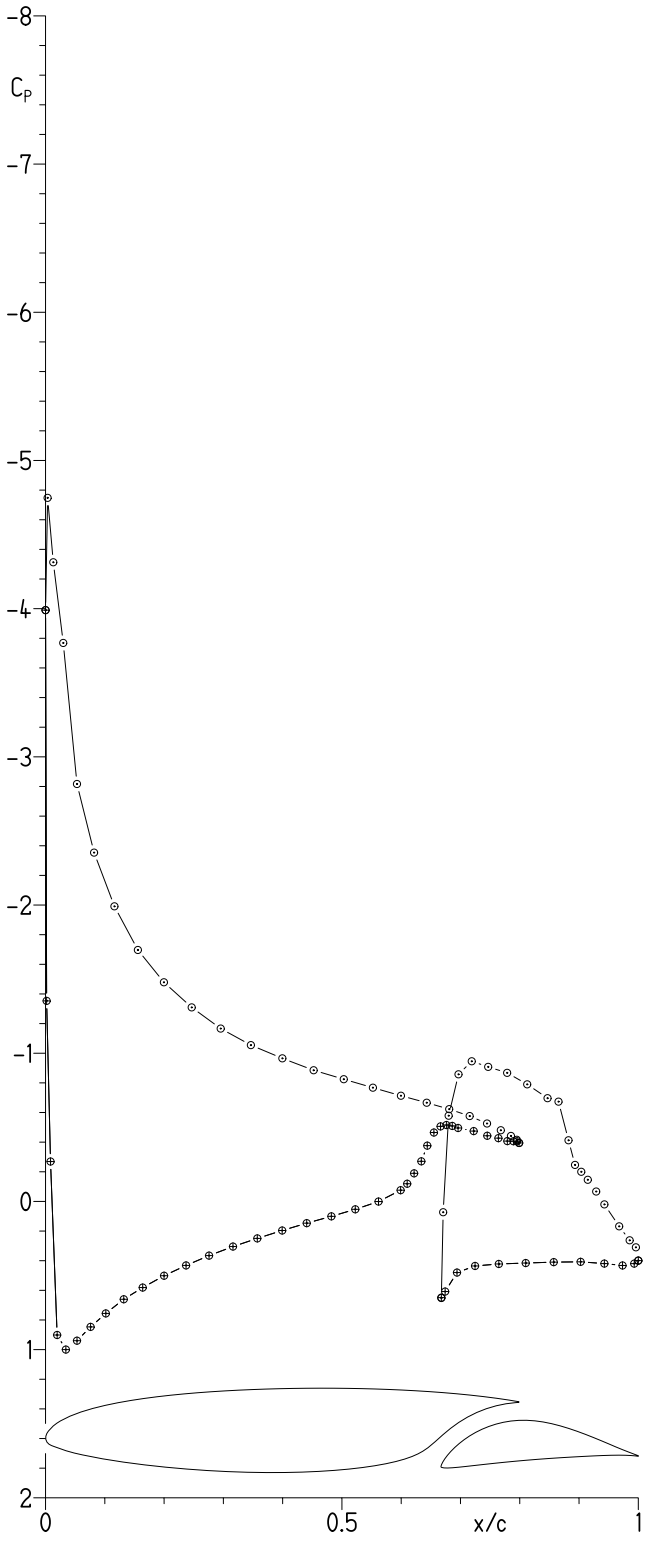

(o) $\alpha = 10.16°$; $c_l = 1.448$; $c_d = 0.02059$; $c_m = -0.1291$.

Figure 7.- Continued.

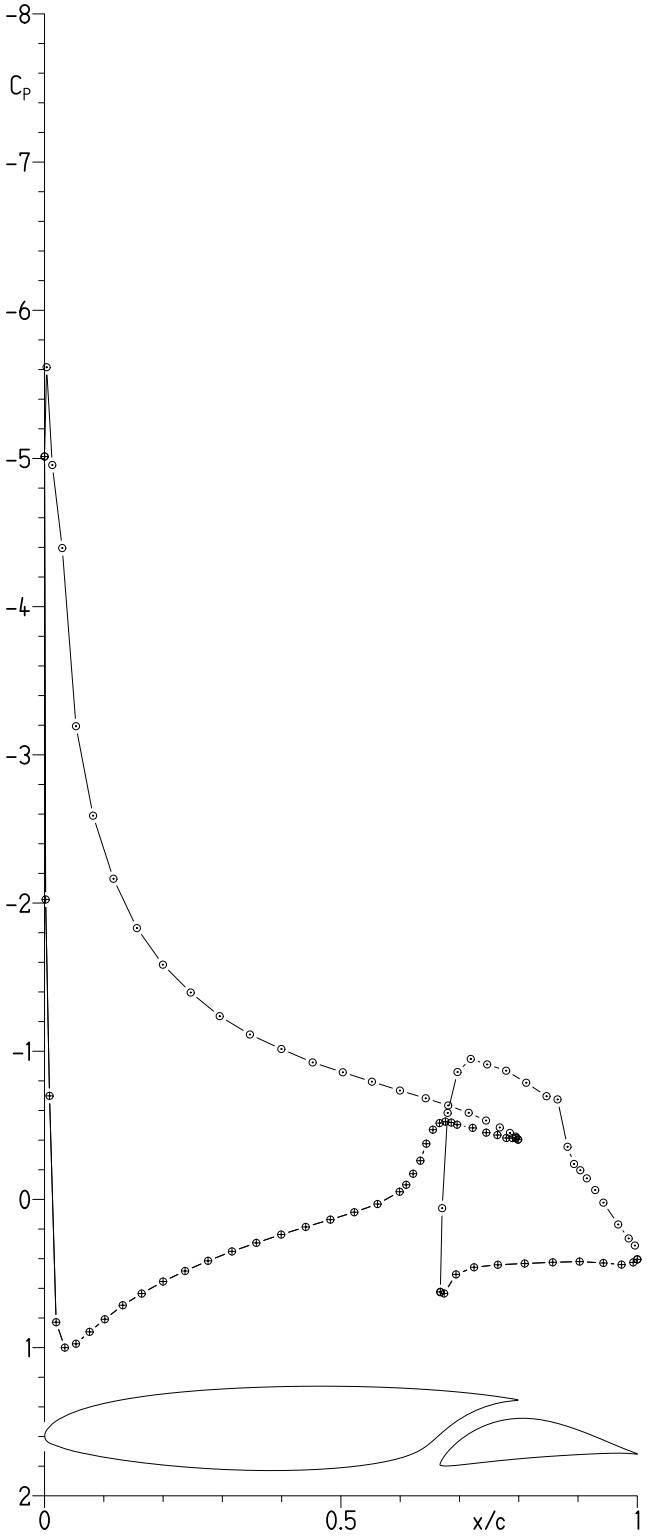

(p) $\alpha = 11.18°$; $c_l = 1.553$; $c_d = 0.02255$; $c_m = –0.1270$.

Figure 7.- Continued.

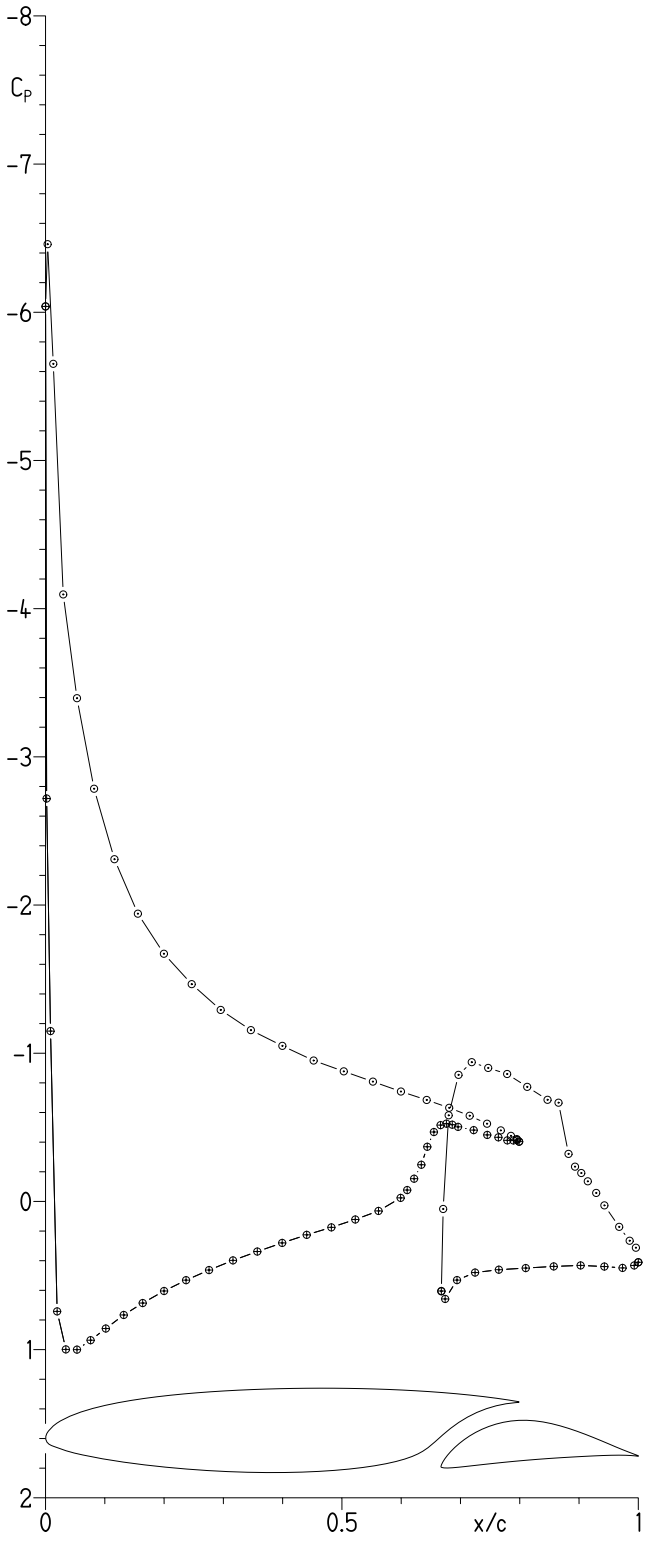

(q) $\alpha = 12.19°$; $c_l = 1.624$; $c_d = 0.02537$; $c_m = –0.1279$.

Figure 7.- Continued.

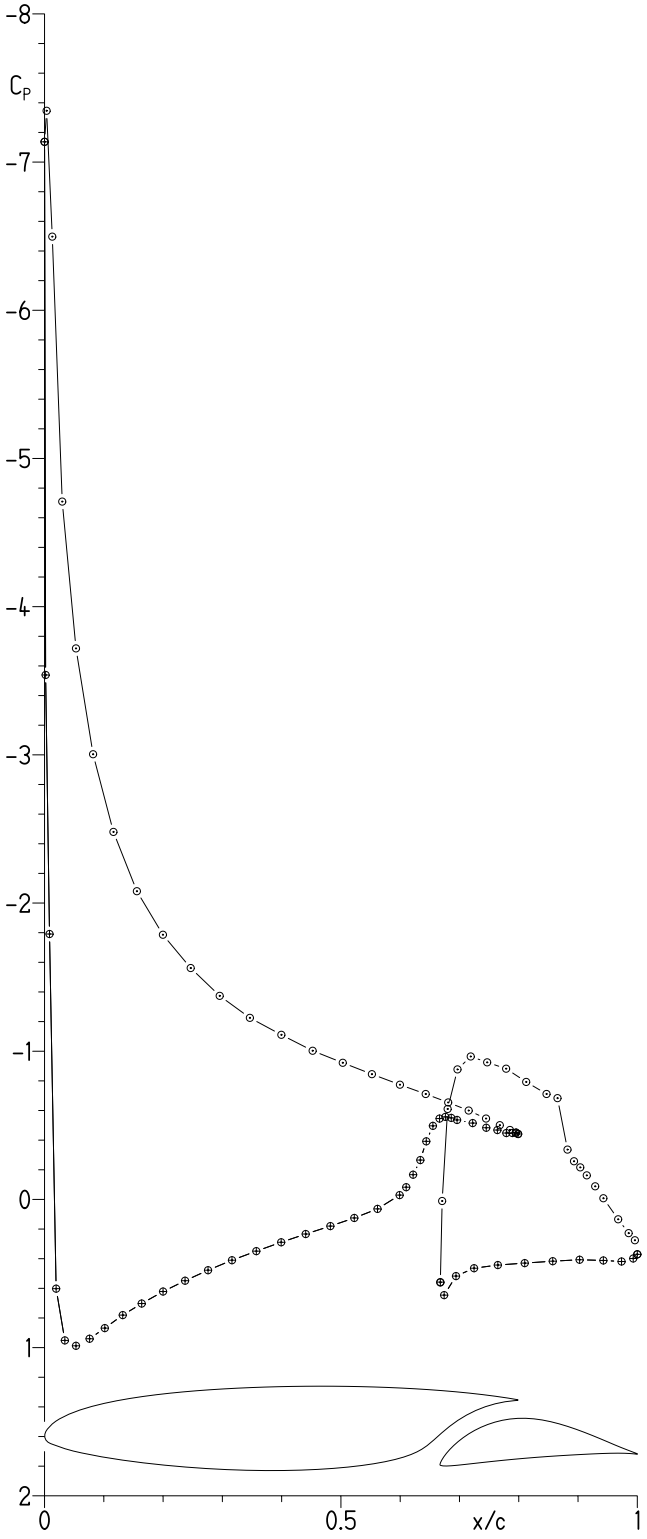

(r) $\alpha = 13.21°$; $c_l = 1.706$; $c_d = 0.02823$; $c_m = -0.1238$.

Figure 7.- Continued.

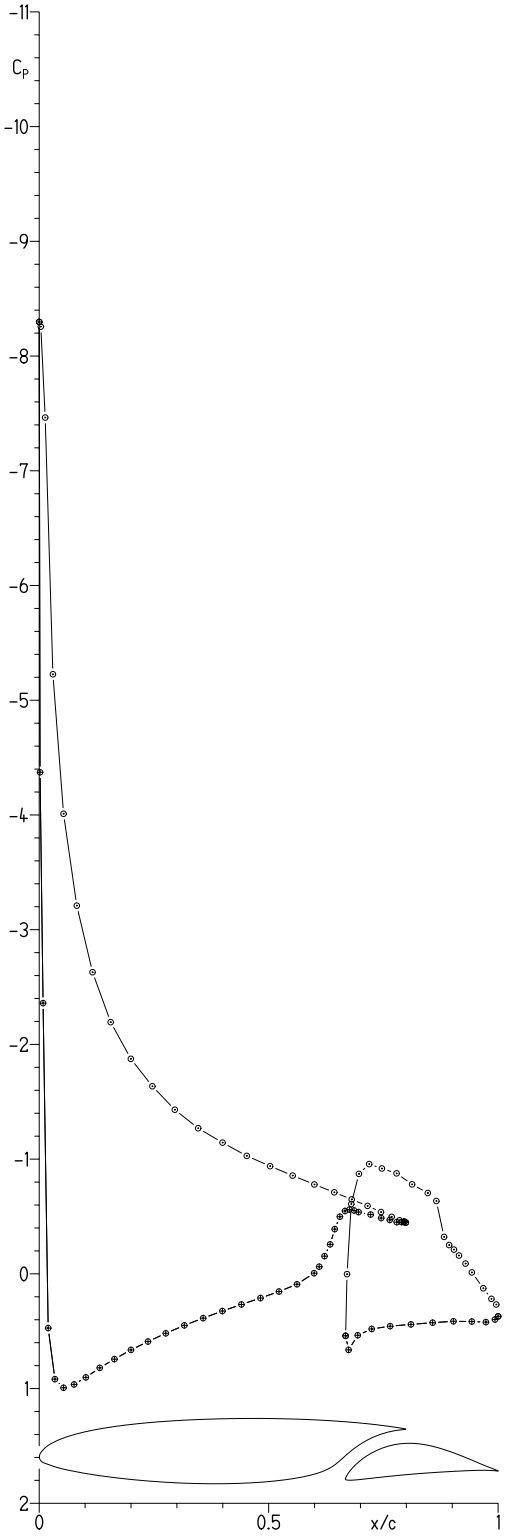

(s) $\alpha = 14.23°$; $c_l = 1.790$; $c_d = 0.03249$; $c_m = -0.1196$.

Figure 7.- Continued.

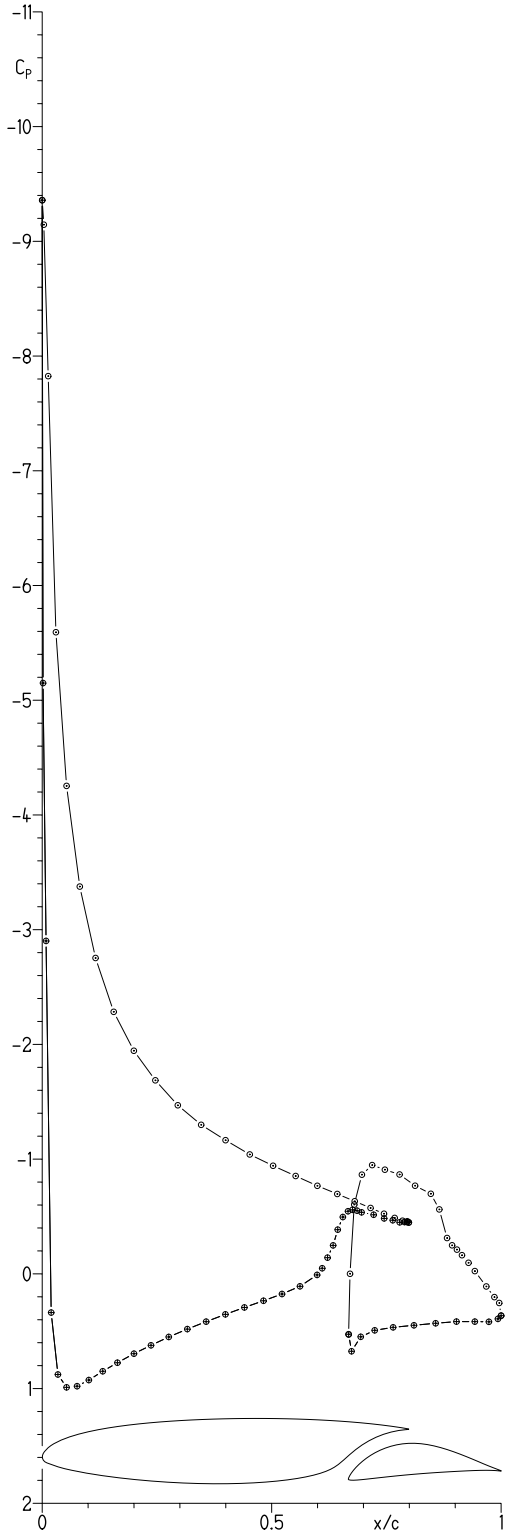

(t) $\alpha = 15.24°$; $c_l = 1.846$; $c_d = 0.03823$; $c_m = -0.1160$.

Figure 7.- Continued.

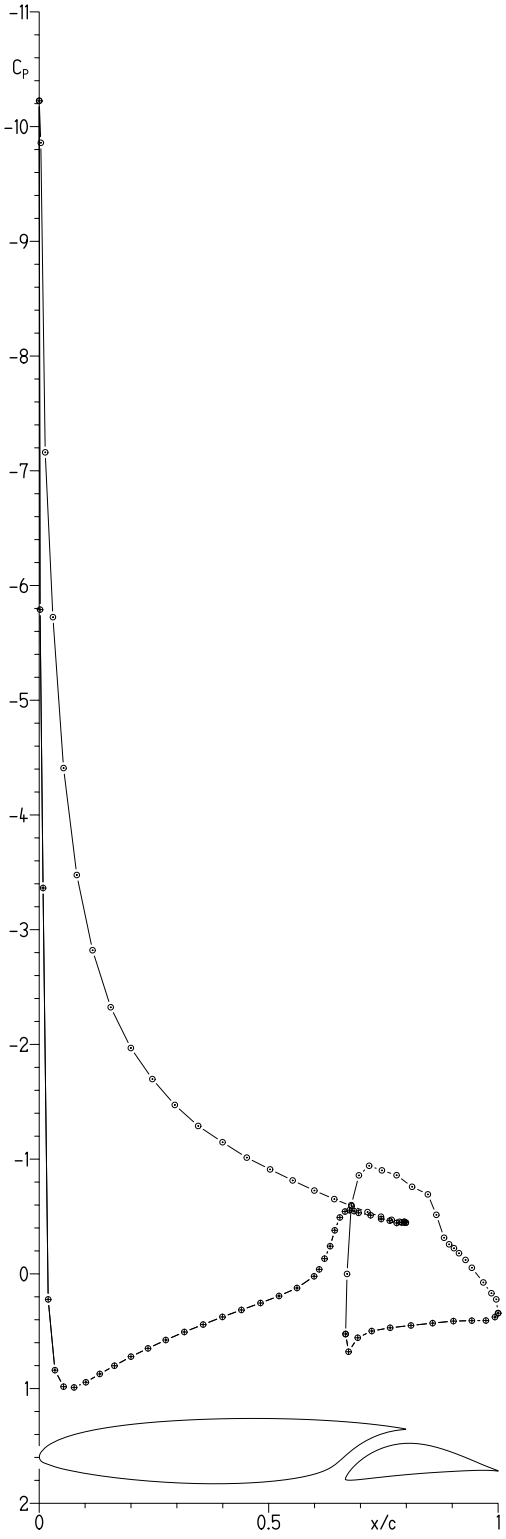

(u) $\alpha = 16.24°$; $c_l = 1.855$; $c_d = 0.04830$; $c_m = -0.1143$.

Figure 7.- Continued.

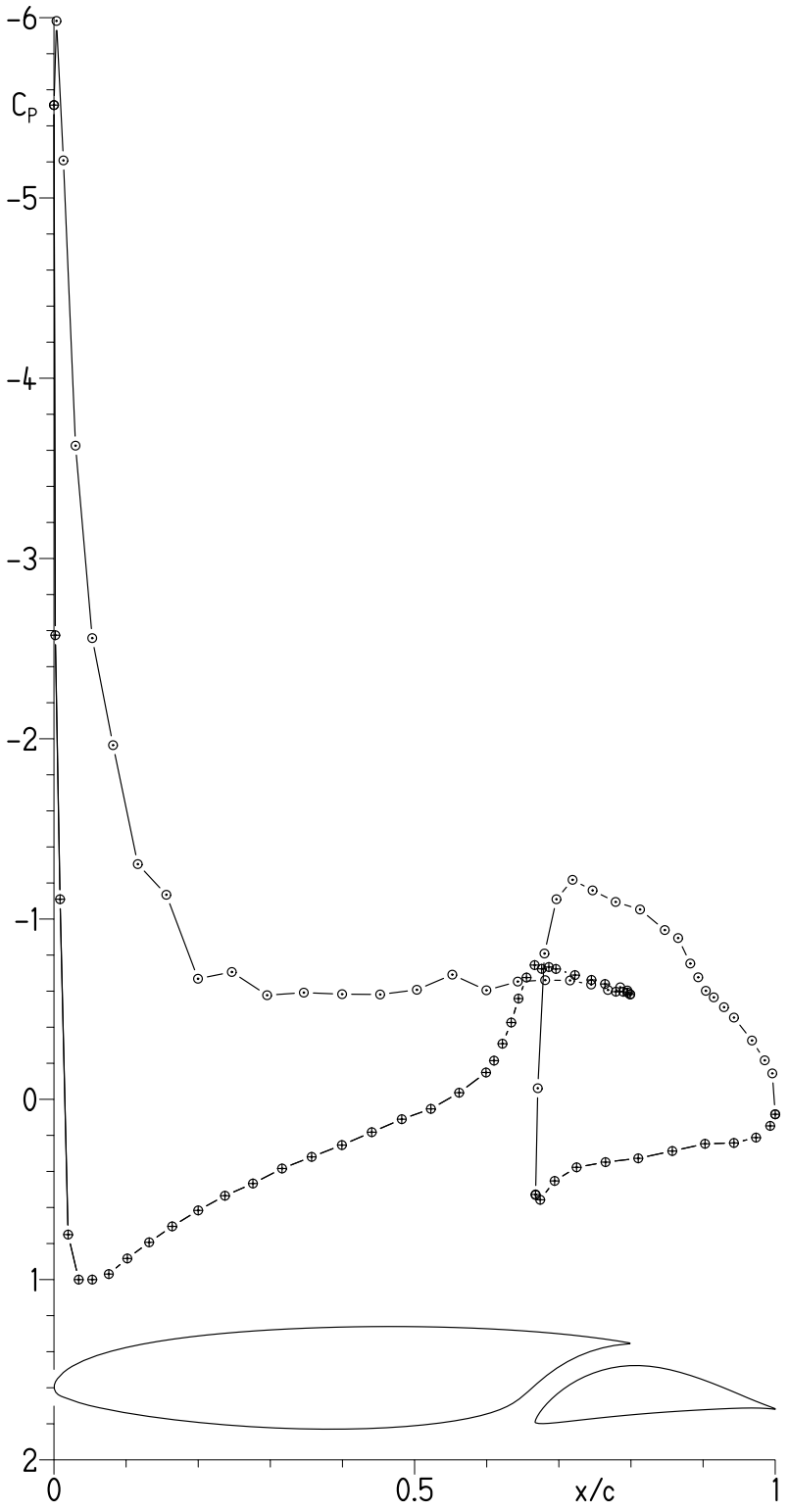

(v) $\alpha = 17.12°$; $c_l = 1.300$; $c_d = 0.08307$; $c_m = –0.1532$.

Figure 7.- Continued.

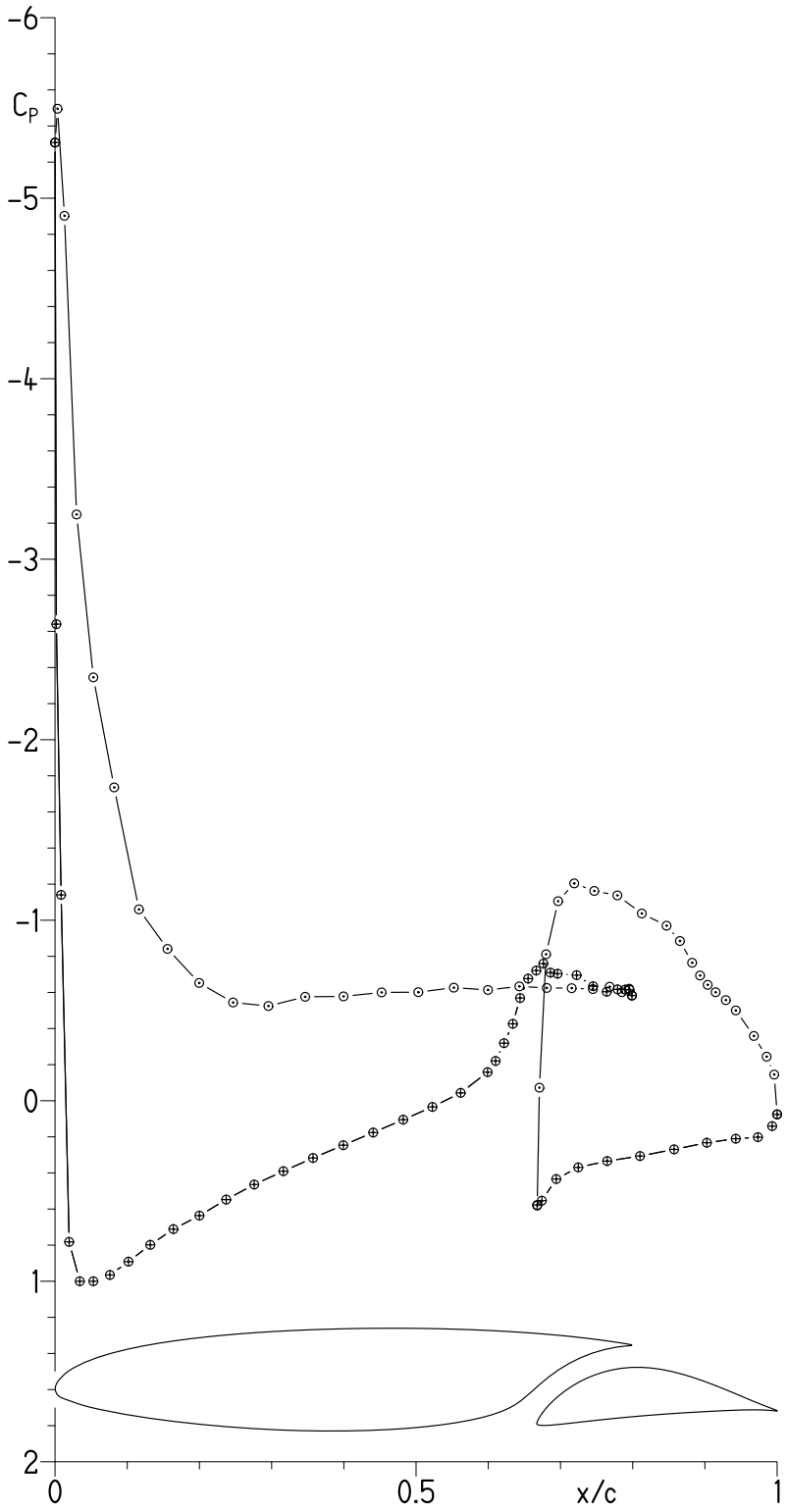

(w) $\alpha = 18.11°$; $c_l = 1.228$; $c_d = 0.11394$; $c_m = -0.1593$.

Figure 7.- Continued.

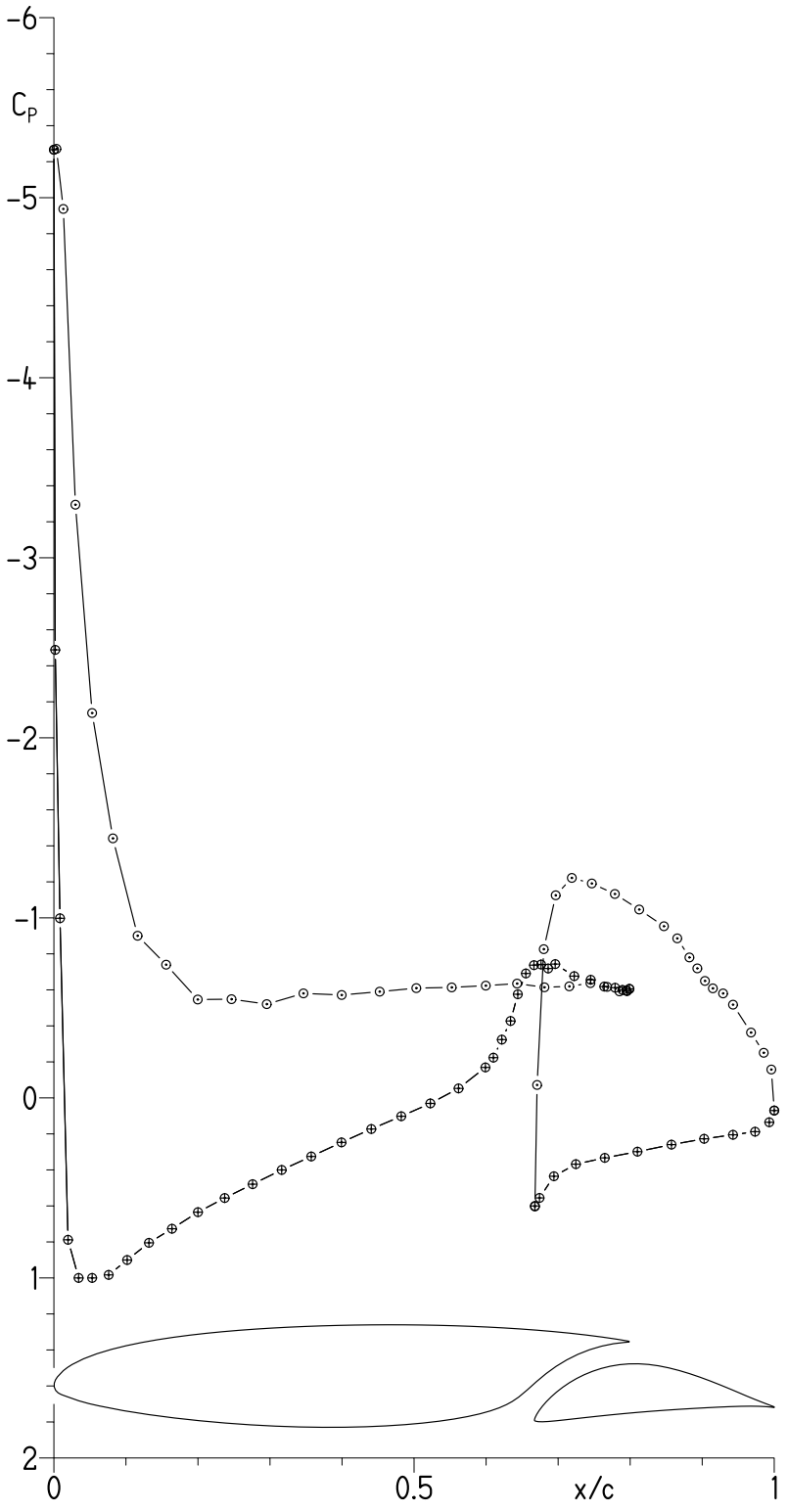

(x) $\alpha = 19.10°$; $c_l = 1.198$; $c_d = 0.13976$; $c_m = -0.1627$.

Figure 7.- Concluded.

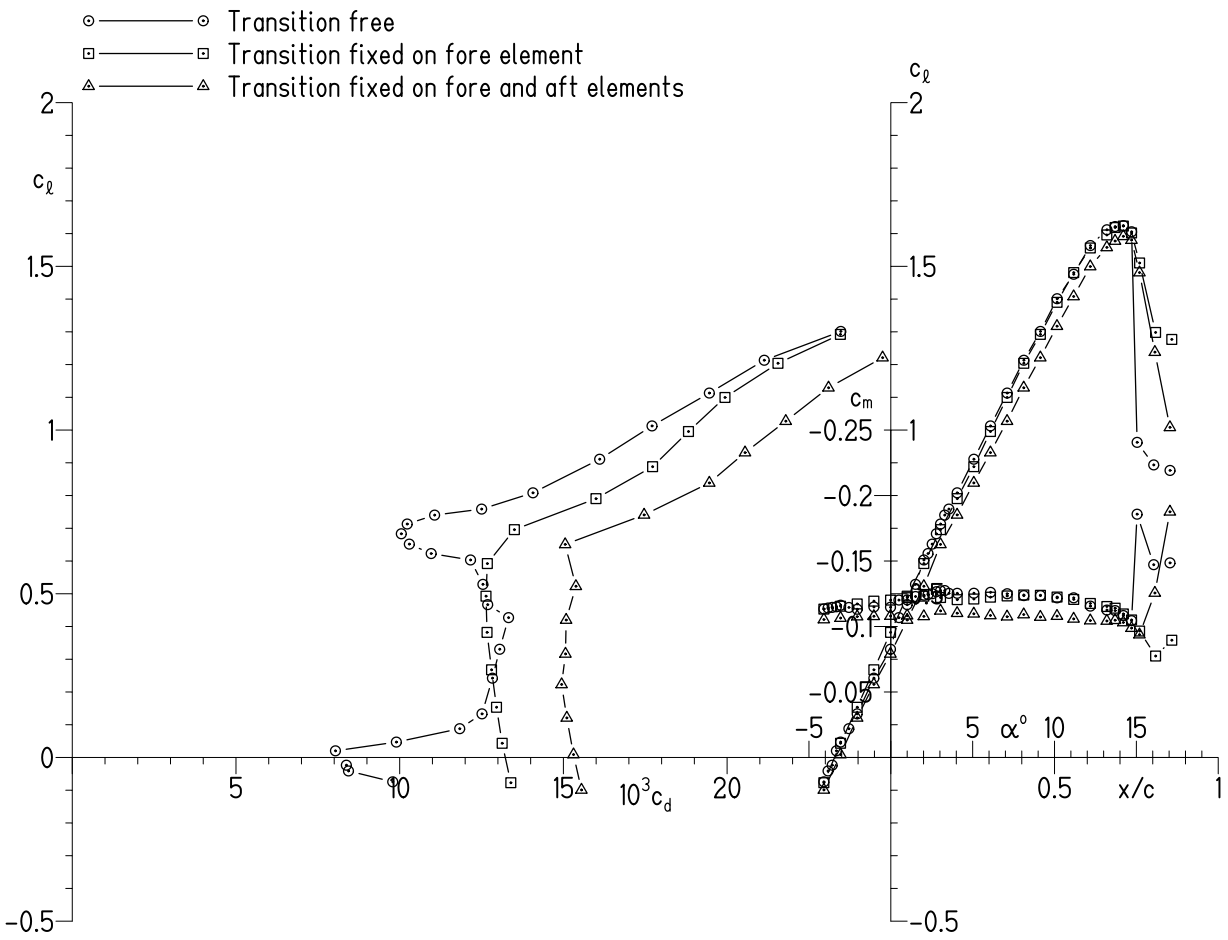

(a) $R = 0.50 \times 10^6$ and $M = 0.05$.

Figure 8.- Experimental section characteristics with transition free, with transition fixed on fore element, and with transition fixed on fore and aft elements.

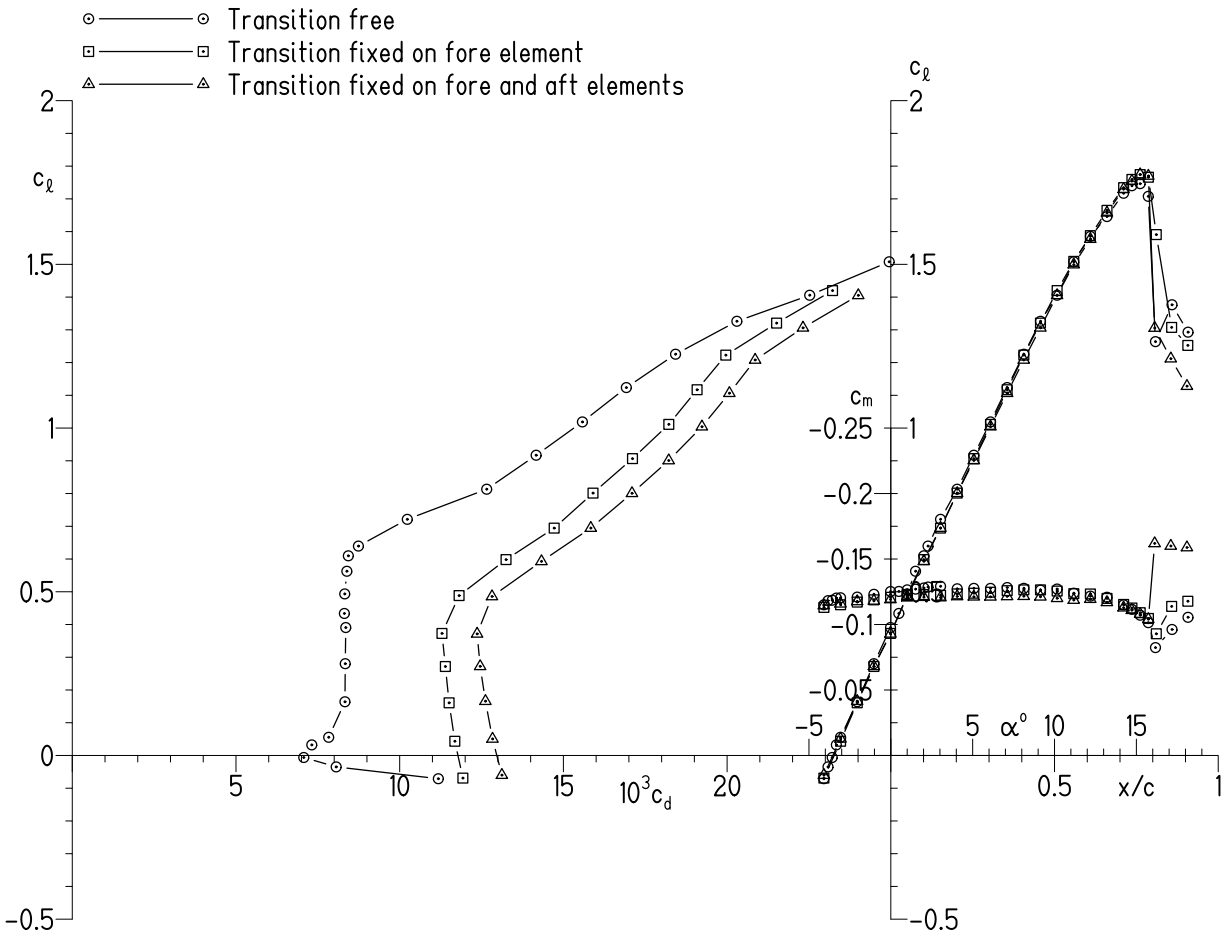

(b) $R = 0.70 \times 10^6$ and $M = 0.07$.

Figure 8.- Continued.

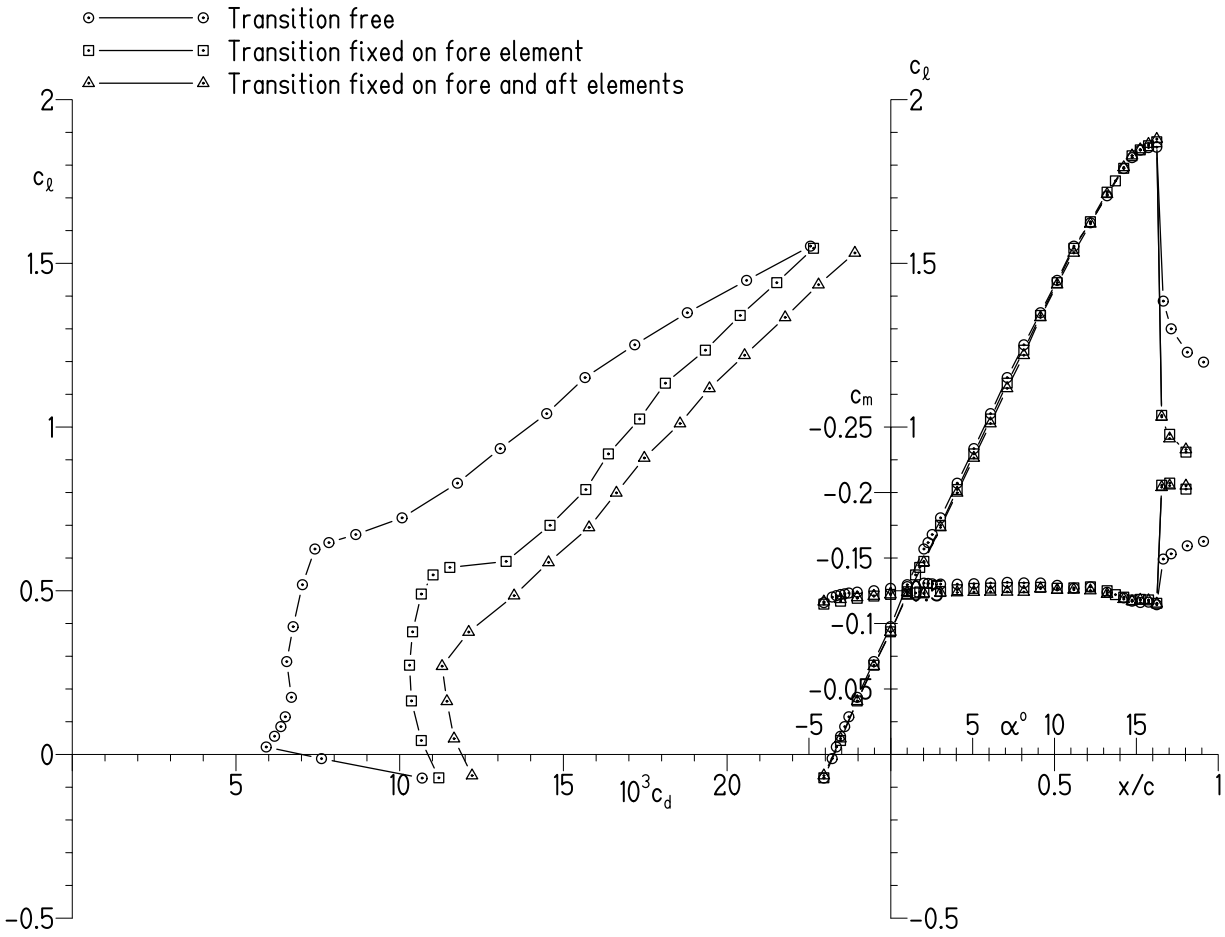

(c) $R = 1.00 \times 10^6$ and $M = 0.10$.

Figure 8.- Continued.

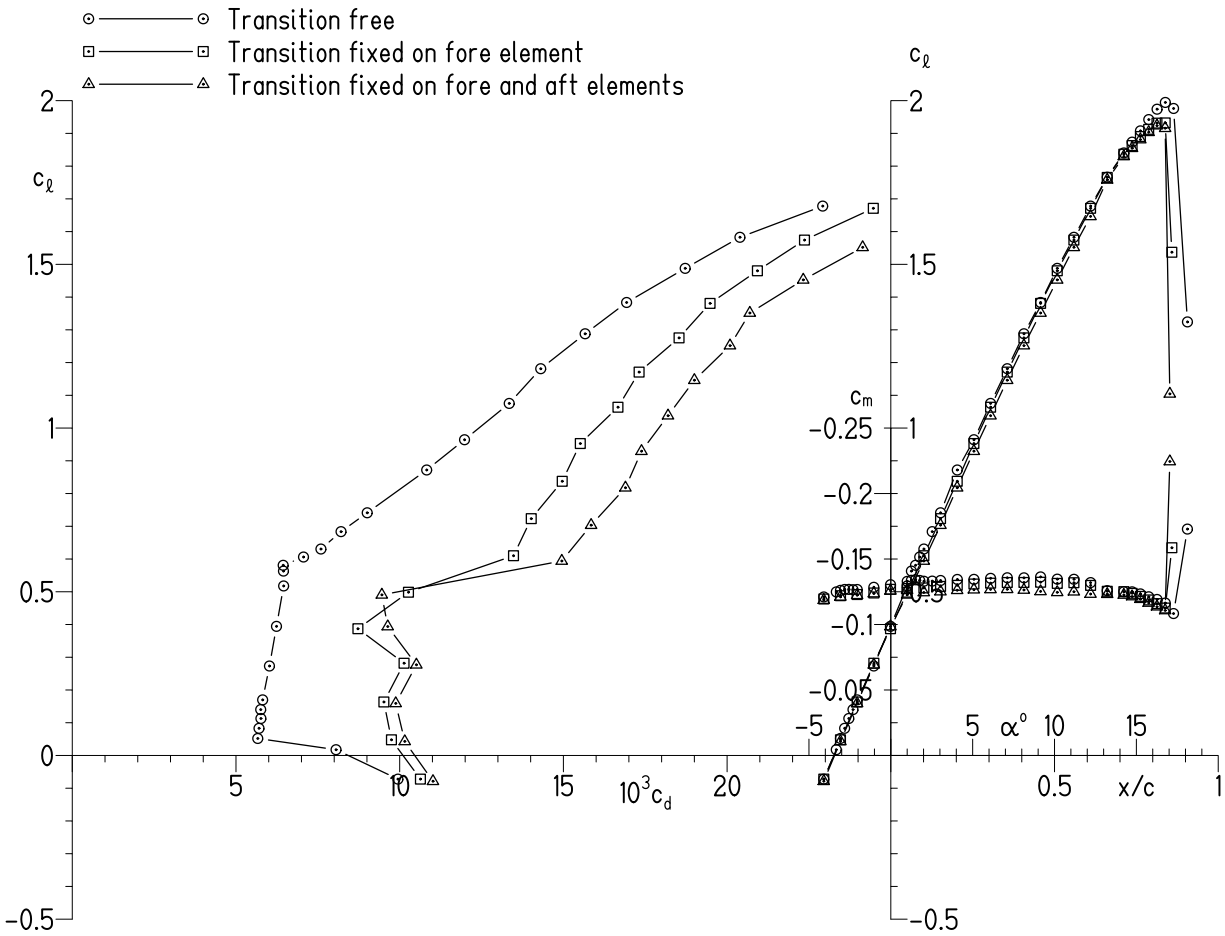

(d) $R = 1.50 \times 10^6$ and $M = 0.17$.

Figure 8.- Concluded.

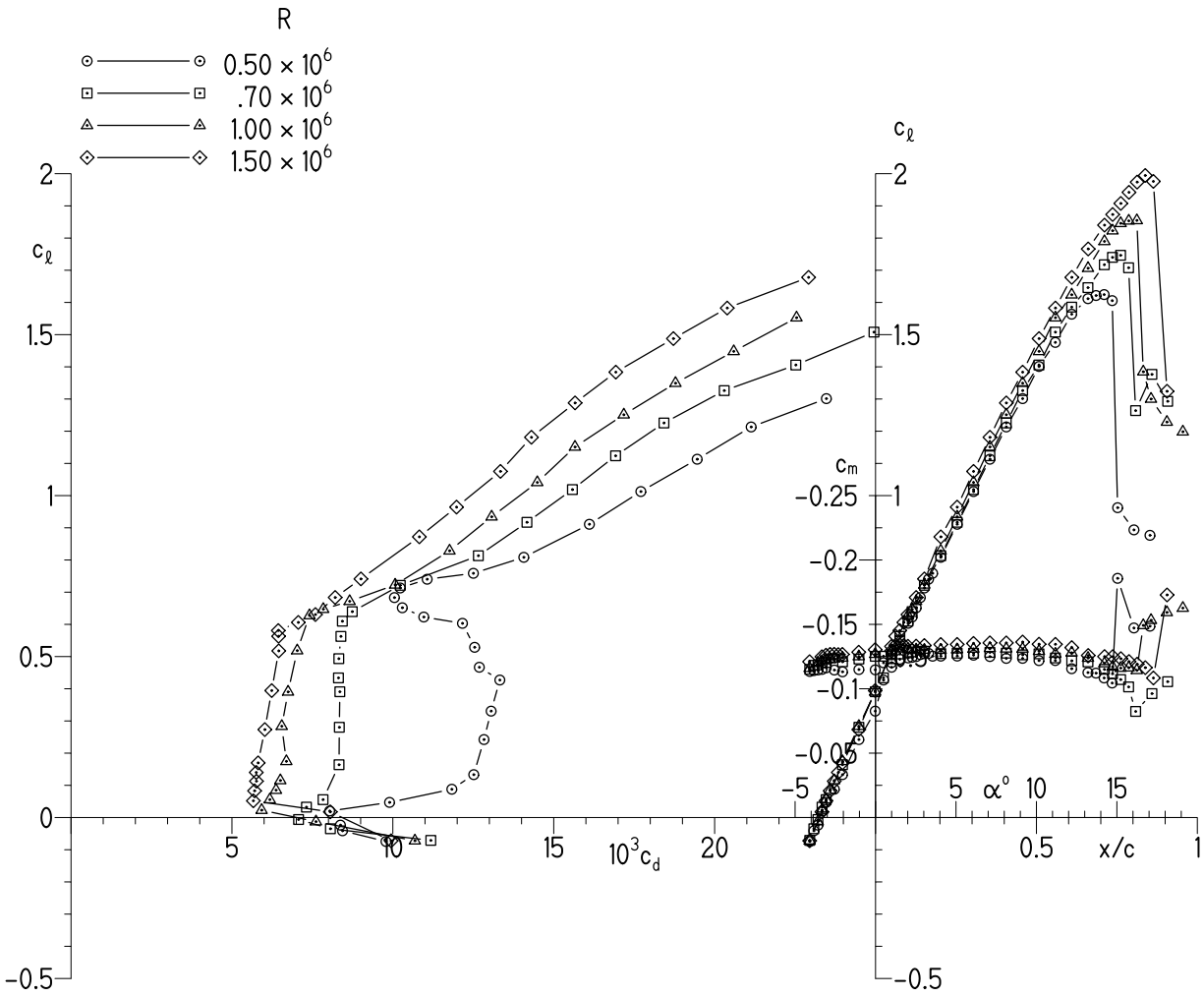

(a) Transition free.

Figure 9.- Effects of Reynolds number on experimental section characteristics.

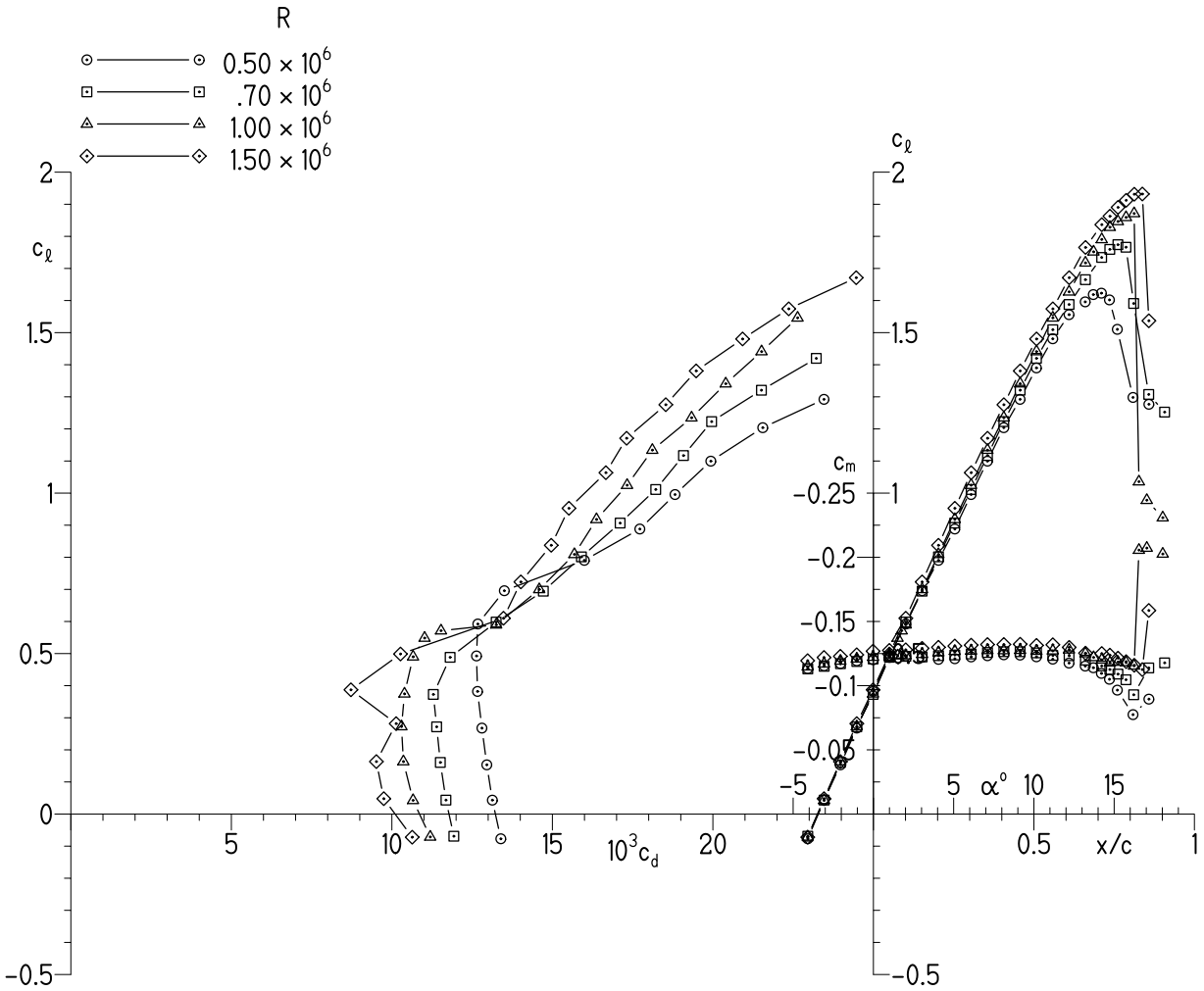

(b) Transition fixed on fore element.

Figure 9.- Continued.

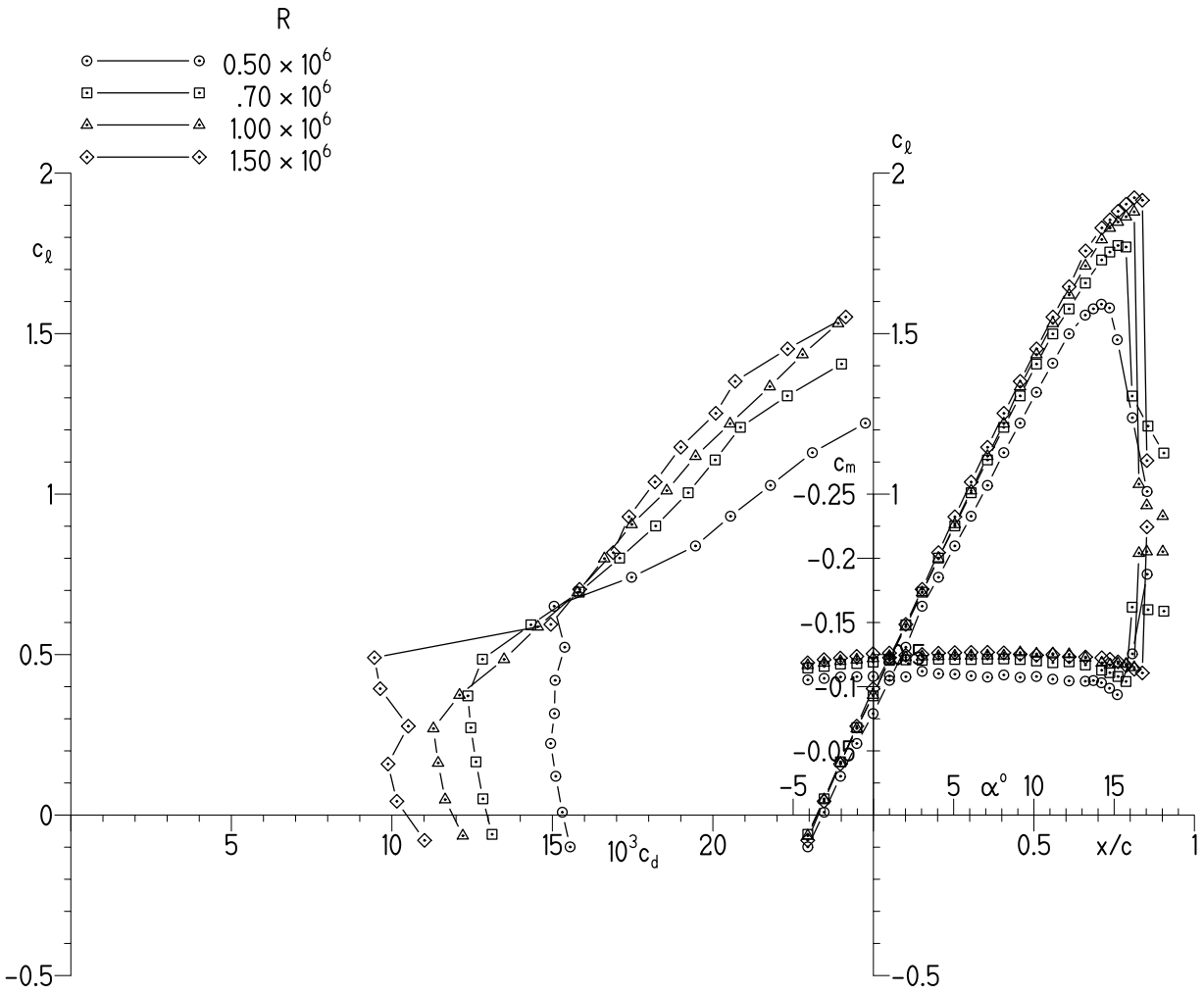

(c) Transition fixed on fore and aft elements.

Figure 9.- Concluded.

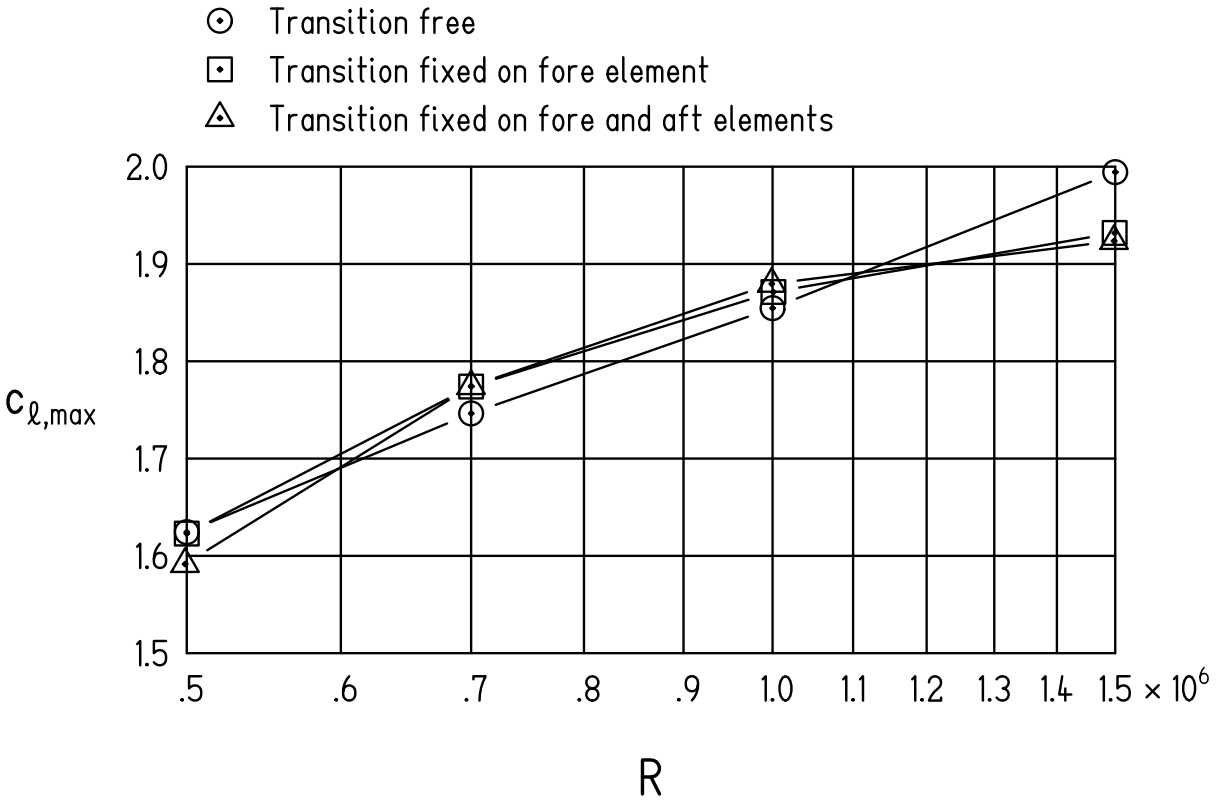

Figure 10.- Variation of experimental maximum lift coefficient with Reynolds number.

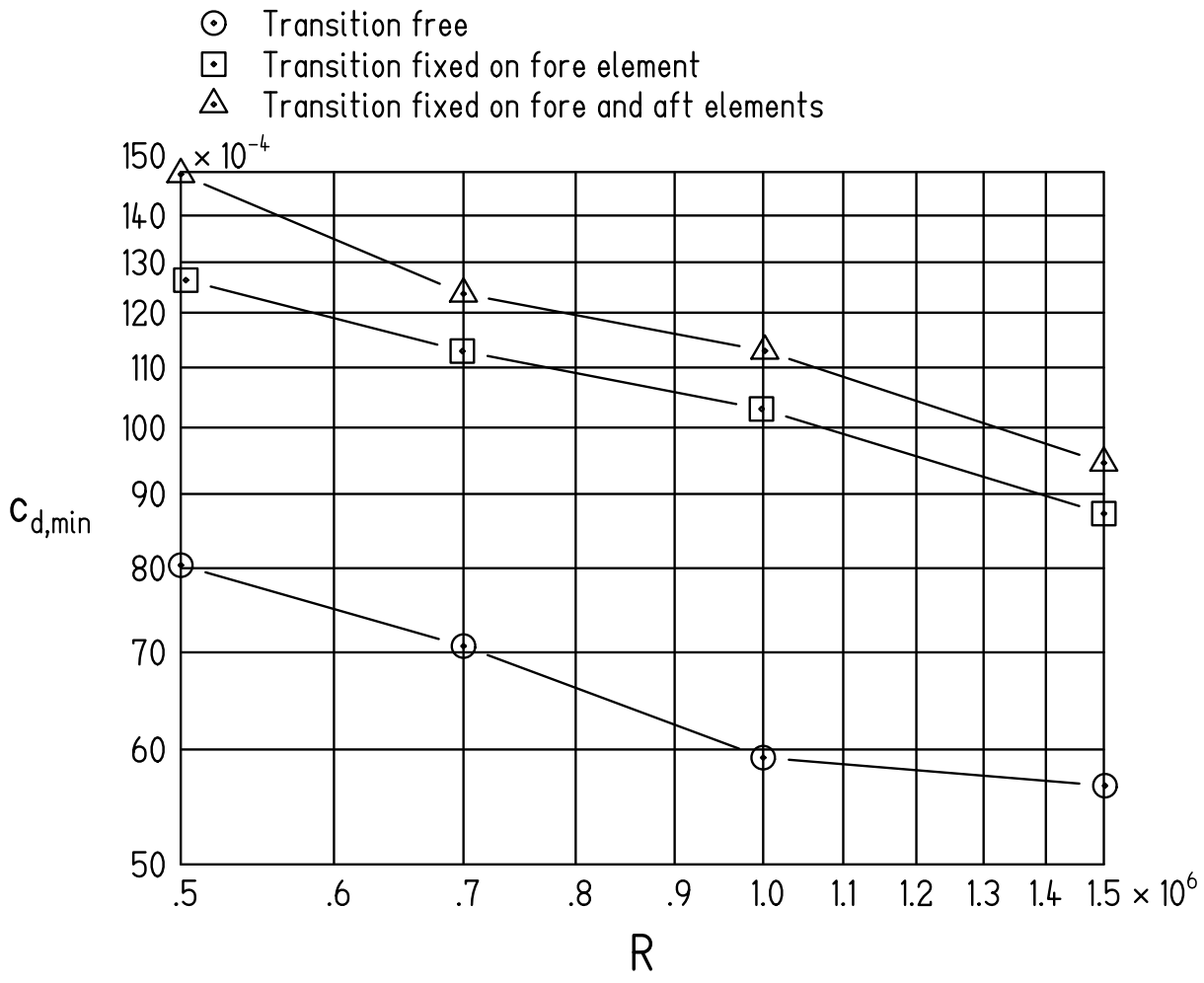

Figure 11.- Variation of experimental minimum profile-drag coefficient with Reynolds number.

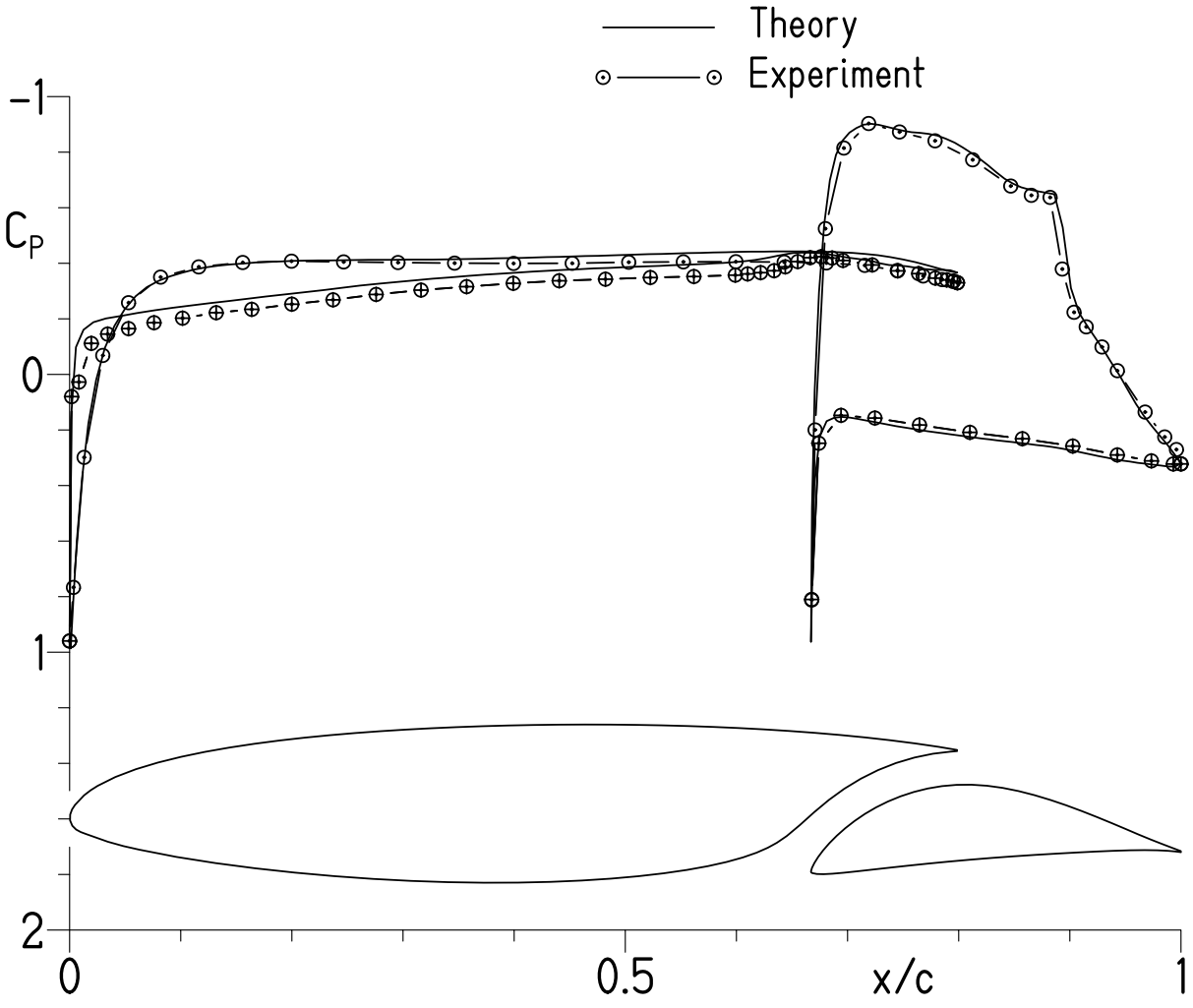

(a) $c_l = 0.28$.

Figure 12.- Comparison of theoretical and experimental pressure distributions for $R = 1.00 \times 10^6$ and $M = 0.10$.

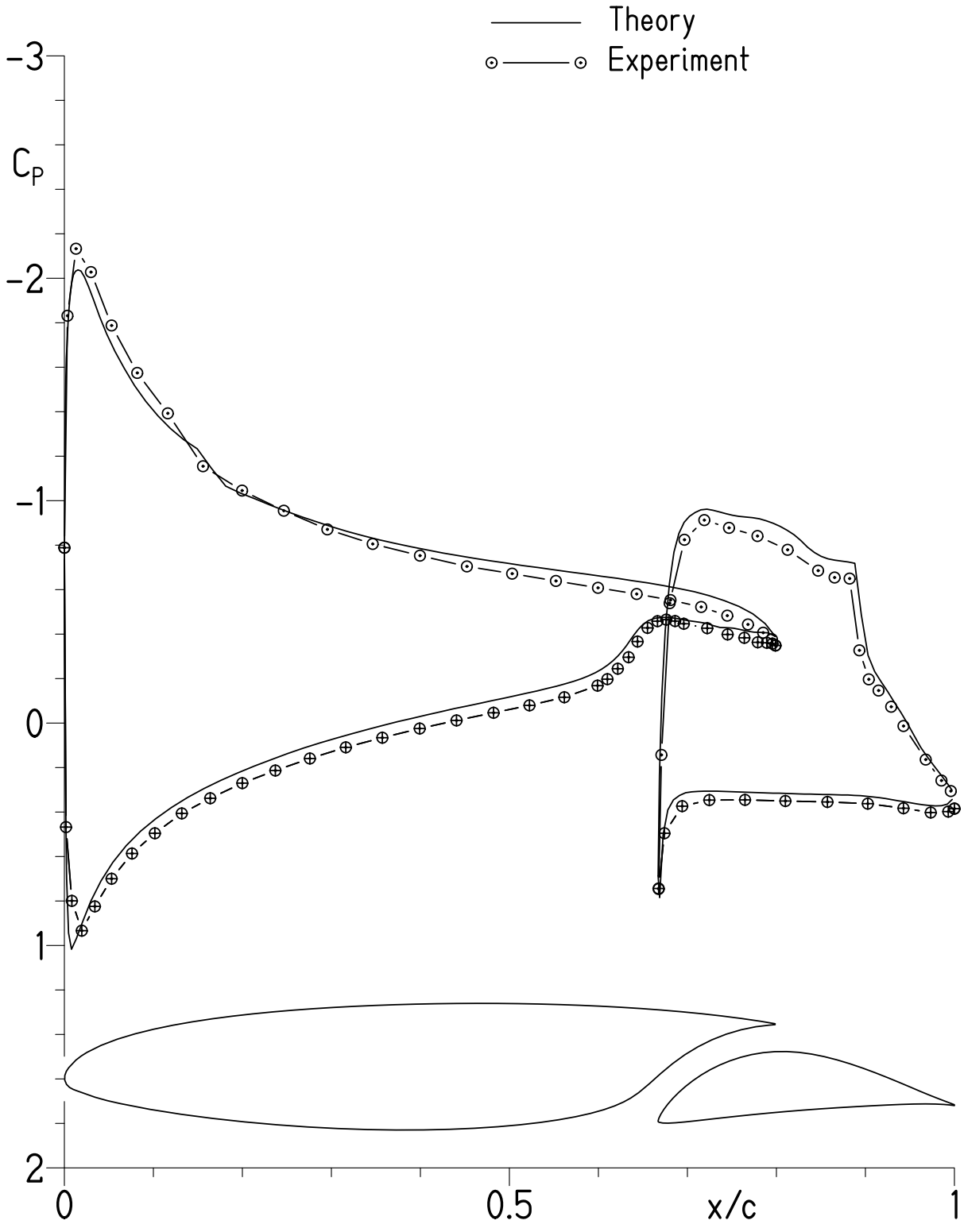

(b) $c_l = 1.04$.

Figure 12.- Continued.

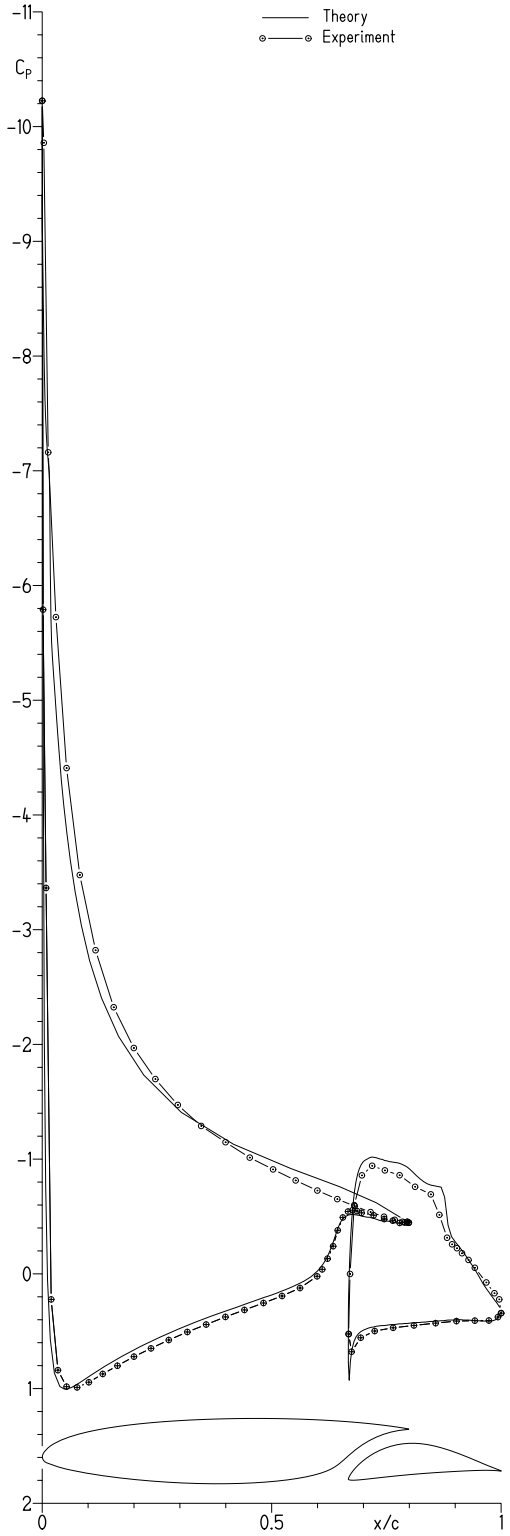

(c) $c_l = 1.85$.

Figure 12.- Concluded.

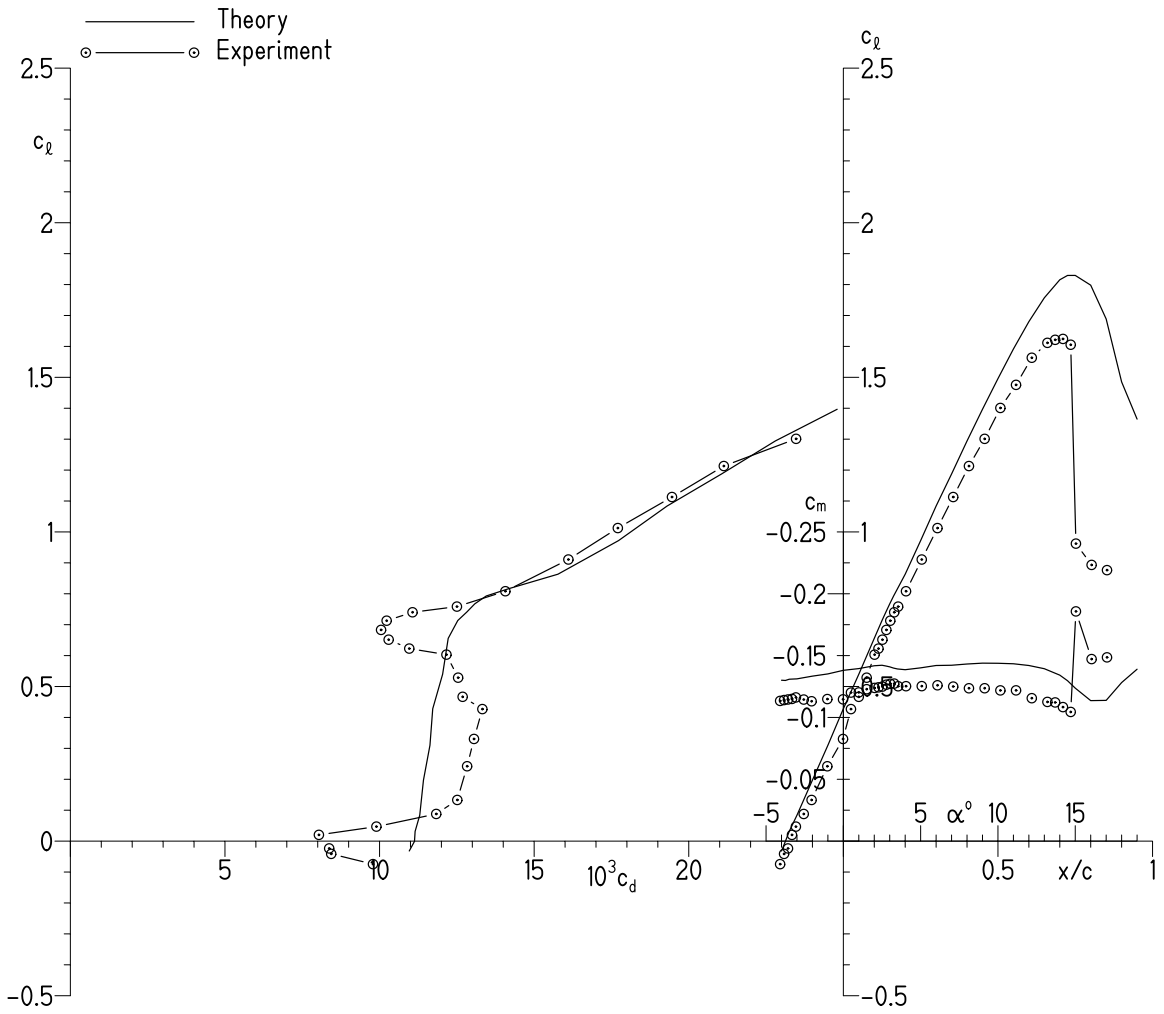

(a) $R = 0.50 \times 10^6$ and $M = 0.05$.

Figure 13.- Comparison of theoretical and experimental section characteristics with transition free.

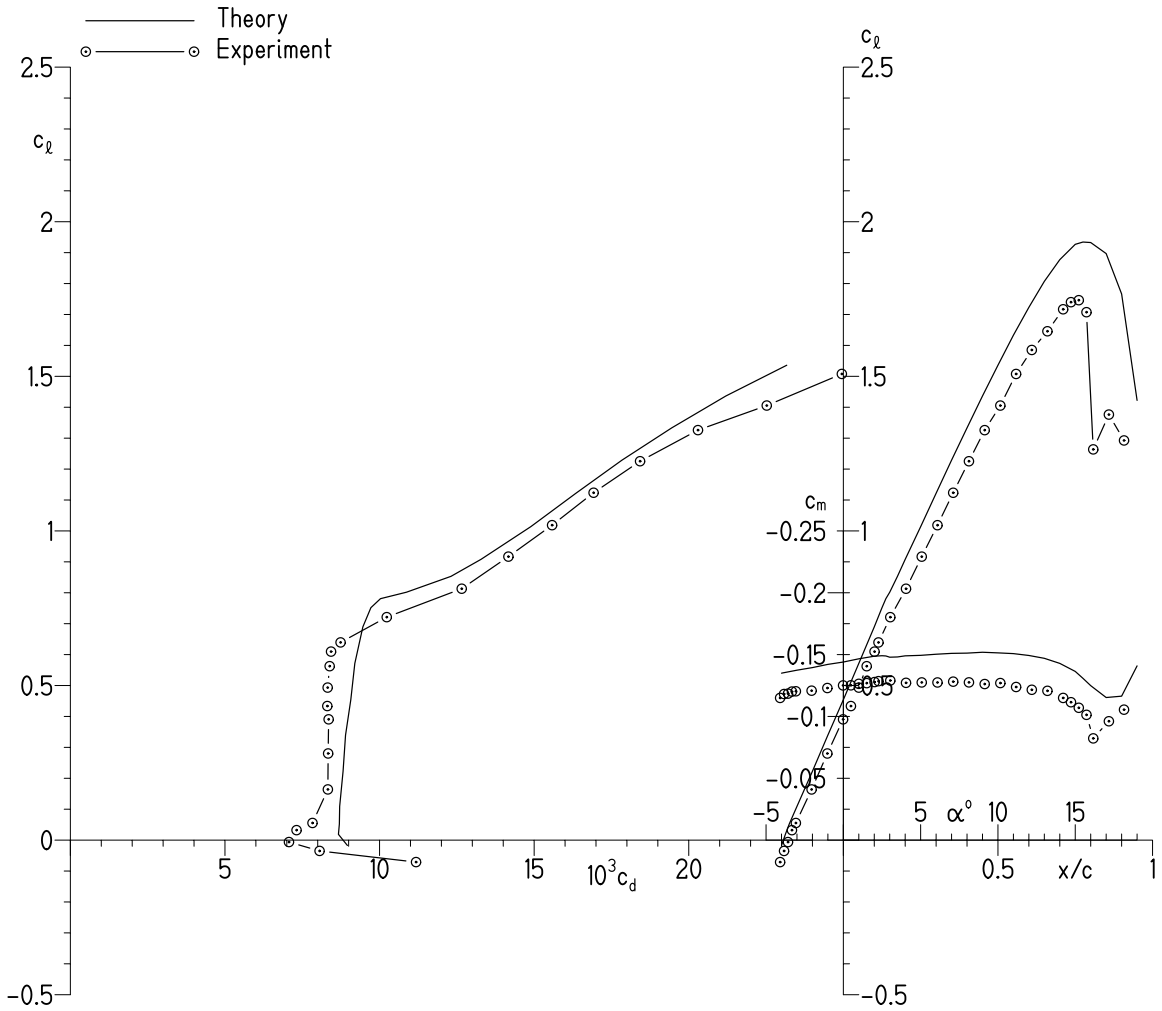

(b) $R = 0.70 \times 10^6$ and $M = 0.07$.

Figure 13.- Continued.

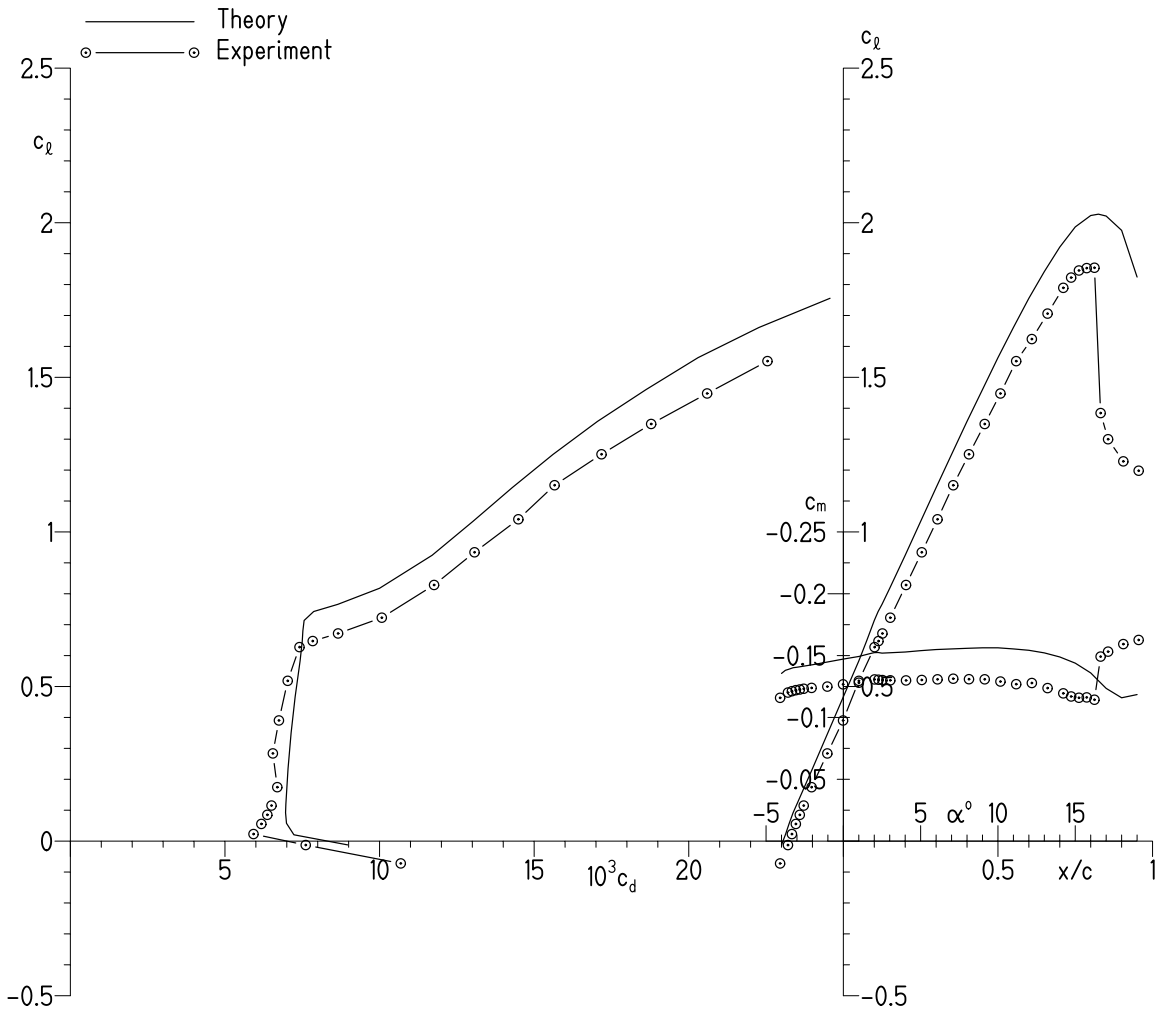

(c) $R = 1.00 \times 10^6$ and $M = 0.10$.

Figure 13.- Continued.

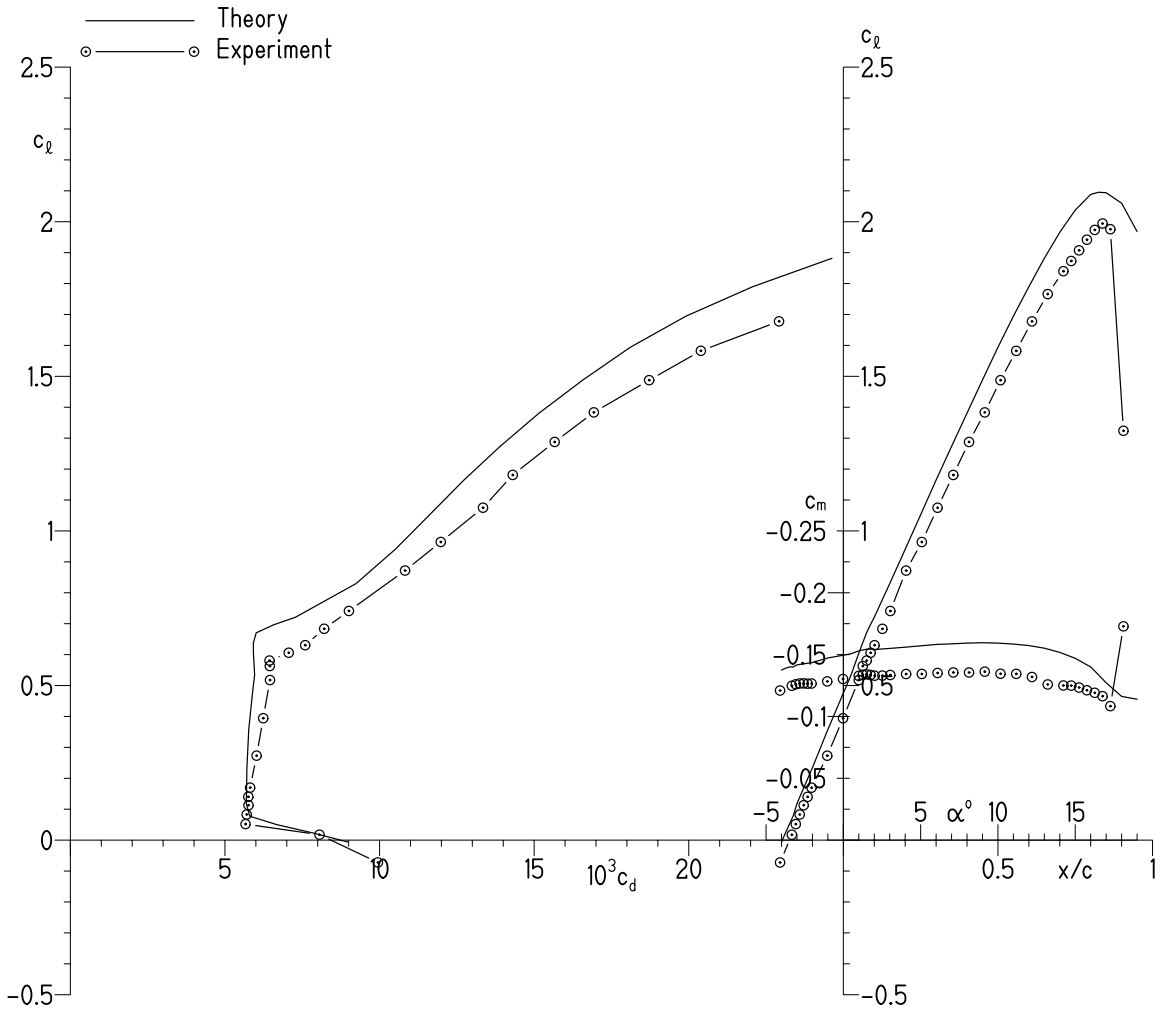

(d) $R = 1.50 \times 10^6$ and $M = 0.17$.

Figure 13.- Concluded.

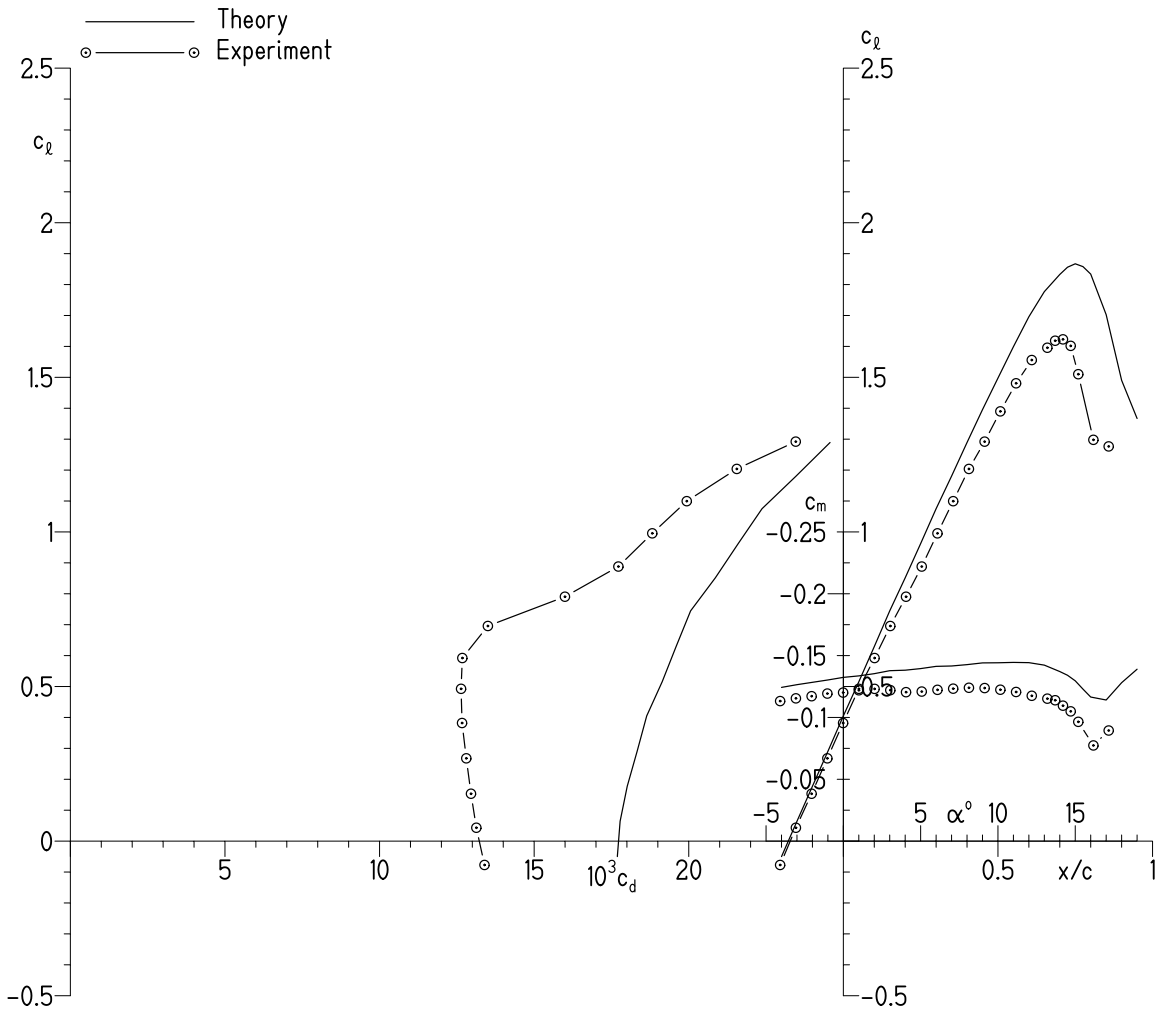

(a) $R = 0.50 \times 10^6$ and $M = 0.05$.

Figure 14.- Comparison of theoretical and experimental section characteristics with transition fixed on fore element.

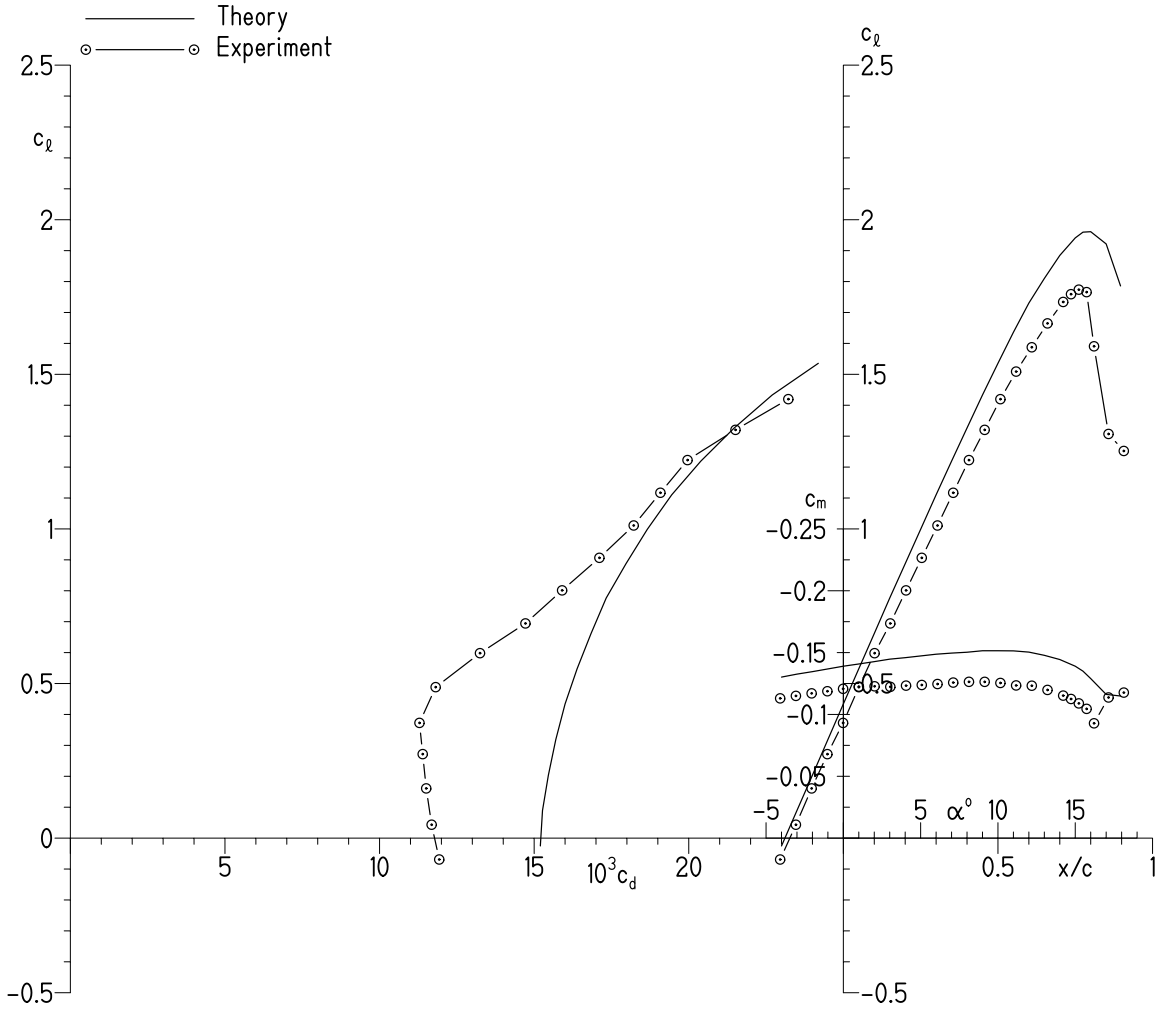

(b) $R = 0.70 \times 10^6$ and $M = 0.07$.

Figure 14.- Continued.

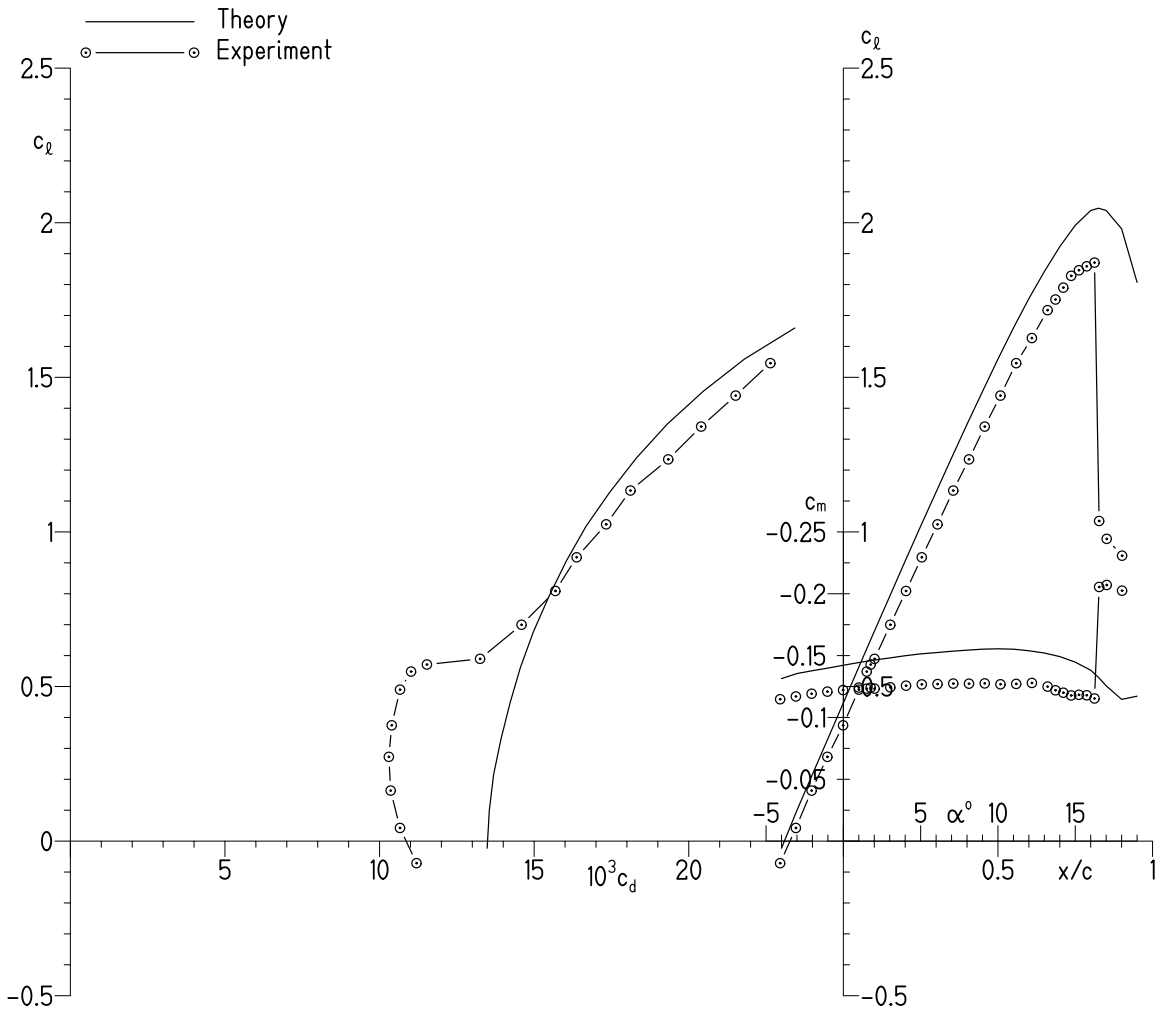

(c) $R = 1.00 \times 10^6$ and $M = 0.10$.

Figure 14.- Continued.

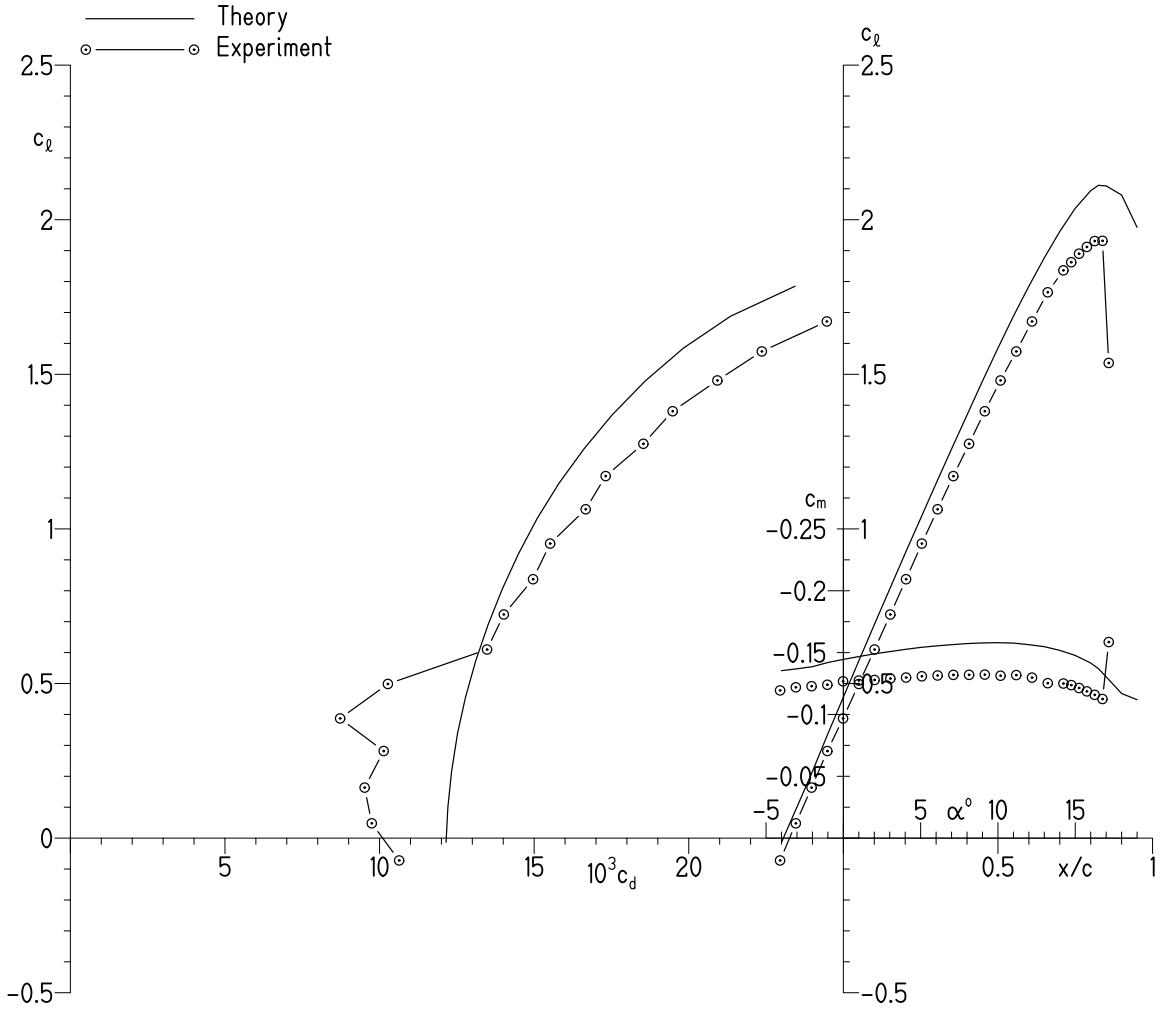

(d) $R = 1.50 \times 10^6$ and $M = 0.16$.

Figure 14.- Concluded.

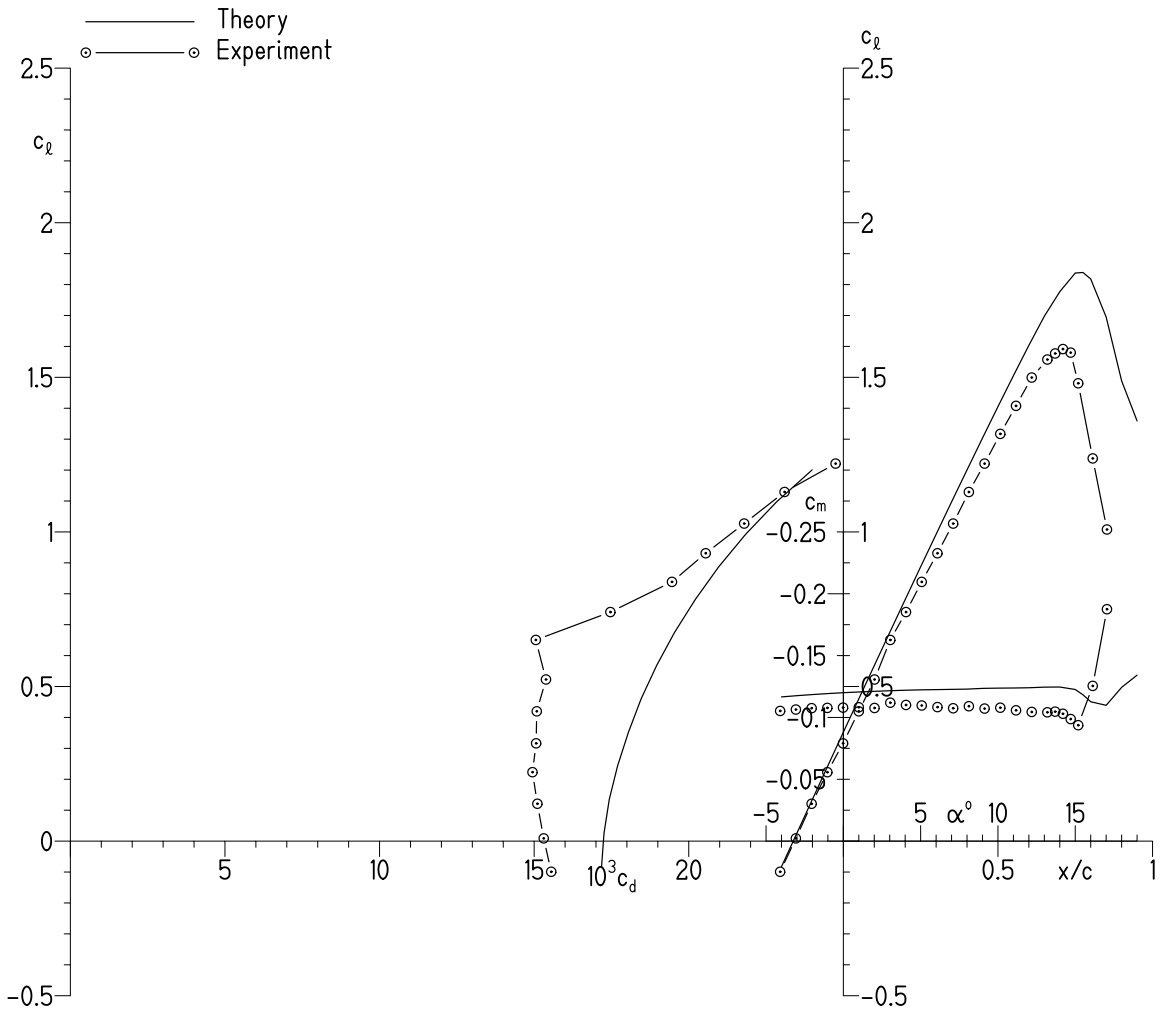

(a) $R = 0.50 \times 10^6$ and $M = 0.05$.

Figure 15.- Comparison of theoretical and experimental section characteristics with transition fixed on fore and aft elements.

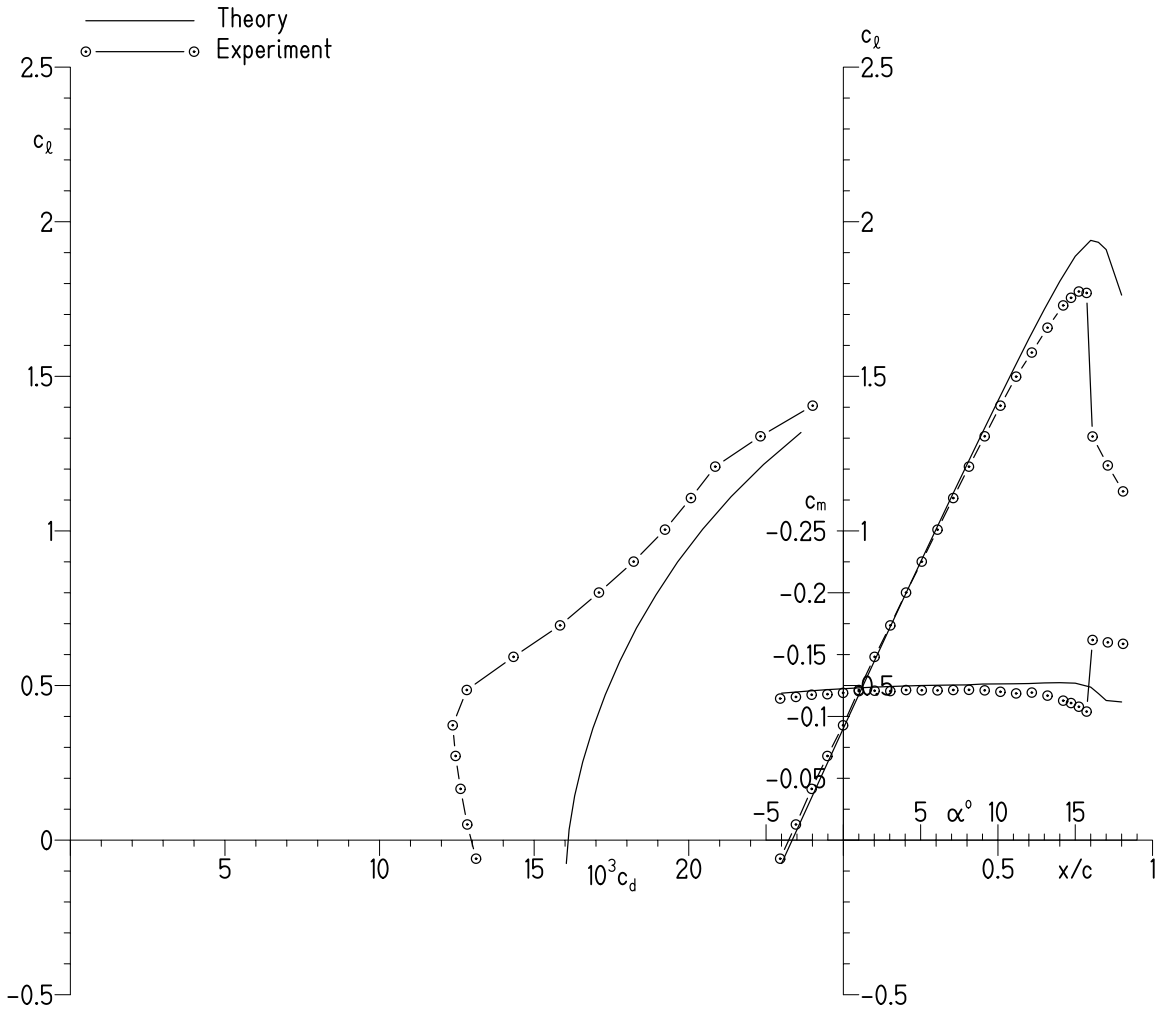

(b) $R = 0.70 \times 10^6$ and $M = 0.07$.

Figure 15.- Continued.

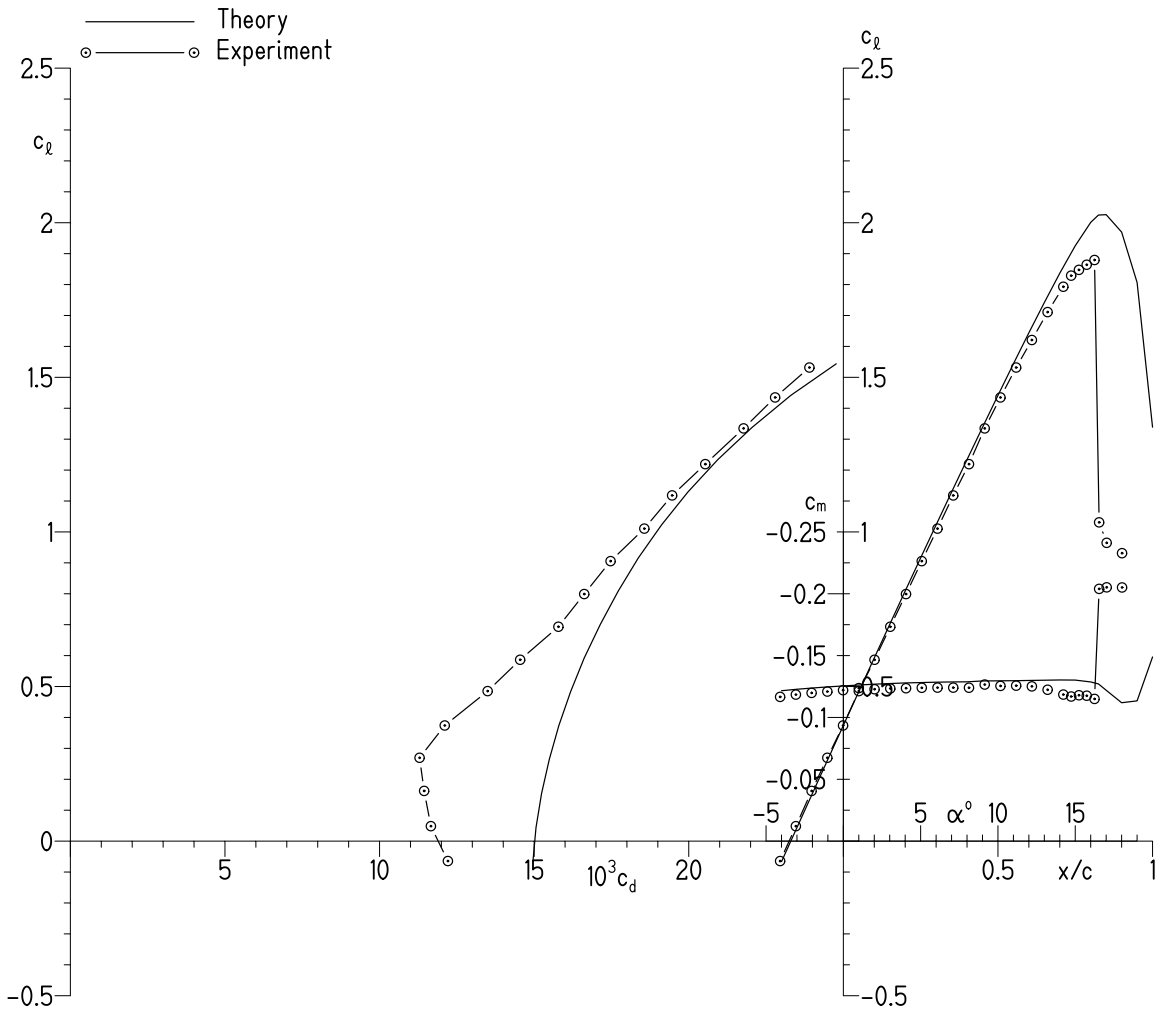

(c) $R = 1.00 \times 10^6$ and $M = 0.10$.

Figure 15.- Continued.

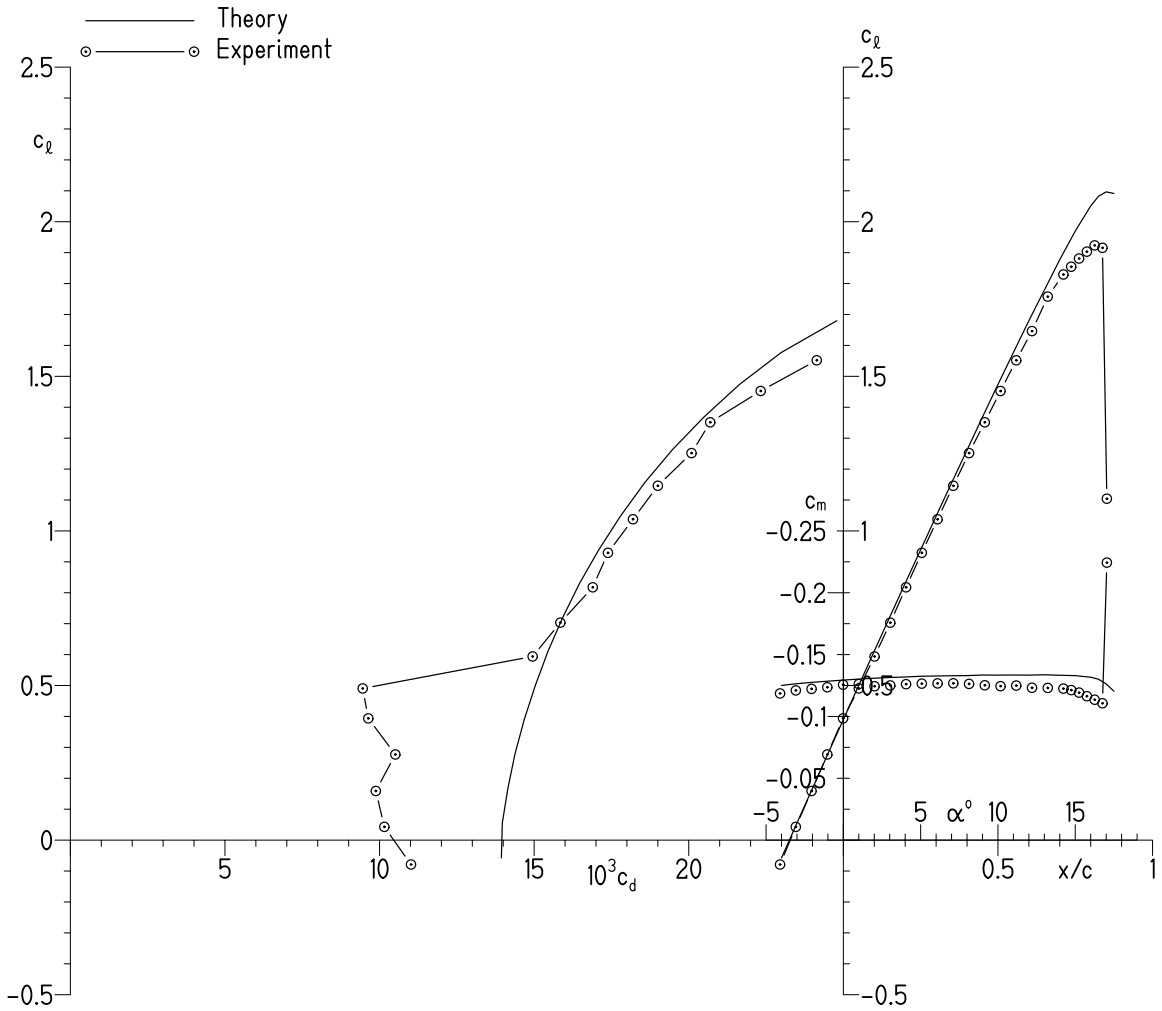

(d) $R = 1.50 \times 10^6$ and $M = 0.16$.

Figure 15.- Concluded.

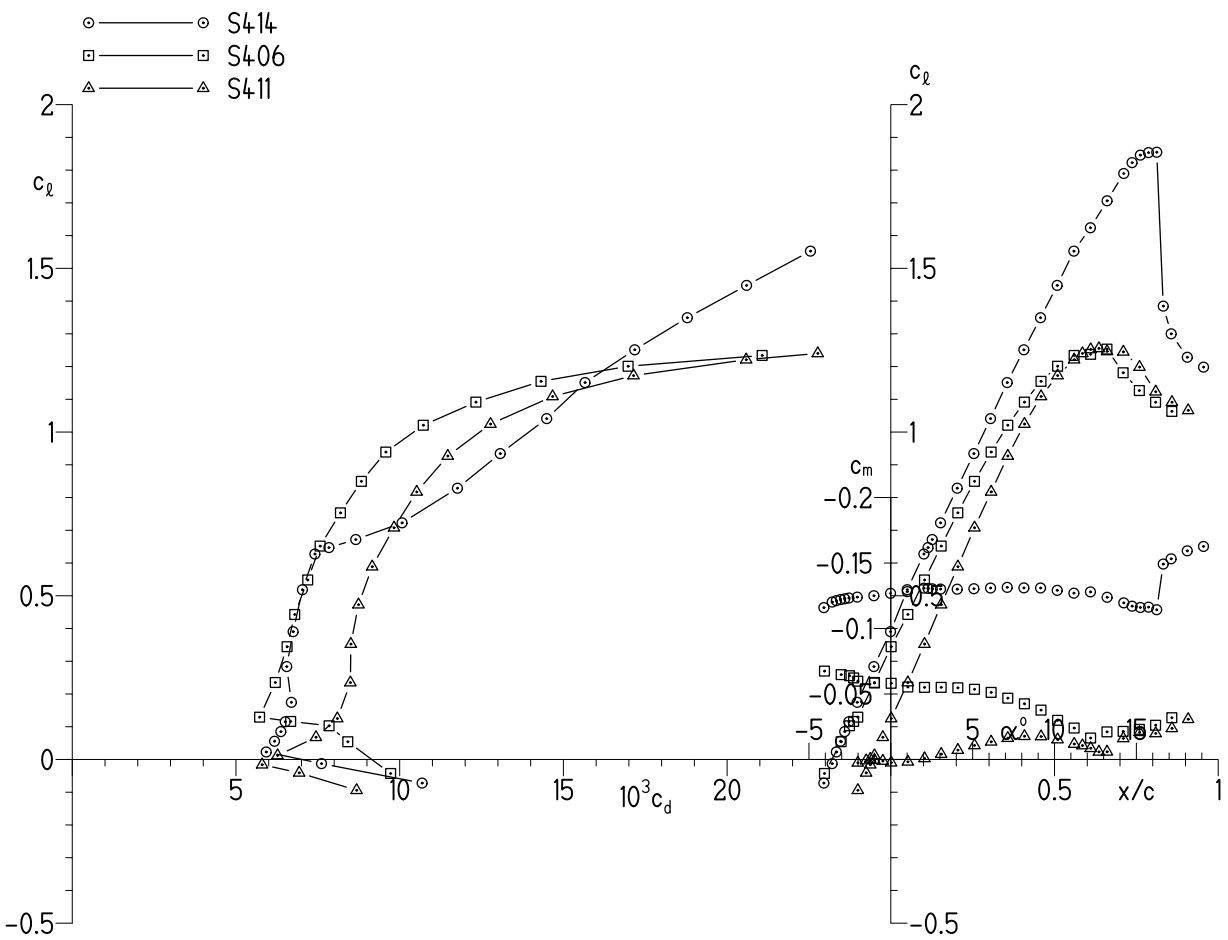

Figure 16.- Comparison of experimental section characteristics of S414, S406, and S411 airfoils for $R = 1.0 \times 10^6$ and $M = 0.1$ with transition free.

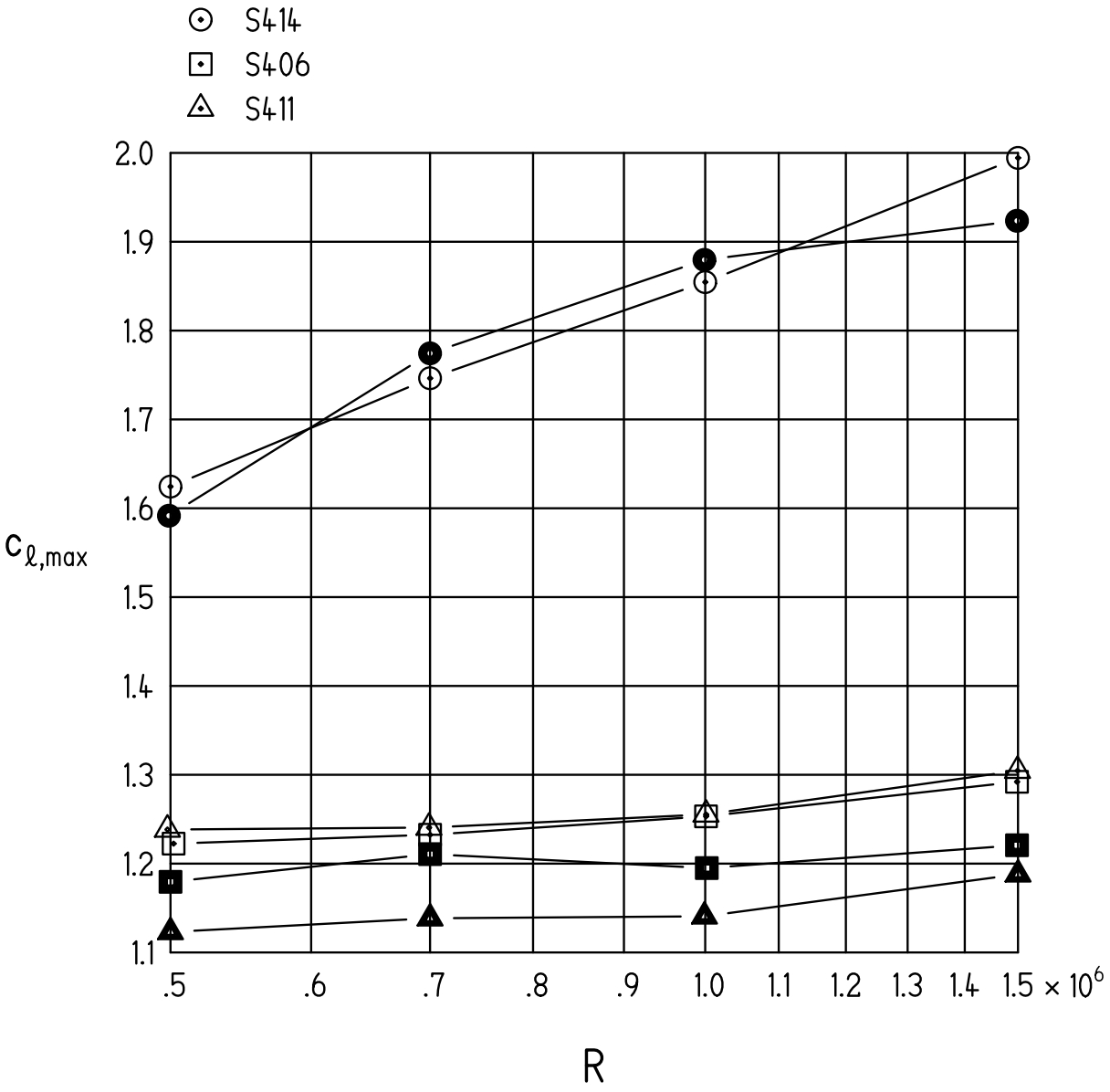

Figure 17.- Comparison of experimental maximum lift coefficients of S414, S406, and S411 airfoils. Open symbols represent data with transition free; solid symbols, data with transition fixed.

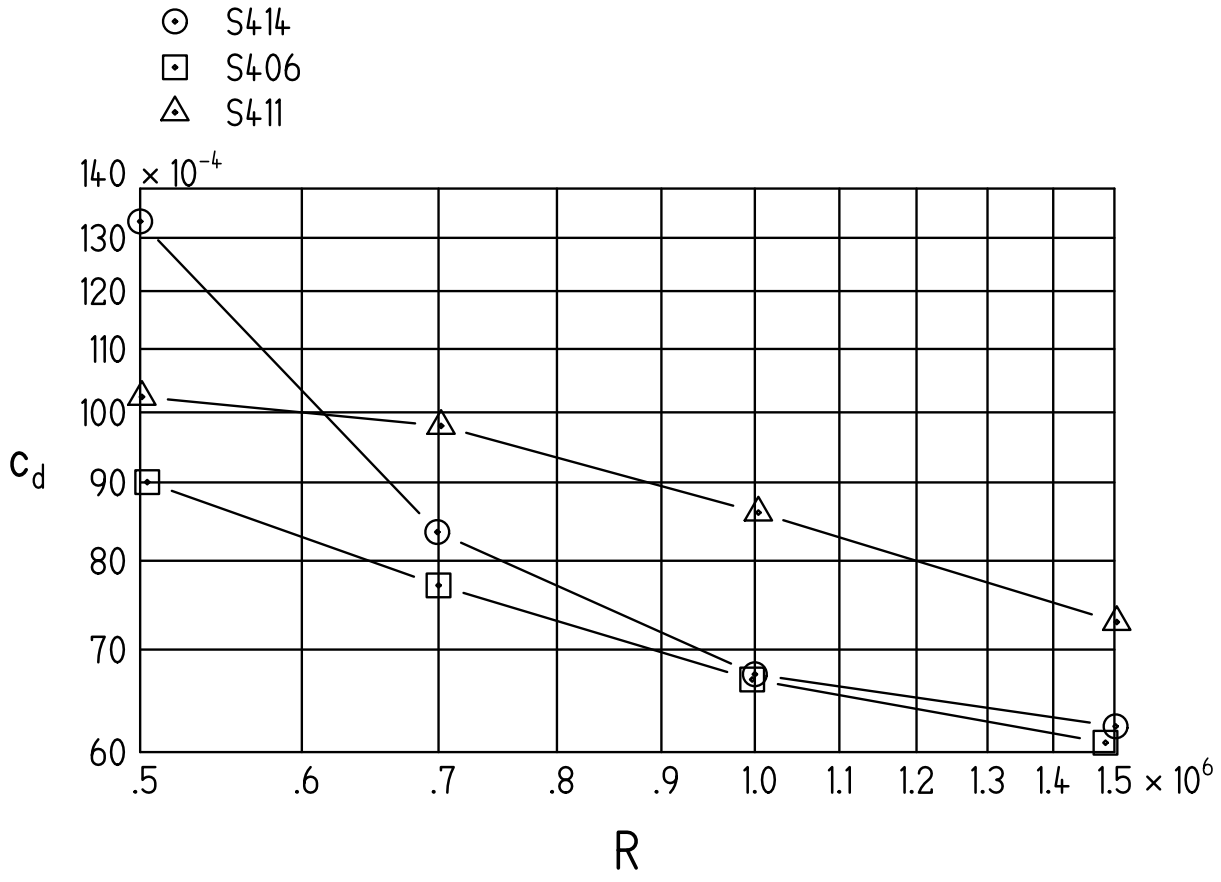

Figure 18.- Comparison of experimental profile-drag coefficients at $c_l = 0.4$ of S414, S406, and S411 airfoils with transition free.

APPENDIX

EXPERIMENTAL SECTION CHARACTERISTICS

$R = 0.50 \times 10^6$, M = 0.05, transition free

α, deg	c_l	c_d	c_m
–4.090	–0.0744	0.009787	–0.11343
–3.835	–.0412	.008436	–.11410
–3.582	–.0236	.008371	–.11458
–3.325	.0203	.008038	–.11504
–3.071	.0470	.009898	–.11624
–2.563	.0879	.011833	–.11452
–2.055	.1332	.012514	–.11314
–1.037	.2422	.012832	–.11492
–.022	.3305	.013054	–.11469
.491	.4271	.013325	–.12017
.997	.4668	.012687	–.12030
1.506	.5287	.012541	–.12289
2.018	.6032	.012163	–.12393
2.271	.6228	.010961	–.12440
2.526	.6516	.010294	–.12501
2.780	.6832	.010049	–.12656
3.035	.7130	.010229	–.12727
3.289	.7402	.011066	–.12744
3.544	.7586	.012502	–.12528
4.052	.8083	.014069	–.12533
5.070	.9109	.016107	–.12538
6.087	1.0126	.017706	–.12607
7.105	1.1130	.019457	–.12501
8.123	1.2132	.021134	–.12359
9.138	1.3012	.023471	–.12362
10.156	1.4011	.025849	–.12187
11.169	1.4758	.028733	–.12190
12.188	1.5635	.032368	–.11557
13.199	1.6117	.037185	–.11256
13.701	1.6215	.041285	–.11214
14.204	1.6244	.045975	–.10837
14.705	1.6056	.052214	–.10445
15.043	.9624	.203635	–.18575
16.057	.8935	.197284	–.14720
17.053	.8766	.216449	–.14859

$R = 0.50 \times 10^6$, $M = 0.05$, transition fixed on fore element

α, deg	c_l	c_d	c_m
–4.090	–0.0771	0.013394	–0.11326
–3.071	.0433	.013130	–.11547
–2.054	.1533	.012957	–.11720
–1.036	.2678	.012805	–.11934
–.017	.3820	.012668	–.12014
1.001	.4926	.012636	–.12199
2.017	.5922	.012677	–.12314
3.035	.6958	.013503	–.12210
4.053	.7905	.015995	–.12047
5.069	.8881	.017724	–.12096
6.086	.9955	.018820	–.12237
7.103	1.0995	.019935	–.12331
8.121	1.2038	.021553	–.12403
9.136	1.2921	.023460	–.12379
10.154	1.3900	.025496	–.12246
11.171	1.4808	.027957	–.12063
12.186	1.5560	.031483	–.11756
13.194	1.5958	.037280	–.11523
13.699	1.6185	.040601	–.11394
14.203	1.6229	.045835	–.10956
14.704	1.6019	.053399	–.10496
15.195	1.5102	—	–.09650
16.172	1.2980	—	–.07741
17.161	1.2767	.030607	–.08948

$R = 0.50 \times 10^6$, M = 0.05, transition fixed on fore and aft elements

α, deg	c_l	c_d	c_m
–4.089	–0.0991	0.015552	–0.10530
–3.071	.0089	.015309	–.10643
–2.053	.1209	.015104	–.10754
–1.036	.2230	.014946	–.10777
–.020	.3163	.015064	–.10798
.998	.4198	.015084	–.10826
2.016	.5228	.015382	–.10770
3.035	.6507	.015054	–.11195
4.051	.7409	.017465	–.11013
5.068	.8385	.019457	–.10971
6.085	.9311	.020548	–.10841
7.102	1.0271	.021792	–.10748
8.118	1.1292	.023098	–.10912
9.135	1.2211	.024749	–.10723
10.151	1.3172	.026665	–.10793
11.168	1.4079	.029120	–.10581
12.185	1.4994	.032316	–.10450
13.195	1.5577	.037478	–.10421
13.699	1.5773	.040984	–.10476
14.202	1.5916	.046306	–.10304
14.704	1.5801	.053833	–.09875
15.191	1.4809	—	–.09378
16.130	1.2379	.045742	–.12557
17.050	1.0081	.170539	–.18757

$R = 0.70 \times 10^6$, M = 0.07, transition free

α, deg	c_l	c_d	c_m
–4.091	–0.0710	0.011180	–0.11503
–3.837	–.0349	.008060	–.11819
–3.582	–.0062	.007070	–.11851
–3.327	.0323	.007315	–.12016
–3.073	.0555	.007831	–.12039
–2.055	.1640	.008328	–.12090
–1.036	.2803	.008337	–.12304
–.019	.3907	.008353	–.12515
.488	.4337	.008310	–.12522
.998	.4934	.008321	–.12643
1.509	.5626	.008386	–.12699
2.017	.6098	.008431	–.12787
2.271	.6395	.008739	–.12859
3.035	.7212	.010232	–.12913
4.052	.8132	.012657	–.12725
5.069	.9170	.014167	–.12757
6.087	1.0187	.015580	–.12754
7.104	1.1236	.016922	–.12820
8.122	1.2255	.018425	–.12761
9.140	1.3261	.020298	–.12627
10.153	1.4056	.022522	–.12707
11.173	1.5078	.024951	–.12388
12.188	1.5854	.028236	–.12164
13.199	1.6459	.032081	–.12079
14.216	1.7170	.037471	–.11504
14.722	1.7400	.041355	–.11157
15.227	1.7464	.046946	–.10708
15.725	1.7076	.055195	–.10138
16.163	1.2639	—	–.08234
17.174	1.3765	.032878	–.09618
18.154	1.2928	.065443	–.10549

$R = 0.70 \times 10^6$, M = 0.07, transition fixed on fore element

α, deg	c_l	c_d	c_m
–4.089	–0.0691	0.011930	–0.11304
–3.071	.0434	.011684	–.11505
–2.053	.1608	.011509	–.11709
–1.035	.2717	.011395	–.11880
–.019	.3727	.011291	–.12077
1.000	.4883	.011814	–.12254
2.018	.5982	.013248	–.12280
3.035	.6944	.014718	–.12236
4.053	.8013	.015904	–.12335
5.070	.9066	.017110	–.12387
6.088	1.0112	.018219	–.12465
7.105	1.1170	.019083	–.12582
8.123	1.2227	.019960	–.12643
9.139	1.3205	.021511	–.12641
10.157	1.4198	.023220	–.12551
11.174	1.5090	.025508	–.12351
12.187	1.5876	.028232	–.12329
13.203	1.6649	.031549	–.11988
14.218	1.7342	.036451	–.11529
14.725	1.7593	.039557	–.11256
15.230	1.7740	.044457	–.10899
15.732	1.7660	.051539	–.10458
16.213	1.5908	.064317	–.09289
17.151	1.3073	.050516	–.11378
18.139	1.2523	.078973	–.11773

$R = 0.70 \times 10^6$, M = 0.07, transition fixed on fore and aft elements

α, deg	c_l	c_d	c_m
–4.088	–0.0600	0.013121	–0.11449
–3.070	.0506	.012836	–.11581
–2.052	.1658	.012619	–.11760
–1.034	.2722	.012458	–.11802
–.018	.3714	.012365	–.11911
1.001	.4856	.012820	–.12049
2.019	.5928	.014331	–.12085
3.036	.6945	.015837	–.12054
4.054	.8007	.017095	–.12138
5.071	.9008	.018217	–.12117
6.089	1.0042	.019231	–.12112
7.106	1.1064	.020070	–.12142
8.123	1.2080	.020856	–.12158
9.140	1.3061	.022318	–.12114
10.158	1.4052	.024007	–.11999
11.175	1.4991	.026330	–.11866
12.188	1.5770	.028912	–.11934
13.204	1.6574	.032401	–.11688
14.219	1.7294	.037301	–.11281
14.725	1.7541	.040777	–.11087
15.231	1.7744	.045552	–.10791
15.733	1.7699	.052740	–.10399
16.118	1.3055	.081579	–.16188
17.104	1.2119	.113903	–.15994
18.090	1.1279	.127516	–.15876

$R = 1.00 \times 10^6$, M = 0.10, transition free

α, deg	c_l	c_d	c_m
–4.092	–0.0721	0.010685	–0.11592
–3.585	–.0127	.007612	–.12018
–3.329	.0229	.005923	–.12127
–3.074	.0556	.006177	–.12211
–2.819	.0851	.006370	–.12265
–2.565	.1151	.006505	–.12325
–2.055	.1745	.006692	–.12395
–1.037	.2837	.006549	–.12501
–.020	.3903	.006745	–.12682
1.001	.5185	.007029	–.12815
2.018	.6275	.007410	–.13079
2.271	.6471	.007838	–.13057
2.526	.6717	.008658	–.13028
3.035	.7227	.010072	–.13009
4.053	.8285	.011763	–.13000
5.071	.9342	.013071	–.13036
6.089	1.0410	.014489	–.13088
7.107	1.1511	.015660	–.13139
8.125	1.2512	.017178	–.13099
9.142	1.3492	.018784	–.13090
10.160	1.4479	.020594	–.12911
11.179	1.5525	.022545	–.12696
12.191	1.6239	.025368	–.12792
13.208	1.7063	.028233	–.12381
14.225	1.7896	.032488	–.11955
14.733	1.8228	.035245	–.11703
15.238	1.8457	.038226	–.11600
15.739	1.8534	.042815	–.11628
16.241	1.8546	.048295	–.11433
16.640	1.3846	.052281	–.14921
17.123	1.3000	.083066	–.15321
18.108	1.2284	.113944	–.15931
19.101	1.1982	.139756	–.16266

$R = 1.00 \times 10^6$, M = 0.10, transition fixed on fore element

α, deg	c_l	c_d	c_m
–4.091	–0.0713	0.011195	–0.11476
–3.073	.0426	.010660	–.11700
–2.054	.1635	.010359	–.11923
–1.036	.2726	.010300	–.12092
–.020	.3746	.010393	–.12219
.999	.4900	.010661	–.12421
1.509	.5484	.011019	–.12330
1.763	.5712	.011531	–.12405
2.016	.5896	.013250	–.12337
3.035	.6998	.014591	–.12441
4.052	.8091	.015685	–.12574
5.070	.9180	.016374	–.12679
6.088	1.0246	.017328	–.12703
7.107	1.1339	.018114	–.12745
8.124	1.2347	.019336	–.12737
9.142	1.3408	.020400	–.12759
10.160	1.4410	.021516	–.12688
11.178	1.5459	.022639	–.12717
12.191	1.6271	.025014	–.12796
13.209	1.7173	.027820	–.12500
13.717	1.7518	.029901	–.12200
14.225	1.7902	.032026	–.12007
14.733	1.8284	.034239	–.11783
15.236	1.8464	.037268	–.11838
15.739	1.8591	.040701	–.11798
16.243	1.8712	.045411	–.11539
16.543	1.0355	.211458	–.20557
17.032	.9777	.252899	–.20716
18.026	.9233	.267834	–.20256

$R = 1.00 \times 10^6$, M = 0.10, transition fixed on fore and aft elements

α, deg	c_l	c_d	c_m
–4.091	–0.0644	0.012210	–0.11666
–3.073	.0484	.011660	–.11851
–2.054	.1624	.011442	–.11989
–1.037	.2696	.011294	–.12097
–.020	.3740	.012108	–.12208
.998	.4852	.013495	–.12376
2.016	.5866	.014547	–.12285
3.034	.6934	.015784	–.12345
4.052	.7991	.016619	–.12366
5.070	.9056	.017471	–.12403
6.088	1.0108	.018563	–.12416
7.107	1.1181	.019462	–.12415
8.124	1.2193	.020534	–.12407
9.142	1.3349	.021773	–.12664
10.160	1.4350	.022793	–.12554
11.176	1.5318	.023902	–.12575
12.192	1.6208	.025952	–.12517
13.210	1.7111	.028818	–.12245
14.227	1.7931	.032476	–.11856
14.734	1.8290	.034809	–.11697
15.237	1.8477	.037643	–.11800
15.740	1.8643	.041191	–.11763
16.245	1.8796	.045431	–.11504
16.544	1.0311	.241072	–.20402
17.031	.9649	.252464	–.20525
18.026	.9314	.270051	–.20516

$R = 1.50 \times 10^6$, M = 0.17, transition free

α, deg	c_l	c_d	c_m
–4.096	–0.0722	0.009946	–0.12102
–3.333	.0176	.008056	–.12487
–3.078	.0519	.005665	–.12607
–2.823	.0829	.005703	–.12673
–2.568	.1129	.005761	–.12679
–2.313	.1401	.005755	–.12655
–2.058	.1698	.005814	–.12671
–1.042	.2732	.006022	–.12840
–.022	.3943	.006237	–.13036
.997	.5177	.006455	–.13290
1.255	.5631	.006450	–.13375
1.507	.5808	.006441	–.13410
1.762	.6061	.007062	–.13361
2.017	.6305	.007594	–.13302
2.526	.6836	.008208	–.13312
3.036	.7412	.009008	–.13359
4.058	.8719	.010824	–.13439
5.074	.9643	.011980	–.13445
6.092	1.0752	.013345	–.13522
7.110	1.1812	.014307	–.13566
8.129	1.2879	.015663	–.13562
9.145	1.3835	.016930	–.13632
10.164	1.4877	.018719	–.13462
11.181	1.5826	.020391	–.13451
12.199	1.6779	.022919	–.13198
13.218	1.7662	.025211	–.12586
14.232	1.8402	.028719	–.12502
14.738	1.8732	.030864	–.12495
15.245	1.9076	.033540	–.12338
15.753	1.9421	.036374	–.12117
16.260	1.9738	.040197	–.11913
16.765	1.9944	.044550	–.11638
17.269	1.9760	.052555	–.10836
18.117	1.3241	.130468	–.17286

$R = 1.50 \times 10^6$, $M = 0.16$, transition fixed on fore element

α, deg	c_l	c_d	c_m
–4.095	–0.0722	0.010633	–0.11946
–3.076	.0479	.009748	–.12197
–2.057	.1634	.009517	–.12286
–1.037	.2817	.010133	–.12404
–.021	.3871	.008724	–.12683
.998	.4986	.010268	–.12748
2.017	.6101	.013476	–.12791
3.036	.7233	.014018	–.12906
4.055	.8374	.014964	–.12988
5.074	.9527	.015516	–.13089
6.093	1.0636	.016666	–.13154
7.111	1.1709	.017312	–.13203
8.129	1.2754	.018532	–.13207
9.147	1.3807	.019479	–.13225
10.165	1.4803	.020925	–.13136
11.181	1.5741	.022363	–.13187
12.200	1.6711	.024465	–.12982
13.218	1.7654	.025727	–.12533
14.231	1.8364	.028878	–.12505
14.737	1.8627	.032356	–.12377
15.243	1.8903	.036433	–.12143
15.749	1.9122	.041617	–.11871
16.255	1.9312	.047183	–.11590
16.758	1.9319	.054215	–.11253
17.163	1.5369	.064182	–.15858

$R = 1.50 \times 10^6$, $M = 0.16$, transition fixed on fore and aft elements

α, deg	c_l	c_d	c_m
–4.096	–0.0788	0.011017	–0.11863
–3.076	.0429	.010155	–.12110
–2.057	.1590	.009879	–.12232
–1.038	.2770	.010510	–.12363
–.019	.3938	.009635	–.12571
.997	.4906	.009455	–.12624
2.017	.5940	.014951	–.12445
3.035	.7034	.015847	–.12511
4.054	.8177	.016895	–.12613
5.073	.9293	.017386	–.12658
6.092	1.0378	.018196	–.12677
7.110	1.1461	.019000	–.12685
8.129	1.2518	.020089	–.12636
9.147	1.3514	.020694	–.12525
10.165	1.4526	.022326	–.12454
11.182	1.5519	.024140	–.12502
12.200	1.6464	.026032	–.12326
13.219	1.7579	.025245	–.12313
14.232	1.8295	.028215	–.12255
14.737	1.8546	.031740	–.12135
15.243	1.8811	.035997	–.11933
15.750	1.9034	.041624	–.11643
16.256	1.9236	.047828	–.11359
16.758	1.9157	.055772	–.11070
17.043	1.1044	.231380	–.22444

REPORT DOCUMENTATION PAGE

Form Approved
OMB No. 0704-0188

1. REPORT DATE *(DD-MM-YYYY)*	2. REPORT TYPE	3. DATES COVERED *(From - To)*
xx 08 2010	FINAL REPORT	Sep 2007 Jun 2010

4. TITLE AND SUBTITLE

Design and Experimental Results for the S414 Airfoil

5a. CONTRACT NUMBER
W911W6 07 C 0047

5b. GRANT NUMBER

5c. PROGRAM ELEMENT NUMBER

6. AUTHOR(S)

Somers, Dan M. and Maughmer, Mark D.

5d. PROJECT NUMBER

5e. TASK NUMBER

5f. WORK UNIT NUMBER

7. PERFORMING ORGANIZATION NAME(S) AND ADDRESS(ES)

Airfoils, Incorporated
Attn: Dan M. Somers
122 Rose Drive
Port Matilda PA 16870 7535

8. PERFORMING ORGANIZATION REPORT NUMBER

SBIR Topic Number A06 006
Proposal Number A2 2972

9. SPONSORING / MONITORING AGENCY NAME(S) AND ADDRESS(ES)

US Army Aviation Research, Development and Engineering Command (RDECOM)
Aviation Applied Technology Directorate (AATD)
Fort Eustis VA 23604 5577

10. SPONSOR/MONITOR'S ACRONYM(S)

11. SPONSOR/MONITOR'S REPORT NUMBER(S)
RDECOM TR 10 D 112

12. DISTRIBUTION / AVAILABILITY STATEMENT

Approved for public release; distribution is unlimited.

13. SUPPLEMENTARY NOTES

UL Note: No proprietary / limited information may be included in the abstract.

14. ABSTRACT

A 14.22 percent thick, slotted, natural laminar flow (SNLF) airfoil, the S414, intended for rotorcraft applications has been designed and analyzed theoretically and verified experimentally in The Pennsylvania State University Low Speed, Low Turbulence Wind Tunnel. The two primary objectives of high maximum lift and low profile drag have been achieved. The constraint on the airfoil thickness has been satisfied. The airfoil exhibits an abrupt stall. Comparisons of the theoretical and experimental results show good agreement overall. Comparisons with the S406 and S411 airfoils, which have similar design specifications, confirm the achievement of the objectives.

15. SUBJECT TERMS

Airfoils, rotorcraft, laminar flow, wind tunnel

16. SECURITY CLASSIFICATION OF:			17. LIMITATION OF ABSTRACT	18. NUMBER OF PAGES	19a. NAME OF RESPONSIBLE PERSON
a. REPORT	b. ABSTRACT	c. THIS PAGE			Dan M. Somers
unclassified	unclassified	unclassified	UU	94	19b. TELEPHONE NUMBER *(include area code)* (814) 357 0500